AN INVESTIGATION OF VARIOUS HYDROCARBON SOURCES IN THE PRODUCTION OF CARBON NANOPARTICLES VIA A PLASMA ENHANCED CHEMICAL VAPOUR DEPOSITION TECHNIQUE

Shivan Royith Singh

Submitted in fulfilment of the requirement for the degree of Master of Science in Engineering to the School of Electrical, Electronic and Computer Engineering, University of KwaZulu-Natal.

As the candidate's Supervisor I agree/do not agree to the submission of this thesis.

Signature: _____ **Name:** _____

Date: _____

DECLARATION

I, Shivan Royith Singh, declare that:

(i) The research reported in this thesis, except where otherwise indicated, is my original work.

(ii) This thesis has not been submitted for any degree or examination at any other university.

(iii) This thesis does not contain other persons' data, pictures, graphs or other information, unless specifically acknowledged as being sourced from other persons.

(iv) This thesis does not contain other persons' writing, unless specifically acknowledged as being sourced from other researchers. Where other written sources have been quoted, then:

  (a) Their words have been re-written but the general information attributed to them has been referenced;

  (b) Where their exact words have been used, their writing has been placed inside quotation marks, and referenced

(v) Where I have reproduced a publication of which I am an author, co-author or editor, I have indicated in detail which part of the publication was actually written by myself alone and have fully referenced such publications.

(vi) This thesis does not contain text, graphics or tables copied and pasted from the Internet, unless specifically acknowledged, and the source being detailed in the thesis and in the References sections.

Signed:_____

ACKNOWLEDGEMENTS

There are numerous people who have, in one way or another, assisted me in this work and it would be remiss not to acknowledge them. Firstly, I owe a great deal of thanks to Clarence Mortlock for all the custom-made glasswork. I must also thank James Wesley-Smith, Priscilla Maartens and Sharon Eggers at the Electron Microscope Unit for their assistance in the Transmission and Scanning Electron Microscopy analysis.

Closer to the School, Alan Moonsamy receives thanks for always promptly and efficiently attending to my purchasing needs. Anthony Lester is thanked for his assistance around the lab, as well as for his invaluable advice. Gratitude is also shown to Daniel Sanderson, Jonathon Archer, Brett Swann, Peter Adigun, Neil Hendry, Timothy Rowell and Jurie Loots for their advice, support and assistance. Big thanks must go to my supervisor, Leigh Jarvis, who always had endless patience and words of encouragement.

Finally, I must thank my parents and my sisters – their support throughout this work has been invaluable and unflagging. It is deeply appreciated.

ABSTRACT

A simple, low cost microwave plasma enhanced chemical vapour deposition (PECVD) technique for the production of carbon nanostructures has been developed in the School's Materials Science Laboratory. The technique utilises a conventional microwave oven as an energy source, various hydrocarbons as a carbon source, a metallic aerial as a catalyst and hydrogen to support the process. The input hydrocarbon and the hydrogen flow rate are independently varied to investigate their effect on the resultant nanostructures. This technique allows for the production of carbon nanotubes (CNTs), onion-like nanostructures structures (ONSs) and amorphous carbon, which has been verified via transmission and scanning electron microscopy. A change in input parameters results in the controllable yield of CNTs versus ONSs. The formation of amorphous carbon is reduced by controlling the hydrogen flow rate. In further experiments, the thermal conductivity of the ONSs is investigated using the „Lee's Disk' method. It was observed that bulk ONS specimens exhibit a thermal conductivity above that of amorphous carbon powder. Insufficient quantities of CNTs were grown using this method to facilitate a comparable thermal conductivity investigation.

TABLE OF CONTENTS

TABLE OF FIGURES

LIST OF TABLES

CHAPTER 1. INTRODUCTION TO CARBON NANOSTRUCTURES

An unpublished, novel microwave plasma enhanced chemical vapour deposition (PECVD) technique to produce carbon nanotubes has previously been developed by a Masters student in the Materials Science Laboratory at the University of KwaZulu-Natal [**1**]. The concept that carbon nanotubes (CNTs) could be produced in a domestic microwave oven was proved in the previous student's work. The work described herein arose from the desire to further explore the original findings to determine the optimal conditions for CNT growth.

This exploration required a number of alterations, such as the addition of flow meters and the redesign of a borosilicate tube and stainless steel aerial, to be made to the original design. A thorough investigation of the effect of various hydrocarbon sources on the quality and yield of CNTs was also conducted. In the course of this investigation [**2**], however, it was observed that onion-like nanostructures (ONSs) could be grown using this technique; with the quantity of ONSs growth far exceeding the quantity of CNTs.

ONSs are a lesser studied carbon nanostructure and the growth of a decent quantity of these structures presents the opportunity to investigate them further. To this end, an investigation of the thermal conductivity of ONSs, embedded in an epoxy-resin matrix was conducted. The thermal conductivity was measured using the well-known Lee's disk method.

1.1 Organisation of this dissertation

Before delving into the details of this project, it is sensible to first describe the layout and structure of this document.

Chapter 1 takes a detailed look at carbon nanostructures: their structure, properties, uses and the three major methods used to synthesise these structures.

In Chapter 2, the experiments conducted in this project are described in detail; from the equipment used, to the planning of the experiments themselves.

Chapter 3 presents the analysis of the experiments, making use of transmission and scanning electron microscopy as tools to provide visual analysis of the grown structures.

Thermal conductivity is discussed in Chapter 4, along with two methods used to measure the thermal conductivity of materials.

Chapter 5 presents the experimental work on the thermal conductivity of ONSs and carbon powder, the production of the samples and a look at the equipment utilised, followed by a

discussion of the results of the thermal conductivity measurements made on ONS and carbon samples.

Chapter 6 concludes this dissertation and incorporates a few suggestions for future work.

1.2 Carbon nanotubes

Numerous carbon nanostructures have been documented – ranging from the quasi-one-dimensional carbon nanotube (CNT) and fullerenes to structures such as carbon nano-necklaces, nano-chains and onion-like nanostructures (ONSs) [**3-12]**. CNTs have been studied intensively since their seminal report describing these structures in 1991 [**3**]. Indeed, CNTs have already been utilised in various applications [**13**]. Investigations of other carbon nanostructures, however, are still in their infancy and there remain numerous avenues for research to follow.

1.2.1 Structure

Carbon nanotubes may be described as quasi-one-dimensional structures due to their high length-to-thickness ratio. The CNT is essentially a rolled up sheet of graphene – a single layer of hexagonally arranged carbon atoms (depicted in Figure 1-1).The bonding of this sheet is strong as a result of the sp^2 bonding between atoms. A carbon nanotube may consist of a single layer of graphene, described as a ‚single-walled carbon nanotube' (SWNT), or many layers of graphene rolled up to form a ‚multi-walled carbon nanotube' (MWNT).

When a single sheet of graphene rolls up the resultant tube resembles a seamless cylinder as shown in Figure 1-2. If we imagine cutting the tube shown in Figure 1-2 along the dashed line and then unrolling it into the sheet form, the carbon atom (indicated by the blue dot) appears twice as a result of the seamless nature of the tube (as shown in Figure 1-3 - with the atom seen at (0, 0) and ‚again' at (8, 4)). When unrolled, the dashed line in Figure 1-2 becomes the ‚tube axis' (indicated by dashed lines in Figure 1-3). The vector which begins at first ‚image' of the carbon atom (i.e. the origin) and terminates at the second "image" is termed the ‚chiral vector', $\underline{\boldsymbol{R}}$, and is defined as $\underline{\boldsymbol{R}} = n\underline{\boldsymbol{a}}_1 + m\underline{\boldsymbol{a}}_2$, where $\underline{\boldsymbol{a}}_1$ and $\underline{\boldsymbol{a}}_2$ are the unit vectors as defined in Figure 1-3. The chiral vector shown in Figure 1-3 corresponds to $\underline{\boldsymbol{R}} = 8\,\underline{\boldsymbol{a}}_1 + 4\,\underline{\boldsymbol{a}}_2$.

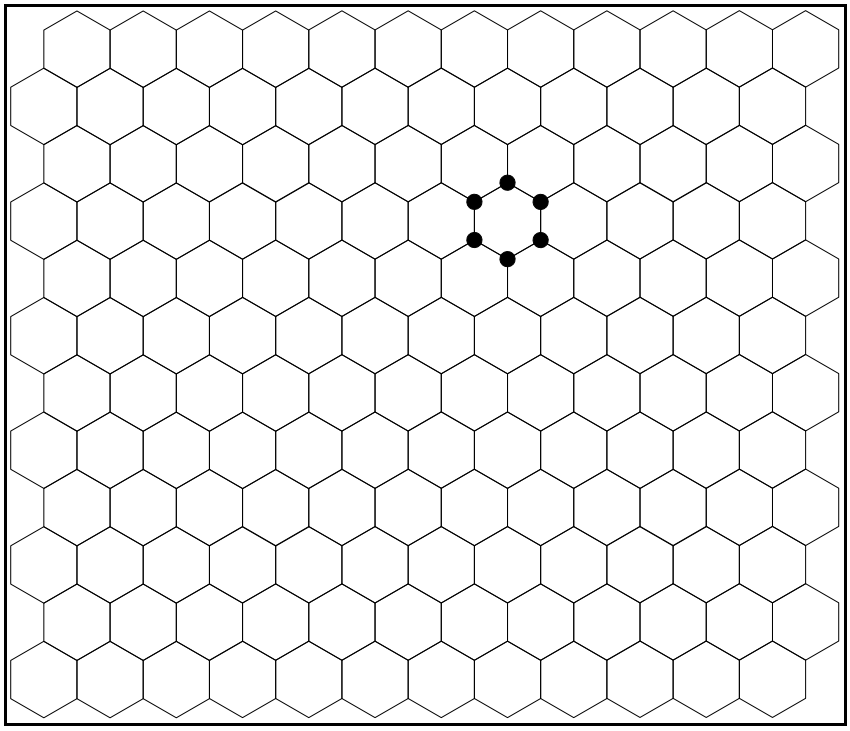

Figure 1-1: The hexagonal structure of graphene. A carbon atom lies at each of the vertices - as indicated by the dark dots.

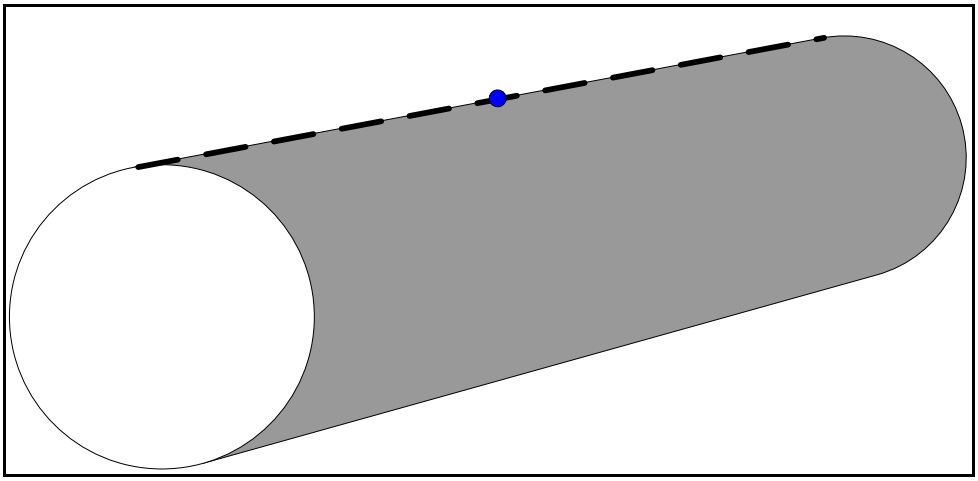

Figure 1-2: The cylinder-like structure of a carbon nanotube. The blue dot indicates a single carbon atom that may be found on the surface of the tube.

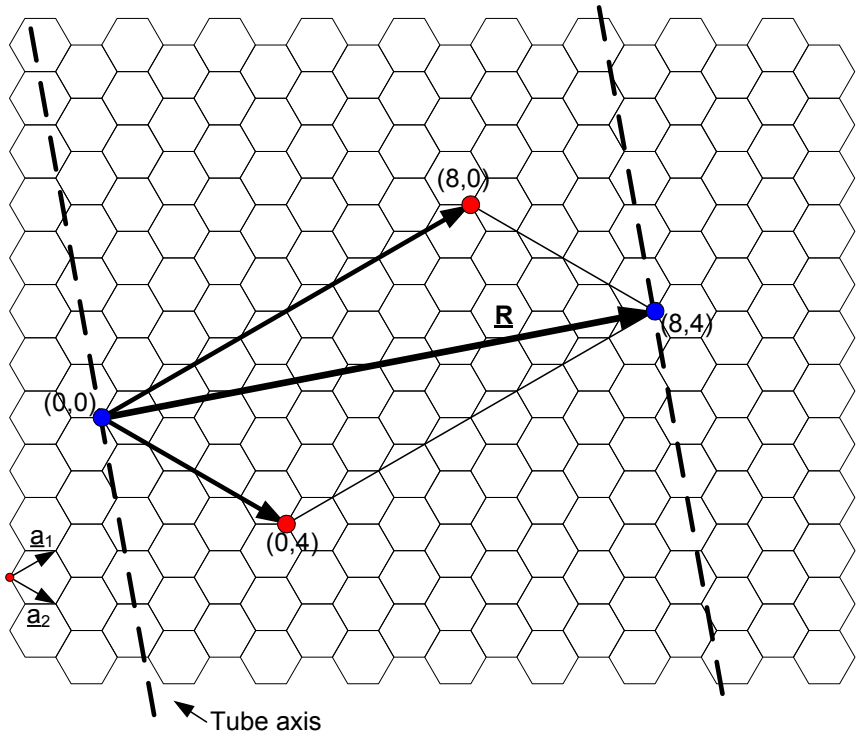

Figure 1-3: An 'unwrapped' carbon nanotube. The unit vectors and the chiral vector, R, are shown.

It is intuitive that $\underline{\boldsymbol{R}}$ lies perpendicular to the tube axis and that the length of $\underline{\boldsymbol{R}}$ is the tube diameter. In order to characterise a CNT, the manner which the graphene sheet rolls up - known as the „chirality' of the tube - must be identified. There are three types of chirality: „armchair', „zigzag' and „chiral' which are indicated in Figure 1-4 by $\underline{\boldsymbol{R}}_{armchair}$, $\underline{\boldsymbol{R}}_{zigzag}$, and $\underline{\boldsymbol{R}}_{chiral}$ respectively. It is the integer pair (*n, m*) that determines the chirality of the tube. When $m = n$, the chiral vector lies in the direction of the green line shown in Figure 1-4 and the resulting tube is called an „armchair' tube. When $m = 0$, the chiral vector - indicated by the red line in Figure 1-4 - is purely in the $\underline{\boldsymbol{a}}_1$ direction and the resulting tube is termed „zigzag'. For any other combination of *n* and *m*, the tube is called „chiral'. An example of the chiral vector corresponding to a chiral tube is the blue line in Figure 1-4 which begins at (0, 0) and terminates at (8, 4).

The wrapping angle, ϕ, is the angle between the chiral vector and the armchair direction (that is, the direction corresponding to $n = m$) and is defined as $0^\circ \leq \phi \leq 30^\circ$. θ is the angle between the chiral vector and the zigzag direction. As the angle between the zigzag and armchair directions is 30°; $\theta = 30° - \phi$.

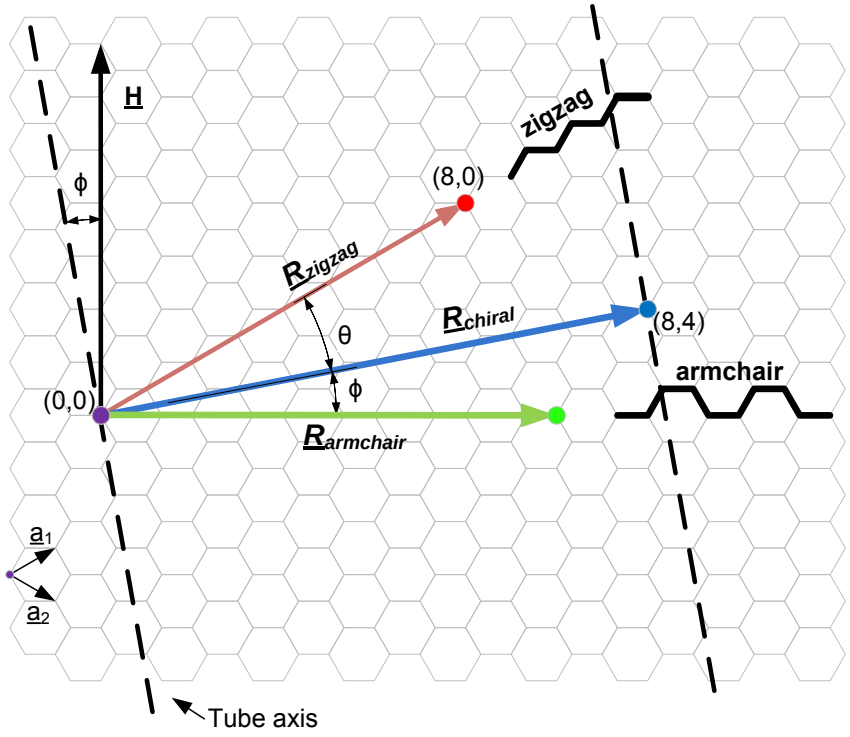

Figure 1-4: The chiralities of the carbon nanotube. The chirality is determined by the indices m and n of the vector R, which begins on a carbon atom and terminates on its 'replica'. The three types of wrapping – zigzag, armchair and chiral are shown.

The vector, ***H*** (indicated in Figure 1-4), lies perpendicular to the armchair direction and is used to identify the „nearest-neighbour' carbon hexagon rows [**14**]. The chirality and tube diameter are important because they determine many of the properties of the tube – such as whether individual tubes are conducting or semi-conducting. It has been observed that the armchair tubes are conductors, while the chiral and zigzag tubes being either conductors or semiconductors [**4**,**5**,**15**].

Occasionally, a carbon nanotube will be enclosed at one end by a hemispherical structure. This hemisphere is essentially „half' of either a C_{60} or C_{80} fullerene. Fullerenes may be described as a spherical arrangement of carbon atoms (unlike the tubular arrangement of the carbon nanotube). The carbon atoms that compose the fullerene do not always form hexagons, but a combination of hexagons and pentagons. The combination of hexagons and pentagons is essential to the formation of the spherical shape (and, in fact, resembles the manner in which old-fashioned football outer-layers were constructed). The structure of a C_{60} fullerene is shown in Figure 1-5.

The formation of the semi-fullerene cap is a result of the method of synthesis - and is not guaranteed to form on every nanotube. Figure 1-6 shows three tubes with the different charities and capped ends.

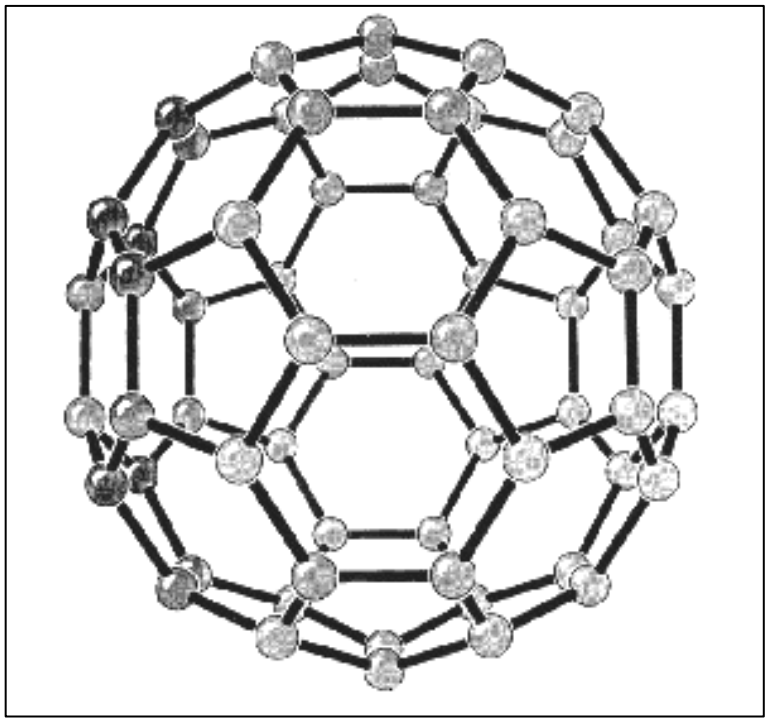

Figure 1-5: C60 Fullerene [16] Note the hexagonal and pentagonal arrangement of carbon atoms that make up the fullerene

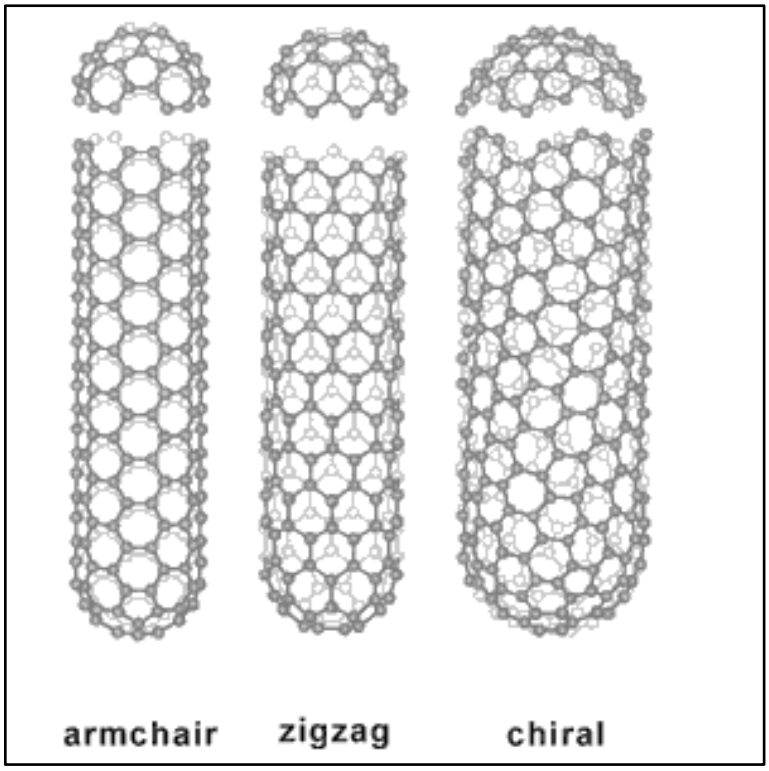

Figure 1-6: The fullerene caps on the ends of the carbon nanotube. The different chiralities are also shown [17].

1.2.2 Properties

It has been discovered that CNTs are semi-metals – occupying the space between a conductor and a semi-conductor – depending on the chirality of the tube. What is remarkable is that a CNT can change from conducting to semi-conducting with the addition or removal of just a few carbon atoms. All armchair tubes are conducting while chiral and zigzag tubes are either conductors or semi-conductors. When $n\text{-}m = 3l$ (where l is an integer) tubes are metallic while for all other cases the tubes are semi-conducting [**14**]. In addition to being a conductor or a semi-conductor, CNTs have also been shown to superconduct [**6**,**18**].

CNTs exhibit a high degree of flexibility and stiffness and, as such, have a high Young's modulus. Materials like silicon carbide have high Young's moduli (approximately 400 GPa). Due to the sp^2 bonding of the carbon atoms in a nanotube, the Young's modulus of a CNT is far greater. Indeed, Treacy *et al.* [**19**] found through their experiments that the Young's modulus for an individual MWNT lies between a minimum of 0.4 TPa (equal to that of silicon carbide) and a maximum of 4.15 TPa. These values, however, are anticipated to be an underestimate due to the difficulties in accurately determining the tube length.

Nanotubes also have a large tensile strength – approximately 22.2 GPa for an individual SWNT [**20**]. This value is about seven times larger than the tensile strength of boron and four times greater than the tensile strength of carbon fibres.

It has been observed that semiconducting SWNTs, when isolated from the metallic nanotubes, exhibit photoluminescence. The light emitted is in the near infra-red and the wavelength may be tuned by carefully selecting the diameter and chirality of the tube [**21**,**22**]. Field emission in CNTs has also been observed [**23**].

The list of properties above is by no means exhaustive, but merely touches the surface of the properties of these remarkable structures. A wide range of applications for these structures have been suggested based on properties that have already been experimentally verified; and there are even more applications mooted for properties that are predicted to exist. Some of these vary from the mundane to the fantastical. A few of these applications are now considered.

1.2.3 Possible applications

It has been suggested that bundles of CNTs could be used for hydrogen storage [**24**]. Early work revealed that the uptake of hydrogen is about 4.2% by weight and more than 75% of the adsorbed hydrogen may be released at room temperature [**25**]. It has also been found that the quantity of hydrogen stored may be increased to as much as 20% (by weight) by doping the

CNTs with lithium or potassium [**26**]. That CNTs are able to store and subsequently release hydrogen is a promising development for high-capacity but light-weight hydrogen fuel cells.

In addition to the adsorption of hydrogen, it has also been shown that open-ended CNTs, with diameters larger than 4 nm, may be filled with liquids by use of capillary forces. This has been shown by Ugarte *et al.* [**27**], who utilized a four-step procedure to fill CNTs with liquid silver nitrate.

A research group at Delft University of Technology in The Netherlands fabricated a field effect transistor (FET), using a single carbon nanotube and two metal electrodes. In their calculations, the group estimate that the maximum switching speed of a carbon nanotube FET could be as high as 10 THz [**28**]. In addition to the potential for incredible switching speeds, it is anticipated that FETs based on CNTs will also consume far less power than their silicon counterparts despite populating integrated circuits far more densely than silicon based devices [**29**].

In 2000, Rueckes *et al.* [**30**] developed a conceptual charge storage device which would act as a non-volatile electromechanical random access memory (RAM) module. Their concept utilises CNTs laid out to form a grid. It is the intersection of the tubes that are the „elements' of this memory. The manipulation of electrostatic forces is used to switch device elements between the ON and OFF states (that is, the tubes either touch or not) at a potential frequency greater than 100 GHz. Not only would this device have great speeds, but it would also have an incredible density – estimated to be approximately 10^{12} elements/cm^2.

Recently, a Finnish group [**31**] developed a different version of nanotube-based memory, where a charge is stored in a single nanotube based on current flowing through the tube. This version has a write/erase time in the region of 100 ns, but is restricted by the short-term storage of the charge (about 42 hours).

As has already been discussed, CNTs are photoluminescent and the emitted wavelengths may be tuned by careful control of CNT diameter. This has raised the possibility of manufacturing thin display panels. Indeed, a flat panel display was demonstrated as early as 2000 using the field emission properties of CNTs [**32**].

Carbon nanotubes are now utilised in the manufacture of some sporting goods, like bicycle frames, golf clubs, tennis racquets and tennis balls to improve balance and mechanical strength. [**33**]. CNTs may be spun into thread and imbedded into composites and then utilised in the manufacture of protective military gear, as demonstrated by a group at Cambridge University in 2007 [**34**]. The performance of the protective gear made from the nanotube threads by this

group is already comparable to the performance of the high-strength, bullet-resistant fibre Kevlar.

There are a myriad of current and potential applications for carbon nanotubes. Even more applications are suggested as more is learnt about the properties. We have looked both at applications that are ready for commercial exploitation and applications that require varying levels of refinement before they are market ready. It is now natural to analyse the processes used to create these remarkable carbon nanostructures.

1.3 Synthesis methods

As revealed in the review of properties and applications, there is tremendous potential for carbon nanostructures, but in order to exploit this potential, there is a need for suitable, low-cost and large scale production of these structures. Currently, there exist numerous techniques to produce various nanostructures and each technique has different results in terms of quality, yield and even the properties of the resultant structures. Each of these techniques is, however, merely a variant of one of three elementary techniques: arc discharge, laser ablation and chemical vapour deposition.

The initial choice of technique is important as each has its own benefit in terms of cost, simplicity, and the type of nanostructure(s) produced. Arc discharge at first appears to be the simplest technique. It produces the best quality CNTs, but at low yields (typically about 30% by weight of source material) [**13**]. The technique itself is also difficult to scale up for industrial-scale production of CNTs. On the other hand, a CVD process produces a copious quantity of CNTs and other nanostructures and allows for industrial-scale production, but suffers from poorer quality CNTs. Laser ablation produces high quality SWNTs at high yields. Laser ablation, however has low growth rates and is difficult to scale up for industrial production. The advantages and disadvantages of each of these techniques pose the question to researchers: „Which is the best technique to produce the nanostructures required for the task at hand?'

There may often be the situation where high quality CNTs are required at high yields and cost is irrelevant – in such situation laser ablation would be the method of choice. In another situation high yield may be required, but the purity of nanostructure is irrelevant – in this scenario arc discharge or chemical vapour deposition would be ideal. In order to understand the compromises required when embarking on carbon nanostructure synthesis, a closer look at the techniques follow.

1.3.1 Arc Discharge

In the arc discharge method, a large current (typically between 50 and 100 A at a voltage between 10 and 20 V, either AC or DC [**35**]) is made to arc between two electrodes located a short distance from each other (this gap is usually approximately 1 mm). Due to the high temperatures during the arcing process, carbon sublimes and then reforms on the cathode (the reformation resembles carbonaceous „soot') and the anode is depleted. It is in this soot that the carbon nanostructures are found. The arc discharge method is, in fact, the method used by Iijima [**3**] in his work which sparked the widespread interest in carbon nanotubes. Typically, the electrodes would be made from high purity graphite, but a recent trend has seen work with electrodes manufactured from more impure sources, like coal [**36**]. MWNTs are formed when the two electrodes are made only from a carbon source, but SWNTs can be preferentially produced by adding a metal to the anode as a catalyst [**7**]. Another consideration in the arc discharge method is the atmosphere in which the process occurs. Typically the process will take place in an inert atmosphere such argon or helium. The pressure of the inert atmosphere, typically between 100-700 Torr, has an effect on the nanostructure yield. The basic arc discharge setup is shown in Figure 1-7.

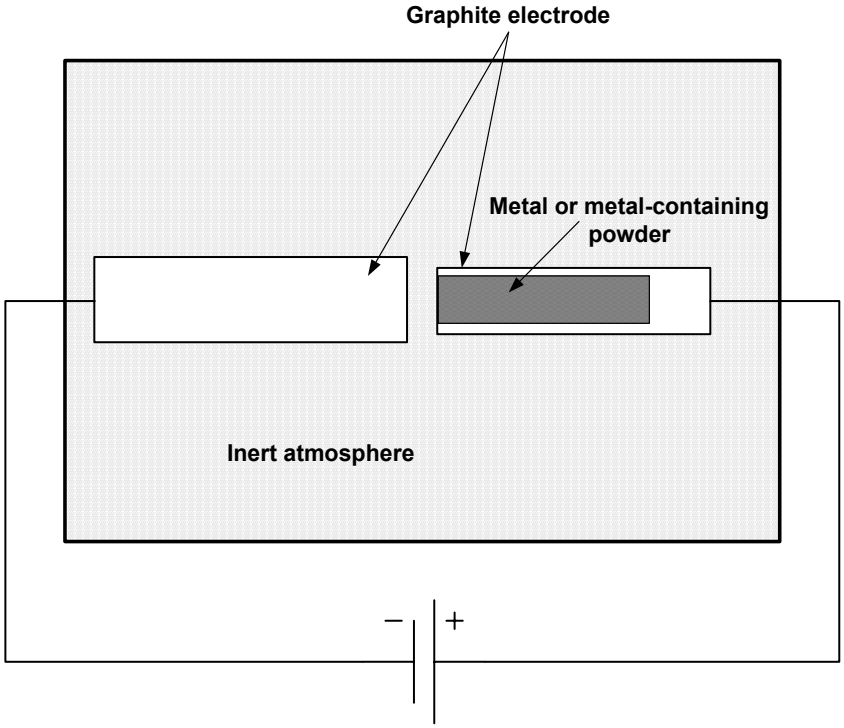

Figure 1-7: Setup of a basic arc discharge method.

1.3.1.1 Catalyst

A metallic catalyst may be added to the anode to promote the growth of SWNTs. This may be done by either placing a piece of metal in a ‚dimple' created on the anode or by packing a powder comprising metal and graphite into a hole drilled through the electrode, as seen in Figure 1-7. Cobalt, nickel, molybdenum and iron are typically used for SWNT production [**37**]. Other metals, and combination of metals – such as NiY, NiCo, FeNi and PtRh **[38-41]** have also been found to produce SWNTs via this method. MWNTs, fullerenes, amorphous carbon and other nanostructures may still be found in the soot which collects on the cathode.

1.3.1.2 Temperature

The temperature of the arc discharge method, in the neighbourhood of the electrodes where the localised plasma forms, is around 4000 K [**42**]. This leads to a situation where a large temperature difference exists between the plasma and the chamber wherein the reaction occurs. This large temperature gradient results in an uneven CNT distribution within the reaction chamber; with the bulk of the CNT growth occurring around the cathode and a small quantity collecting around the chamber walls. The large temperature gradient also accounts for the formation of a variety of nanostructures.

To investigate the effect of the temperature of the environment, Zhao and Liu [**43**] used a temperature-controlled chamber to vary the ambient temperature between 25 °C and 900 °C. The results of their work was telling: by increasing the ambient temperature from 25 °C to 300 °C the CNT yield increased from 25.9 g/h to 33.2 g/h; with purity increasing from 20% to 30%. Increasing the chamber temperature even further to 600 °C resulted in the yield and purity increasing to 64.7 g/h and 70%, respectively. Further increases in temperature to 700 °C led to a decrease in both yield and purity. It was thus determined that the optimal chamber temperature for the process was 600 °C. Additionally, it was found that as the temperature increased from 25 °C to 600 °C, the diameters of SWNT bundles decreased – from 10-50 mm at 25 °C to between 7-20 nm at 600 °C. Zhao and Liu [**43**] postulated that "The environmental temperatures preheat the catalyst, which leads to the shorten of the time for catalyst to activate and accelerates the growth of carbon nanotubes. When the temperature is 700 °C or higher, the yield decreased, which may be explained by the thermal decomposition of SWNTs or a decrease of catalytic activity".

Nishio *et al.* [**44**] determined that the highest yield occurred at the highest arc-plasma temperatures – around 6000 K for their work. Colbert *et al.*, [**45**] however, report that sintering of the CNTs occurred when the electrode itself became too hot. If the temperature was high

enough, then the sintering could result in the reflectivity of the sintered tubes resembling that of graphite. By water-cooling the electrodes, they were able to reduce the sintering of the CNTs and eliminate the production of the ‚graphite-like' product.

1.3.1.3 Atmosphere

The atmosphere wherein the process occurs plays an important role in the production of carbon nanostructures via the arc discharge method. Typically, the process will occur under a helium or argon atmosphere, but hydrogen and methane have also been successfully used [**46**,**47**]. When the arc discharge method occurs in a gaseous atmosphere, it has been determined that helium is more effective than argon for the growth of fullerenes [**8**]. It was later determined by Hinkov *et al.* [**48**] that the same applies for CNTs. Specifically, Hinkov *et al.* observed (through the development of a model and measurement) that (i) helium is more efficient than argon in the production of nanotubes and fullerenes and (ii) that fullerenes are preferentially formed at higher pressures (of either gas). Figure 1-8 shows the plot of nanotube growth rate versus argon and helium pressure obtained from their calculations. It is quite clear that the expected CNT growth is far higher for helium than for argon.

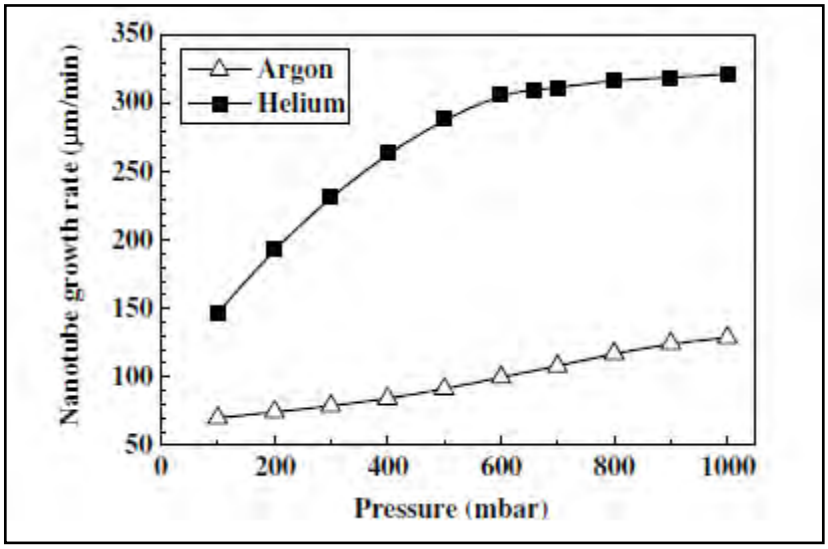

Figure 1-8: Nanotube growth rate versus pressure calculated for helium and argon. I = 100 A [48**].**

The arc discharge method has also been conducted in a liquid environment such as water or liquid N_2. Water or liquid N_2 not only acts as the atmosphere, but also serves to cool the electrode preventing sintering of the product and eliminates the need for the pressure regulators and related equipment needed for argon or helium. In addition to the production of CNTs, other nanostructures, such as onion-like structures, may be produced in the liquid environment [**9**]. Ishigami *et al.* [**49**] claimed that their liquid N_2 technique could be scaled-up to provide

continuous production of high quality MWNTs – all that is required is a constant liquid N_2 supply and a continuous feed of a graphite cathode. Another group reported a yield of up to 70% MWNT in a liquid N_2 atmosphere [**50**].

The drawback of the liquid nitrogen atmosphere, however, is the cost related to liquid nitrogen itself. Water, therefore, provides an interesting avenue of exploration. CNTs have been produced in water [**51**], but they are of low purity and are produced at slow rates (approximately 7 mg/min). It was also discovered that the production time had to be limited to approximately 2 minutes because the water began to etch the nanotubes – this compares unfavourably to the continuous method proposed by Ishigami *et al.* [**49**].

1.3.1.4 Growth mechanisms

1.3.1.4(a) Vapour-phase growth model

The vapour-phase growth model is based on the assumption that the nucleation and growth of carbon nanotubes and other carbon nanostructures occurs as a result of carbon vapour (which is produced due to the high plasma temperatures produced during arcing) condensing [**52**]. In their analysis of the arcing process, Gamalay *et al.* [**53**] found that, during the discharge process, there is a layer of carbon „vapour' which forms near the surface of the cathode. This layer, which is suitable for the growth of the various nanostructures, contains two groups of carbon particles with differing velocity distributions. One group, consisting of carbon evaporated from the cathode, has a temperature-dependant, isotropic distribution (dictated by the temperature of the inter-electrode plasma). The other group consists of ions being unidirectionally accelerated. The „competing velocities' are thought to be the mechanism behind the nanostructure growth.

As the arc discharge begins, the „isotropic group' dominates, resulting in the formation of asymmetric 3-D nanostructures. As the arcing continues the „directed ions' begin to increase, resulting in the formation of open-ended structures. These open-ended structures are effectively the seeds for CNT growth. As the arcing process continues and stabilises, carbon ions collide with the cathode and these collisions result in the formation of CNTs in a particular direction. Eventually, instabilities in the arcing process will begin and this leads to the formation of caps at the end of the structures and thus terminates growth [**53**].

A different version of the vapour-phase growth has been proposed by Louchev [**54**]. In this model, Louchev suggests that the growth of the tubular structures occurs due to the surface diffusion of carbon atoms (which had been adsorbed on the surface of the growing structure) towards the open ends.

1.3.1.4(b) Liquid-phase growth model

de Heer *et al.* [**55**] observed that MWNTs grown in the arc discharge method appeared as though they had "been dipped in a viscous liquid' and that there were beads present in their sample. One can see from the TEM micrograph (Figure 1-9), that the tube seems to be „threaded through' the bead – like a necklace. The bead was found to have a density very similar to that of liquid carbon (1.4 g/cm^3 compared to 1.5 g/cm^3). In addition, a meniscus is seen at the bead-tube interface. This evidence leads to the conclusion that the beads are formed as a result of a previous liquid phase, and that the formation of the „hardened' beads is similar to the manner in which glass solidifies from its molten state. de Heer *et al.* explain that, during the arcing process, the anode is locally heated by the electrons from the cathode. This area of the anode is liquefied as a result of the heating and liquid carbon is ejected from the anode. Due to the high vapour pressure of the liquid carbon, the globule's surface cools quickly far quicker that the core of the globule does. The disparity in the cooling rates leads to the liquid carbon beginning to supercool. Carbon nanostructures are believed to nucleate, and then grow, within these supercooled cores [**55**].

1.3.1.4(c) Solid-phase growth model

The solid-phase growth model was suggested by Harris *et al.* [**56**]. Once fullerenes - which were grown via the arc-discharge method - were removed, the soot which remained was heated to 3000 °C. When analysed, it was observed that carbon „nanocones' and tubular structures were grown. This led that group to conclude that, during the arc discharge, fullerenes and fullerene-like structures will first form. These structures are subsequently subjected to the intense temperatures of the discharge process. The structures then begin to form seeds from which the nanotubes will begin to grow. Growth will continue until there is insufficient carbon to continue or the arcing process is terminated.

1.3.1.5 Summary

The arc discharge method remains an attractive, and relevant, option for nanostructure synthesis due to its simplicity and the availability of a wide range of input parameters in addition to producing the most graphitised tubes. The current density, the size and shape of the electrodes may be varied – either independently or even in tandem. That there exists a large „state space' means that there is still the possibility that yield, purity and continuity of the method may be improved sufficiently to make arc discharge the foremost option for industrial-scale synthesis.

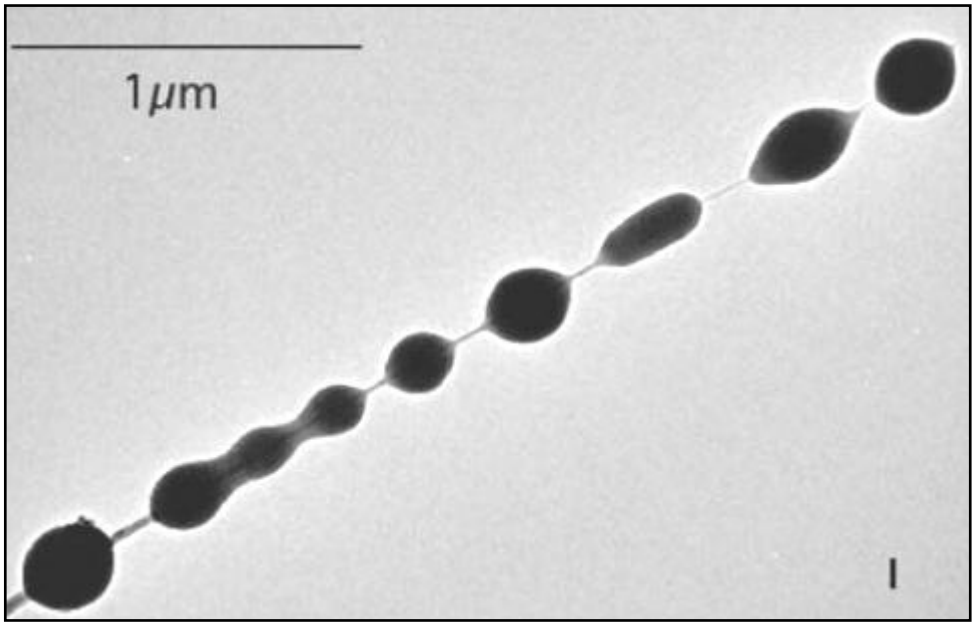

Figure 1-9: Carbon nanotube with the 'beads' which form in the arc discharge method [55**].**

1.3.2 Laser Ablation

The laser ablation method is primarily used for the production of SWNT, although there have been reports of the production of MWNTs [**57**] and other nanostructures via this method [**57**,**58**]. A laser is directed at a metal-doped carbon target, which is then locally vapourised. It is in this vapourisation process that the SWNTs form. The laser may be either continuous [**59**], pulsed [**58**] or „dual-pulsed' [**60**]; and is typically a Nd:YAG laser (although other types like an XeCl laser have also been used [**61**]). The entire process usually occurs in an inert atmosphere within a furnace. The process is schematically depicted in Figure 1-10.

Early work by Guo *et al.* [**58**] showed that the nanotube yield increases with an increase in furnace temperature (up to the limit of their furnace – 1200 °C) ; and that changing from a „single-metal' catalyst to a bimetal catalyst increases yields by up to 100 times (yield has been estimated at about 50%). The SWNTs produced by laser ablation appear to be „cleaner' than the SWNTs produced via arc discharge. Usually SWNTs produced by arc discharge will be coated with a layer of amorphous carbon, but there is less coating observed on tubes produced by laser ablation [**58**].

SWNTs produced by laser ablation occasionally organise themselves into a rope-like structure, consisting of a few hundred tubes. This occurs because of van der Waals force experienced between tubes [**60**].

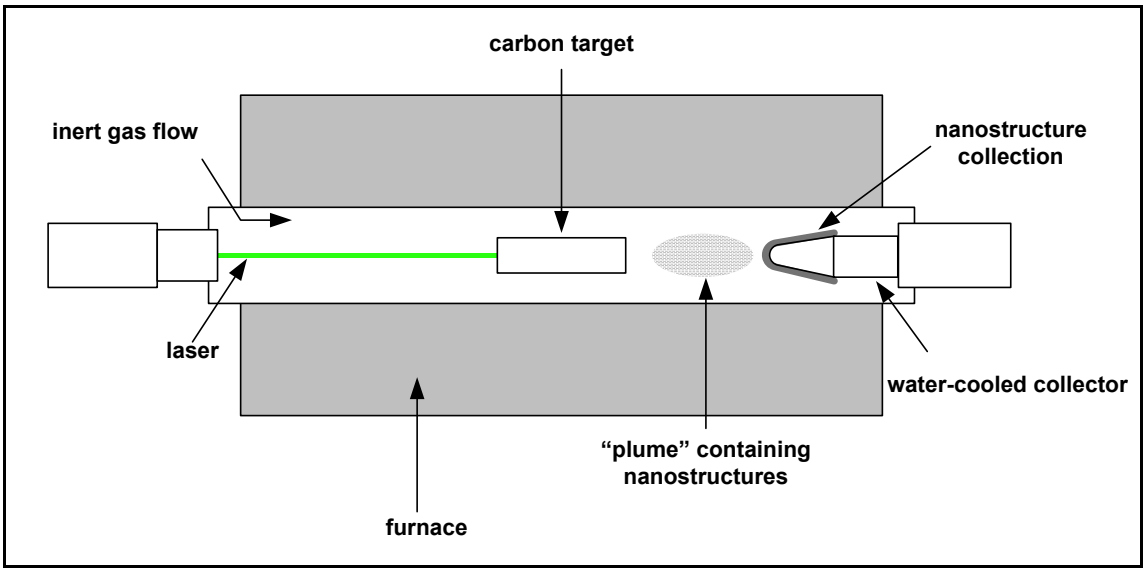

Figure 1-10: Schematic of the laser ablation method utilised for SWNT synthesis.

1.3.2.1 Effects of temperature

As mentioned earlier, SWNT yields could be increased by increasing the furnace temperature [**58**]. Under similar conditions, it has been observed that increasing the furnace temperature above 1350 °C results in a decrease in yield with the Co-Ni catalyst [**62**]. When the catalytic source is changed from Co-Ni to Rh-Pt, the yields continue to increase even at temperatures greater than 1350 °C. It is thought that the growth of SWNTs is suppressed once the furnace temperature has increased past the eutectic point of the alloyed catalyst [**62**].

1.3.2.2 Effect of gas environment

Kataura *et al.* [**62**] observed that, under typical laser ablation conditions (i.e. the process occurs with a heated furnace and in an argon atmosphere at 500 Torr), lower argon flow rates produce SWNTs of smaller diameter. Muñoz *et al.* [**59**] investigated the effect of varying the conditions of the atmosphere wherein the process occurs and found that argon and nitrogen provide a suitable atmosphere between 200 and 400 Torr. Furthermore they found that helium produced a minimal quantity of SWNTs. The Muñoz group attribute the poor SWNT growth to the low mass of the gas and the subsequent larger cooling rates and temperature gradient. Argon and nitrogen also have a poorer SWNT growth at pressures outside the 200-400 Torr boundary – and this is also attributed to an accelerated cooling rate [**59**].

1.3.2.3 Summary

Laser ablation is suitable for high-yield, high-purity production of CNTs but is no longer seen as a viable option for up-scaling for industrial-level production of CNTs because of the high cost associated with the required apparatus. In addition, while yields may be good (up to about 70%) the actual growth rate is poor (around 1g/day [**63**] compared with 25.9g/hr in arc discharge [**43**]). The growth mechanisms of the arc discharge and laser ablation methods are thought to be similar and have been presented earlier.

1.3.3 Chemical Vapour Deposition

The basic Chemical Vapour Deposition (CVD) method, occasionally referred to as „thermal decomposition' involves the application of energy to dissociate a gas[1] into its constituent atoms. These atoms may then combine with atoms from other gases (this depends, of course, on the desired product) and then nucleate onto a substrate located within the system. The CVD process is perhaps the simplest of all the carbon nanostructure production methods to upscale and, as such, presents an exciting avenue for researchers of carbon nanostructure production. In addition to the „easy upscaling', there are also numerous parameters (such as input gas, the introduction of catalysts, process pressure, etc) that may be varied in order to modify desired properties of the resultant structures.

The CVD process typically occurs within a chamber, such as a vacuum furnace or within an enclosed quartz tube (a number of groups utilise a quartz tube within a vacuum furnace) **[10, 64-66]**. A carbon-carrying gas, such as vapourised ethanol, toluene or carbon monoxide is introduced into the chamber where it is energised (by the application of a large quantity of heat or by plasma) until it dissociates. This dissociation occurs in the presence of a substrate and a catalyst and, if the conditions are suitable, the carbon atoms nucleate on the substrate surface and begin to form the carbon nanostructure.

The CVD method is very flexible, with a great degree of control of the input parameters available to researchers. As briefly mentioned earlier, the carbon carrying precursor, the catalyst and process pressure (to name just a few of the parameters), may be varied (either individually or all at once) and this, in turn, allows the purity, yield and morphology of the resultant structure to be controlled. Indeed, the degree of control extends as far as being able to grow the carbon nanostructures in a predetermined pattern by careful catalytic-doping of the substrate. In addition to the large degree of control, the CVD method allows for the use of cheap, abundant,

[1] Liquids may also be used, but they are usually introduced into the system as a mist or by evaporation of the source.

yet highly pure carbon precursors like ethanol. It is for these reasons that the CVD method quickly became the most frequently cited technique for the production of carbon nanostructures.

There are, inevitably, a number of variants of the CVD process as a result of the endless combinations of input parameters, but all maintain the basic concept outlined above. We will now study these process parameters in greater detail.

1.3.3.1 Growth mechanisms

In the CVD method, once the carbon-carrying precursor has been dissociated into its constituent atoms by the application of energy, the carbon atoms adsorbs onto a nano-sized metallic catalyst. The adsorbed carbon then diffuses through the catalyst and, subsequently, a carbon nanostructure (CNTs, onion-like structures or beaded nanotubes) precipitate out of the catalyst **[11, 67-70].** The role of the catalyst here is rather important as it not only decomposes carbon compounds, but also forms metastable metal-carbides and facilitates the diffusion of carbon into and over the carbides [**67**]. Carbon nanostructures always grow out of the catalytic particles and, depending on the strength of the bond between the nano-sized catalyst and the substrate, the metal particle will either (a) remain rooted to the substrate and the carbon nanostructure grows out of it in what is known as the „base-growth' or „root-growth' mechanism or (b) break its bond with the substrate and move upward as the carbon nanostructure grows in what is known as the „tip-growth' mechanism **[68, 70-72].** Both of these growth mechanisms are illustrated in Figure 1-11.

As the growth of the carbon nanostructure occurs from the metallic catalyst, it is logical to assume that the size of the catalytic particle would have an effect on the size of the resultant carbon nanostructure. This assumption, which has its foundation on the growth mechanism outlined above, has been modelled or verified experimentally by various groups [**67**,**73**,**74**].

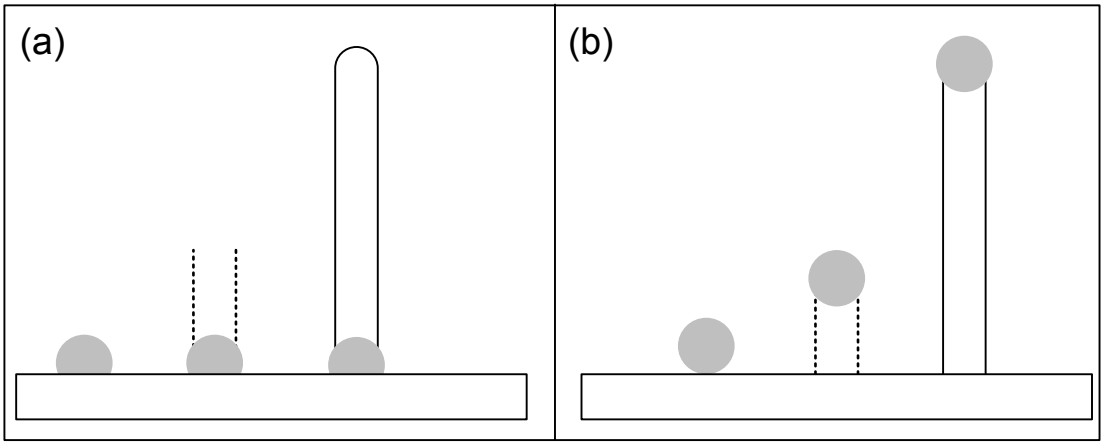

Figure 1-11: Two growth mechanisms for carbon nanotubes. (a) is the base or root growth mechanism, (b) is the tip-growth mechanism. Whether root or tip-growth occurs is a result of the strength of the bond between the catalyst particle and the substrate.

1.3.3.2 Precursor

Unlike the laser ablation and arc discharge method, where only a few carbon sources have been used for the growth of carbon nanostructures, the CVD method has seen a multitude of carbon precursors used.

Sources such as hexafluoroethane (C_2F_6) or tetrafluoroethylene (C_2F_4) [**75**], produce two-dimensional structures termed "carbon nanowalls" which stand vertically from the substrate.

Carbon monoxide (CO) has been utilised in a thermal CVD method, along with iron pentacarbonyl ($Fe(CO)_5$) [**76**]. Here, iron pentacorbonyl is thermally decomposed into iron clusters which form nucleation points for the growth of carbon nanotubes. Carbon is produced through the Boudouard reaction (that is, $CO + CO \rightarrow C_{(solid)} + CO_2$). Highly pure SWNTs with diameters between 0.7 nm and 2.4 nm were grown via this method, with weight yield near 40%. The authors, Nikolaev *et al.*, did note, however, that the thermal decomposition of hydrocarbons is far quicker than the disproportionation of CO at the same pressure; this results in greater yield for hydrocarbon-based CVD processes.

Camphor ($C_{10}H_{16}O$), was found to produce carbon nanotubes – aligned perpendicular to the substrate surface, at low yield (25% by weight), but with negligible formation of amorphous carbon – with purity around 90% [**77**,**78**]. Other carbon sources, such as coal-gas [**79**], dichloromethane (CH_2Cl_2) [**80**], iron carbonyl [**81**] and tetraethoxysilane ($Si(OC_2H_5)_4$) [**82**] have been utilised to grow carbon nanotubes in a variety of CVD methods.

Hydrocarbons are, however, the most commonly used precursors. Indeed, ethanol (C_2H_6O) [**64**,**68**,**83**], xylene (C_8H_{10}) [**69**,**70**], toluene (C_7H_8) [**72**,**73**], hexane (C_6H_{14}) [**84**], methane (CH_4)

[**11**,**85**,**86**], turpentine ($C_{10}H_{16}$) [**87**] and acetylene (C_2H_2) [**71**,**88**] have all been successfully used to grow CNTs and related structures.

In their work on CNT production, Smiljanic *et al.* suggested that hydrocarbons with higher hydrogen to carbon ratio appear to yield better results – with ethylene (C_2H_4) and methane (CH_4) performing better than acetylene (C_2H_2) [**89**].

It is noteworthy that ethanol is not a pure hydrocarbon because of the oxygen component. Murayama *et al.* found that the performance of ethanol and methanol (CH_3O) is somewhat superior to the performance of pure hydrocarbons; this was explained by the oxygen component, or more specifically the OH radical, attacking „nearby carbon atoms with a dangling bond to form CO'. This process then halts the formation of unwanted amorphous carbon at an early stage [**90**]. A similar effect is suggested to be observed in the production of nanotubes by the thermal decomposition of camphor [**77**].

1.3.3.3 Catalysts

Similar to the arc discharge and laser ablation methods, the CVD method utilises metallic catalysts to promote the growth of carbon nanostructures (especially carbon nanotubes). Catalysts may be introduced either on a substrate (supported catalyst) or in particle form in a stream of gas (floating catalyst).

Nanoscale iron particles deposited on a substrate are typically used as catalysts [**11**,**70**,**74**,**85**,**88**]. Other metals, such as nickel and cobalt may also be used [**68**,**73**,**91**]. In the case of a supported catalyst method, there is a great deal of pre-processing that occurs before the substrate is ready for use. „Doping' of the substrate with a catalyst may be done in a number of methods: the substrate may be dipped in an aqueous solution containing the catalyst [**66**,**68**], nano-sized catalysts may be embedded into a porous substrate [**88**], or a pre-deposited catalyst may be exposed on a substrate in a pre-determined pattern by lithography [**86**,**92**]. It is also possible introduce the catalyst as an electrode [**93**].

It is possible to introduce the catalyst without a substrate. This could be done by injecting the catalyst as a solid into the reaction chamber, or by introducing both the precursor and the catalyst as a single stream – as is often the case with ferrocene ($C_{10}H_{10}Fe$) [**69**,**70**,**83**,**84**,**89**].

The choice of the type and size of catalyst is, of course, very crucial to the process (recall that carbon first diffuses through the catalyst and then precipitates into the nanostructure; and that the catalyst determines the diameter of the grown nanostructure). It is for this reason that a lot of research of the CVD method focuses on the selection of catalyst and methods to selectively

pattern catalytic sites for *in situ* growth of nanotubes for commercial uses such as the field emission display proposed by Ago *et al.* [**94**].

1.3.3.4 Gas

Usually the CVD process has to be supported by the introduction of a gas into the system. Argon is one of the common support gases [**66**,**70**]. However, hydrogen is the most utilised gas of all. Hydrogen may be explicitly added as a support gas [**65**,**86**], or included as part of the chemistry of the precursor [**89**]. Indeed, it appears that hydrogen actually has quite a pronounced effect on the CVD growth of carbon nanostructures - with some CNT production processes being completely unsuccessful without the addition of hydrogen [**83**].

Li *et al.* [**83**] reported that a high hydrogen flow rate suppressed the formation of carbon, but the removal of hydrogen altogether resulted in the formation of particulate carbon instead of nanotubes. Li *et al.* also state that SWNTs may be preferentially grown, rather than MWNTs, by increasing the hydrogen flow rate. A similar trend is by Zheng *et al.* [**65**]. In their work, Zheng *et al.* combined hydrogen with carbon monoxide as a precursor for the growth of CNTs. They found that there was little or no nanotube growth when carbon monoxide was used alone, and that the highest SWNT yield was obtained between 35% and 65% of hydrogen in the H_2-CO mixture. They propose two interpretations for this effect in the CO-H_2 system. Firstly, the carbon deposition is accelerated by the hydrogenation of CO (through the reaction $CO + H_2 = C + H_2O$). The second interpretation is that the adsorption of H_2 on the catalyst surface catalyses the disproportionation of CO (through the reaction $2CO = C + CO_2$). These interpretations are also proposed by Kim *et al.* [**86**] who state that the flow of the precursor and hydrogen enables the continuous feeding of carbon for the growth of tubes whilst preventing the catalyst from being ‚poisoned' by amorphous carbon and that hydrogen sustains the growth of nanotubes. Endo *et al.* [**69**] who favour the first interpretation with the claim that "Hydrogen scavenges for oxygen and prevents the loss of carbon to carbon dioxide".

Regardless of the exact mechanism through which hydrogen affects the production of nanotubes, the effect is clear to see. There exists an ideal ratio of hydrogen-to-carbon for the grown of carbon nanotubes. Too little hydrogen will result in the formation of no nanotubes. Too much hydrogen will suppress nanotube growth.

1.3.3.5 Promoters

A promoter is typically added to the precursor in order to modify the structure of the grown nano-product. Sulphur, bismuth and lead have been used as promoters [**95**]. The nature of the promoter is rather different from the catalyst in that it does not provide nucleation sites for the

growth of nanostructures - even in the case of metals like bismuth. The promoter, rather, improves the yield of the carbon nanostructure and increases the diameters of carbon nanotubes, often resulting in the formation of double-walled nanotubes [**96**]. The promoter stabilises the intermediate species during nucleation and that sulphur promotes the growth of large carbon clusters which eliminate dangling bonds and extend the carbon lifetime [**95**].

Thiophene (C_4H_4S) is commonly used as a promoter [**70**,**71**,**73**,**84**], but may also be added to the CVD process as a precursor as a result of the carbon content. It has been observed that the sulphur content of thiophene results in the growth of SWNTs and the removal of amorphous carbon. A further increase in sulphur content, however, results in the growth of MWNTs [**97**]. Any further increase in the sulphur content results in the destruction of the catalytic effect of metals present in the system [**98**], suppressing the growth of carbon nanotubes. The trend is thus to add only a small quantity of sulphur or thiophene to the system.

1.3.3.6 Effect of temperature

As mentioned in the discussion on the laser ablation and arc discharge methods, the temperature at which carbon nanotubes are grown plays an important role in the quality of the structure. Due to the crystalline nature of carbon nanostructures, it is expected that the same also applies to the CVD process. The attraction of the CVD process is the possibility of decreasing the growth temperature of the reaction to the point where nanotubes may be grown *in situ* for certain commercial applications like field emission displays, especially if the CVD process utilises a plasma to dissociate the carbon precursor [**85**].

In their detailed analysis of the effect of temperature on the formation of carbon nanotubes, Li *et al.* [**99**] state that "NTs can not grow at either low (600 °C) or high (1050 °C) temperature". Further reading reveals, however, that it is not uncommon to see the successful growth of nanotubes outside of this range. Indeed, van Quy *et al.* [**84**] state that the precursor conditions could be optimal for one temperature but out of range for another. Further, Wang *et al.* [**85**] grew a variety of carbon nanostructures using a plasma-enhanced CVD (PECVD) method at a reaction temperature below 520 °C, while Smiljanic *et al.* [**89**] estimated that the growth of SWNTs in their plasma-enhanced CVD method occurred at a temperature in excess of 1300 K.

It has been observed that an increase in temperature leads to an increase in both the yield of nanotubes [**99**] and an increase in tube diameters [**72**,**89**,**99**], but this could come at the cost of the graphitisation of the tubes [**70**,**84**]. An increase in temperature will, in some experimental setups, change the structure of nanotubes grown from MWNT to SWNT. Li Y.-L. *et al.* [**83**] observed this change of structure when they went from synthesising MWNTs at a temperature

between 1100 °C and 1180 °C to synthesising SWNTs at 1200 °C in their work. Li W. *et al.* [**99**] reported that they achieved well-structured nanotubes at 700 °C, but bamboo-like tubes began to form at 750 °C. At 800 °C, bamboo-like tubes dominated the sample.

It is noted that nanotubes will usually only form at temperatures above 550 °C, with growth near this temperature characterised by low yields. An increase in temperature may result in increased yield but with a simultaneous increase in diameter. Elevated temperatures (beyond 1000 °C) will begin to suppress the growth of nanotubes and promote the growth of related structures. There are exceptions to this general trend and it is difficult to pinpoint the exact cause due to the disparity in process conditions from between different research groups. These variations may not just be due to temperature, but also the nature of the energy source, the type of precursor, catalyst and support gases. What is definite is, for a given process, a change in temperature does play a vital role in determining the morphology of the carbon structures formed.

1.3.3.7 Variants of the method

There exist many variants of the CVD method, separated by process parameters. The two major methods are thermal CVD - where the reagents are dissociated by the application of high temperatures, and PECVD - where energy is used to generate plasma which is responsible for the dissociation of the reagents. Each of these methods are then further differentiated by certain characteristics, such as pressure (for example atmospheric pressure thermal CVD or low-pressure CVD), and the method of introducing the reagents into the system (such as aerosol assisted CVD or direct liquid injection CVD). A general representation of both the thermal and the plasma-enhanced CVD methods are presented in Figure 1-12.

Thermal CVD is relatively straightforward compared to PECVD, and the actual application only occasionally varies from that shown in Figure 1-12. Plasma-enhanced CVD, however, differs in that there are numerous methods to generate the plasma. The remainder of this section is therefore devoted to the discussion of the PECVD method.

In the PECVD method, the plasma may be generated by any energy produced by a number of sources, including hot-filament [**100**], DC discharge [**101**], microwave radiation **[102-104]**, inductively coupled RF [**105**] or capacitively coupled RF [**66**,**75**]. One of the noteworthy aspects of plasma-enhancement is that the reaction temperatures may be lowered significantly – even compared to thermal CVD [**105**].

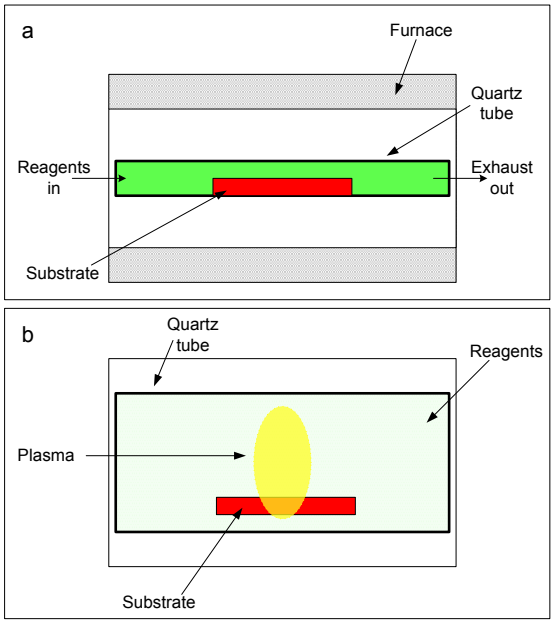

Figure 1-12: Illustrations of the two major types of CVD processes. (a) is the thermal CVD process, where the reagents are subjected to high temperatures within a furnace. (b) shows a plasma-enhanced CVD process, where the reagents are exposed to a plasma.

PECVD has also shown remarkable capacity to grow CNTs in alignment, something which is particularly useful for the development of nanotube-based field emissive devices [**106**]. The alignment of the nanotubes is a result of the electric field that the growing tubes are exposed to [**105**]. Aligned tubes may also be grown in the thermal CVD method if the tubes are exposed to an electric field [**107**]. The electric field that the growing structures are subject to is a result of the electrical self-bias field on the substrate surface as a result of the plasma [**108**]. A micrograph of such aligned growth in a microwave PECVD method is presented in Figure 1-13.

Of further interest in the work by the Bower group [**108**], was the effect that the plasma had on the tubes themselves. They found that, when subjected to the plasma, the tubes would grow straight (which also assisted in the alignment). However, when the plasma was stopped and the process changed into a thermal CVD process, the tubes began to „curl'. The growth rate, in terms of length of the tubes, slowed from approximately 100 nm/s to approximately 150 nm/min. This curling effect occurred towards the bottom of the CNTs, which suggest a base-growth for this process. This curling effect was interpreted as confirmation that the alignment was an effect of the plasma. Had the alignment been a result of van der Waals force experienced between the tubes then the alignment and „straight-tube' growth would have continued once the plasma was discontinued [**108**]. The „straight-curl' growth is illustrated in Figure 1-14.

Kinoshita *et al.* [**102**] found that the length and growth rate of CNTs is improved by placing the substrate so that it is located slightly away from the plasma zone. This was attributed to the

irradiation of the substrate by the plasma disturbing the synthesis of the tubes by either etching the growing tubes or by reducing the reaction paths.

As can be seen in the work by Bower *et al.* [**103**,**108**], it is possible to combine the PECVD and thermal CVD method. A similar method is also employed by Smiljanic *et al.* [**89**]. The difference with the technique employed by the Smiljanic group is that the plasma is at an unusually high temperature for a PECVD technique which they estimate to be in excess of 1300 K. The ‚thermal CVD component' of their technique is added to ensure that the formation of amorphous carbon as a result of a large temperature gradient is curtailed. Such a technique may be referred to as a ‚thermal plasma torch'.

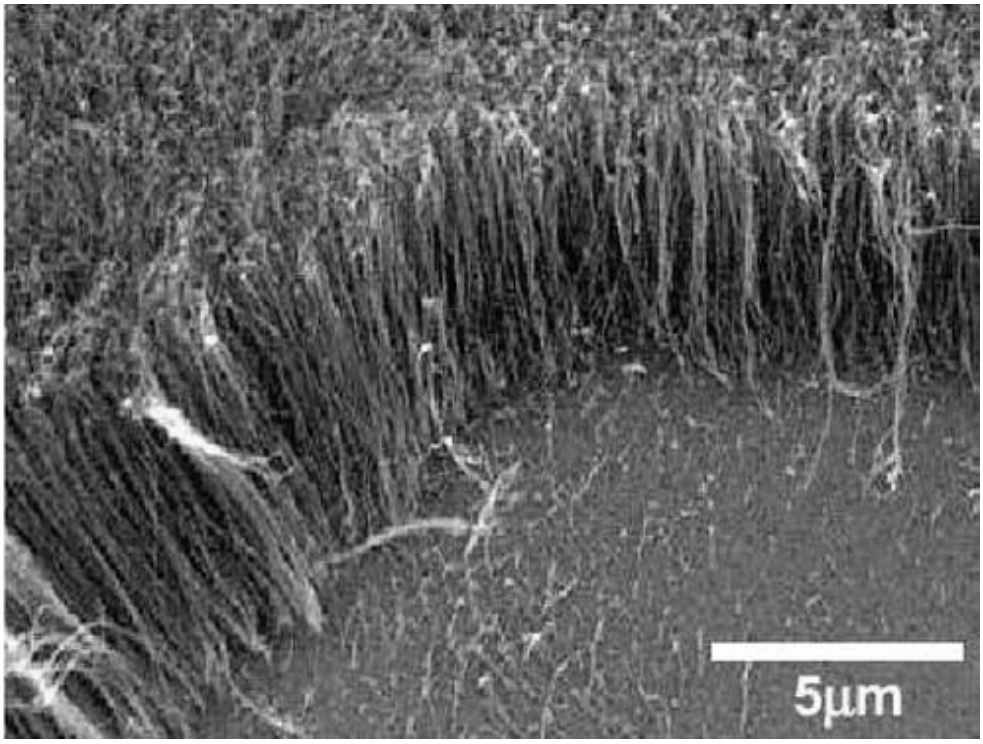

Figure 1-13: 'Forest' of vertically aligned carbon nanotubes grown via microwave plasma enhanced chemical vapour deposition by Kinoshita *et al.* [102**].**

1.3.3.8 Summary

As seen with the other synthesis methods discussed thus far, the CVD method has many procedural variations as well as parametrical variations (catalysts, precursors, support gases, etc.) that provide for a large research space. This great degree of variance in the research space also results in a large variance in the yield, quality and morphology of the resultant carbon nanostructures. The benefits of the CVD method are manifold: the temperature of the growth process may be lowered by the introduction of plasma; growth may be done in predetermined

patterns by using a catalytic masking process on substrates; nanotubes may be grown in alignment via the introduction of an electric field; the process may be made continuous by exploiting the possibility of introducing a floating catalyst; the process allows for low-cost growth of carbon nanostructures through the use of nothing more than cheap, yet highly pure precursors (like ethanol, for example) and a furnace. That the CVD process appears simple to scale-up for industrial scale production of carbon nanostructures makes it a viable method for the continued research and application of this method.

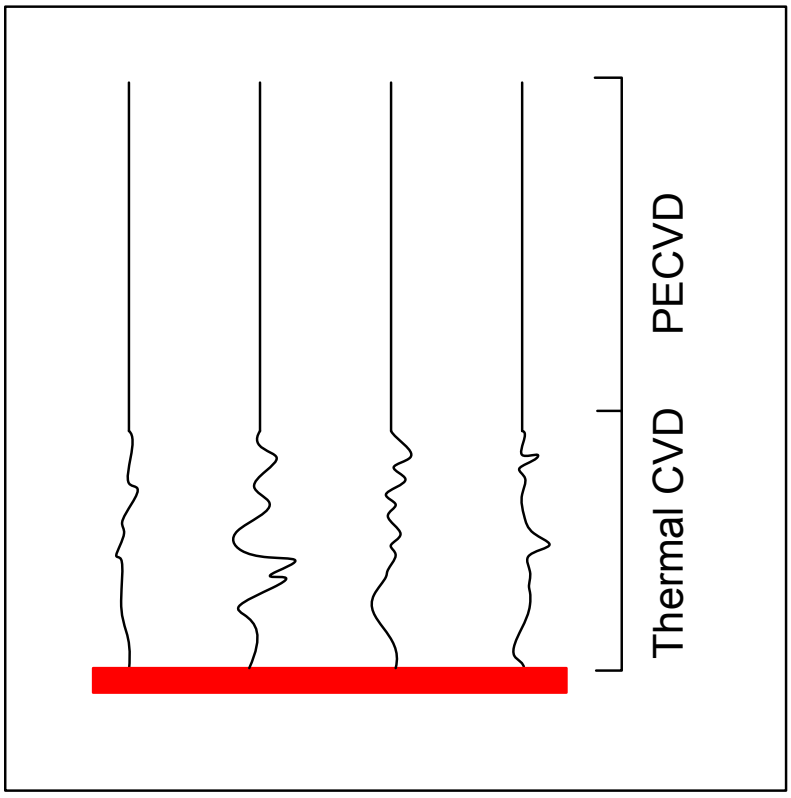

Figure 1-14: Illustration of the curling of carbon nanotubes when plasma is discontinued and a thermal CVD process is subsequently used [108**].**

1.3.3.9 CVD Summary

As seen with the other synthesis methods discussed thus far, the CVD method has many procedural variations as well as parametrical variations (catalysts, precursors, support gases, etc.) that provide for a large research space. This great degree of variance in the research space also results in a large variance in the yield, quality and morphology of the resultant carbon nanostructures. The benefits of the CVD method are manifold: the temperature of the growth process may be lowered by the introduction of plasma; growth may be done in predetermined

patterns by using a catalytic masking process on substrates; nanotubes may be grown in alignment via the introduction of an electric field; the process may be made continuous by exploiting the possibility of introducing a floating catalyst; the process allows for low-cost growth of carbon nanostructures through the use of nothing more than cheap, yet highly pure precursors (like ethanol, for example) and a furnace. That the CVD process appears simple to scale-up for industrial scale production of carbon nanostructures makes it a viable method for the continued research and application of this method.

1.3.4 Summary of synthesis methods

The diversity amongst the three main techniques methods (arc discharge, laser ablation and CVD) for the production of carbon nanostructures has been discussed, along with the large variations in parameters within these methods themselves. From method-to-method, the carbon source, catalysts, environment, synthesis temperature and energy source may be changed to produce a host of carbon nanostructures, from nanotubes, onion-like nano-structures, Y-branched tubes, nano-horns, beaded tubes and so on. The myriad of choice available in the production of carbon nanostructures leads to a rather difficult situation where comparison and analysis of results within an individual method is problematic; and the difficulty in inter-method comparison is even more distinct. As such, determining the exact effect of a single parameter is a complex task.

CVD certainly provides a low-cost and relatively simple entry-point for the production of carbon nanotubes. This presents a research group such as ours with the opportunity to participate in research that would otherwise require tremendous initial expenditure (on specialised equipment) to establish. In the previous study [**1**] it was found that all that was required for the production of carbon nanotubes was a domestic microwave oven, some ethanol and other items that would normally be found in laboratories such as a rotary pump and relevant glassware.

The earlier work explored the concept of producing carbon nanotubes using a microwave PECVD process within a domestic microwave oven[2]. The motivation for the work presented within this document arose from a desire to further characterise and find an optimal point for the process formerly developed by our group and additionally perform measurements of some of the properties of the grown structures. Added to the initial investigation is the determination of the effect of the composition of the precursor, the flow rate of support gases and promoter

[2] This method was initially used for experimental work on the production of MgB_2 thin film superconductors in the Hybrid Physical-Chemical Vapour Deposition technique, demonstrating the versatility of this low-cost apparatus [**1**].

concentration has on the growth of carbon nanotubes. Some elements of the earlier work have now been redesigned, with other elements reconfigured in order to streamline the pre-experimental process. A detailed description of the apparatus and experimental method utilised for this investigation is provided in the next chapter.

CHAPTER 2. EXPERIMENTAL: PRODUCTION OF NANOSTRUCTURES

2.1 Introduction

The method used to produce the carbon nanostructures is a microwave PECVD method which utilises a domestic microwave oven as an energy source. To briefly describe this method, the reactions take place within a chamber placed within the microwave oven. This chamber has tubes attached to allow the process inputs into the chamber and also for the out-gassing of the chamber. The substrate, in the form of an aerial is also located within this plasma chamber. The experimental set-up will now be described in detail.

2.2 Apparatus

2.2.1 Microwave Source

The microwave source is a Samsung M1977NCE 1000 W microwave oven, like those found in many homes across the world. The only modification made to the microwave was the replacement of the standard hinged door with an aluminium sheet. The new aluminium door is secured to the chassis of the microwave oven with 3 mm stainless steel screws. The safety switches for the door were bypassed to enable the operation of the microwave oven with the aluminium door. The aluminium door has three holes punched in its surface for the inlet and outlet tubes to pass through.

2.2.2 Plasma Chamber

The plasma chamber consists of a standard 1000 mL borosilicate laboratory flask with two glass inlet tubes attached tangentially to the sides. A laboratory standard 24/25 outlet, through which a tube is inserted – leading to a rotary pump, is located at the bottom of the flask. This configuration is shown in Figure 2-1.

The plasma chamber, with the glass tangential attachments, has been designed so that the gases that enter the chamber swirl around and mix prior to – and during – the plasma process.

As mentioned earlier, a hollow borosilicate glass tube is inserted into the outlet of the plasma chamber and acts as an interface between the plasma chamber and a rotary pump – in addition, the tube also acts as a stand for an aerial which is placed within the plasma chamber. An earlier design of the tube proved cumbersome and impractical and was abandoned in favour of a second design. This favoured design of the tube consisted of a hollow 8 mm (outer diameter)

borosilicate tube approximately 30 cm in length. One end of the tube had glass „olives', around which rubber piping could be securely fitted. The other end of the borosilicate tube was made into a stopper, and further extended into a stand for an aerial. The stopper section consists of a standard 24/25 borosilicate stopper – with its upper and lower surfaces removed. The portion of the tube, which forms the stand, has holes made on the surface to allow gas to be drawn into the hollow section of the tube by a rotary pump, via the rubber tubing. The stopper section of the tube is shown in Figure 2-2.

Figure 2-1: Image of the plasma chamber. The glass tubes attached tangentially to the sides of the chamber are used as inlets, with the opening at the bottom used as an outlet.

2.2.3 Aerial

The aerial's purpose is twofold; firstly to induce breakdown of the gas in the immediate vicinity of the point of the aerial (thus confining the plasma to the neighbourhood of the aerial), and secondly to act as a nucleation point for the growth of the carbon nanostructures. As the chamber is constructed from borosilicate glass, it is important that the plasma is located away from the chamber walls as the plasma can become hot enough to cause the melting of the chamber (borosilicate glass softens around 820 °C). The aerial itself comprises two parts: the base and the tip. The base, made from stainless steel, is 25 mm high, with a diameter of 10 mm in its middle section. The upper and lower sections have differing diameters and these are 16 mm and 6 mm respectively. The base has a 2 mm diameter, 15 mm deep hole wherein the aerial tip fits. The aerial tip is a 20 mm long piece of 2 mm diameter Nilo K wire. Nilo K is a metal

composite, comprised of 53% Fe, 29% Ni, 17% Co with the remaining 1% made up of sulphur and other metals. Guo *et al.* [**58**] noted, for the laser ablation method, that the presence of a bi-metallic catalyst resulted in an increase in yield by up to 100 times. There is thus sufficient reason to explore the use of this composite. Once the sharpened aerial tip is inserted into the base, the total height is 30 mm, which is approximately one quarter of the wavelength of the microwave radiation. The aerial base is shown in Figure 2-3; with the composite aerial shown in Figure 2-4.

2.2.4 Process control elements

The inlet and outlet tubes are interfaced to the process control elements via rubber LPG tubing. The control elements are, specifically:

- An Edwards „18' two-stage rotary pump
- A Techfluid variable area flowmeter, calibrated so that 100% corresponds to 10 Lt/min of hydrogen

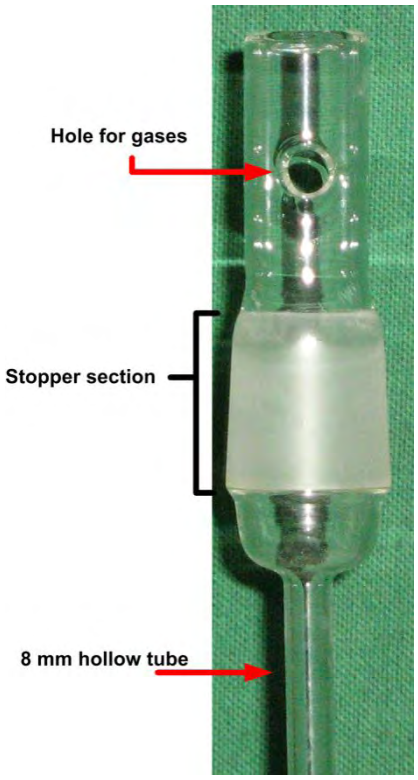

Figure 2-2: Tube to be inserted into the opening of the plasma chamber. Shown, is the hole on the surface to allow gases to be drawn into the hollow core of the tube; the 24/25 stopper section and the 8 mm extension. At the very top of the tube, there is a surface which acts as a stand for an aerial to be placed.

Figure 2-3: Stainless steel aerial base. This aerial has been blackened from multiple uses. The three sections, of differing diameters are clearly visible. The aerial tip is inserted into the hole at the top if the aerial base.

Figure 2-4: The stainless steel aerial with Nilo K tip. The aerial tip is sharpened to aid the breakdown of the electric field.

2.3 Process inputs

The precursors used in the synthesis of the nanostructures are all liquid hydrocarbons. The hydrocarbon is introduced into the plasma chamber in its gaseous form by opening the appropriate valve and pumping on the liquid.

The hydrocarbons for use were selected based on the hydrogen-carbon ratio. A high hydrogen-carbon ratio is thought to better promote the growth of CNTs [**89**]. The selected hydrocarbons precursors used in these experiments are: 99.5% purity ethanol (H-C ratio of 3:1), 99% purity toluene (H-C ratio of 8:7) and 98.6% purity xylene (H-C ratio 5:4).

The catalyst is included in the system as the aerial tip whereon the plasma is focussed. This aerial is made from Nilo K, which is a composite of iron, nickel, cobalt and sulphur. Recall that iron, nickel and cobalt are the preferred catalysts for nanotube growth in the CVD process, and that sulphur leads to improved structure and the growth of nanotubes of larger diameters.

In addition to the Nilo K aerial, ferrocene is also used as an additional catalyst in selected experiments. In these experiments, ferrocene is added to the hydrocarbon solution.

Thiophene is used as the promoter for these experiments. Thiophene contains sulphur and sulphur improves the structure of the nanotubes grown in a CVD process. Varying quantities of liquid thiophene (from 0% up to 1.5% thiophene by weight) is added to ethanol in order to study the effect of the thiophene concentration on the production of carbon nanostructures in this process. It is important to note, however, that although the thiophene is added to the ethanol in a specific proportion, the evaporated hydrocarbon gas entering the plasma chamber may not contain that same ratio of thiophene-to-ethanol. The ethanol-thiophene solution is agitated to aid the proportional transfer of the thiophene and ethanol in the gas drawn into the plasma chamber.

The support gas utilised in these experiments is hydrogen. A variable area flow meter is used to control the hydrogen input between 0 Lt/min and 10 Lt/min. The hydrogen used for these experiments is Afrox 99.999% purity H_2. As mentioned earlier, hydrogen has been shown to play an important role in the growth of CNTs in a CVD process. It is hoped that the range of 0 Lt/min to 10 Lt/min if hydrogen flow is large enough to facilitate the determination of the optimal hydrogen point for this process.

2.4 Physical setup

The microwave oven is mounted with the door facing toward the ground. The outlet and two inlet tubes protrude from the door and are connected to the appropriate source via rubber LPG tubing.

The outlet tube is connected to the rotary pump with LPG piping which is clamped onto a brass flange. The flange is coupled to the inlet of the pump with the appropriate seals and clamps. The outlet tube of the plasma chamber lies directly above the inlet of the pump to ensure that there is minimal bending of the LPG tubing.

One inlet is connected, via the LPG piping and a valve, to a borosilicate flask containing the liquid hydrocarbon precursor. When the valve is opened, and the pump switched on, the liquid hydrocarbon is evaporated and drawn in to the plasma chamber. The other inlet tube is connected, via LPG piping and a variable area flow meter, to the support gas source. The setup is shown, schematically, in Figure 2-5.

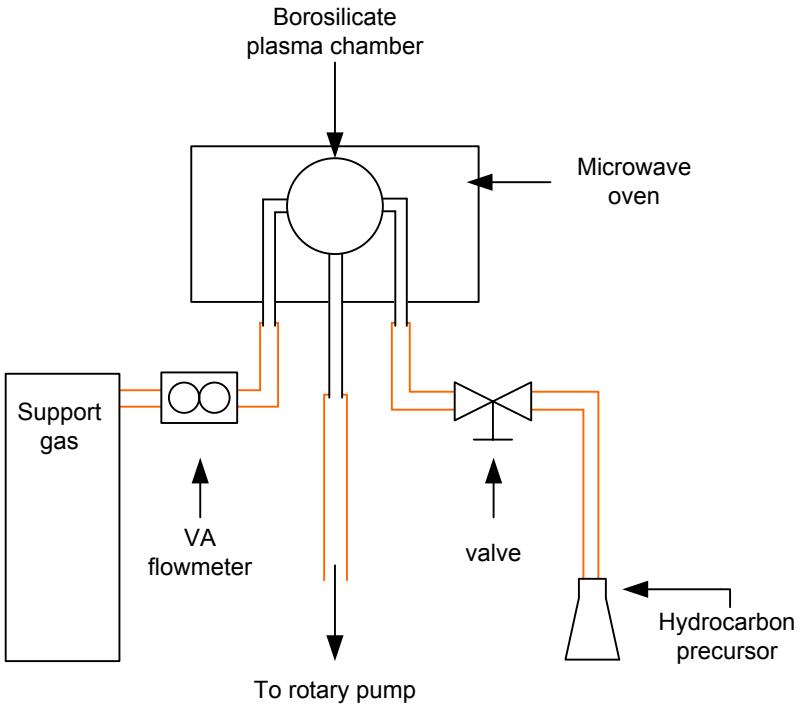

Figure 2-5: Schematic representation of the plasma system.

2.5 Experimental process

In order to determine the effect the different inputs have on the type of nanostructure formed, the experiments have been divided into numerous experiment sets. There are six sets, labelled from A to F, separated by the hydrocarbon precursor choice. Each set is further divided into subsets – each subset having a different hydrogen flow rate – these are allocated a number for identification.

The main experiment sets are:

A. Ethanol only
B. Ethanol with 0.5% thiophene (by weight)
C. Ethanol with 1.5% thiophene (by weight)
D. Xylene only
E. Toluene only
F. Ethanol with 1.5% thiophene (by weight) and 2.5% ferrocene (by weight). This experiment was conducted after the analysis of experiment sets A to E was conducted. Experiment set F, therefore, consists of just the single experiment – which was based on what was deemed to be the ‚most successful' experiment, based on CNT production.

The main sets are divided, and numbered, accordingly:

0. 0 Lt/min hydrogen
1. 1 Lt/min hydrogen
2. 5 Lt/min hydrogen
3. 7.5 Lt/min hydrogen
4. 10 Lt/min hydrogen

Each synthesis process followed a particular order. Firstly, the rotary pump was switched on to pump out the plasma chamber, after a brief wait (typically 30 seconds or so), the microwave oven was turned on and the plasma thus ignited. The valve controlling the flow of the hydrocarbon vapour into the plasma chamber was then fully opened. Once all of the above had been done, the hydrogen flow (if required) was regulated. Typically, the period from the ignition of the plasma to the regulation of the hydrogen flow would take no longer than 10 seconds. It should be noted that in all experiments the precursor solution was agitated throughout the duration of the experiment to ensure proper mixing of the solution.

The carbon nanostructures usually coated the Nilo K aerial; this meant that a small quantity could be scraped off for analysis. All samples were analysed using a JEOL JEM 1010 transmission electron microscope (TEM), with selected samples analysed under a LEO 1450 scanning electron microscope (SEM).

The flow rates of the hydrocarbons precursors have been calculated. These, along with the experiments conducted, are summarised in Table 2-1.

Table 2-1: Table of Experiments for Nanostructure Production.

SET	NUMBER	ETHANOL (Lt/min)	THIOPHENE (% ethanol weight)	XYLENE (Lt/min)	TOLUENE (Lt/min)	HYDROGEN (Lt/min)
A	0	0.00320	0	0	0	0
	1					1
	2					5
	3					7.5
	4					10
B	0		0.5	0	0	0
	1					1
	2					5
	3					7.5
	4					10
C	0		1.5	0	0	0
	1					1
	2					5
	3					7.5
	4					10
D	0	0	0	0.00310	0	0
	1					1
E	0	0	0	0	0.00985	0
	1					1
	2					5
	3					7.5
	4					10
F	2	0.00320	1.5	0	0	5

CHAPTER 3. PRODUCTION OF NANOSTRUCTURES

This chapter documents the transmission electron microscopy (TEM) and scanning electron microscopy (SEM) analysis of the experiments conducted. TEM analysis was conducted first, with SEM analysis performed on selected samples. The analysis revealed that CNTs were only grown in the ethanol-based experiments. The quality of CNTs initially improves with the addition of hydrogen and thiophene. It has been observed, however, that the addition of too much hydrogen or thiophene adversely affects the quality of the CNTs and deformations such as uneven tube walls and branching have been noted. ONSs were found regardless of input hydrocarbon while no CNTs were synthesised when toluene or xylene were used as the input hydrocarbon. The presence of ONSs could be prevented in the ethanol-based experiments by an increase in hydrogen or thiophene content in. Large quantities of ONSs were synthesised when toluene and xylene were used. Analysis of the nanostructures found in each experiment is now presented in detail.

3.1 Experiment Set A (Ethanol; 0% Thiophene)

3.1.1 Results of Experiment A0 (0 Lt/min Hydrogen)

This experiment was conducted with ethanol as the hydrocarbon source, no hydrogen support gas and the Nilo K aerial as the catalyst. When observing the flask containing the ethanol, with the pump switched on and the valve controlling the ethanol vapour flow, the ethanol bubbled furiously - indicating good flow of ethanol vapour to the plasma chamber. The plasma itself converged well on the aerial tip and started as a bright purple glow, and progressively turned orange as more ethanol was introduced to the system. The purple glow is indicative of low pressure and the colour change is related to the change in pressure as more ethanol is drawn into the plasma chamber. Each experiment ran for a duration of 5 minutes[3].

The results from this experiment were predictably poor. The absence of hydrogen meant that negligible quantities of carbon nanostructures were formed. From TEM measurements, only two CNTs were found in the sample examined, as shown in Figure 3-1. The sample produced appears to have a large content of amorphous carbon as shown in Figure 3-2.

[3] The first two experiments were done as a single 5 minute run. This was changed in further experiments to prevent the melting of the plasma chamber.

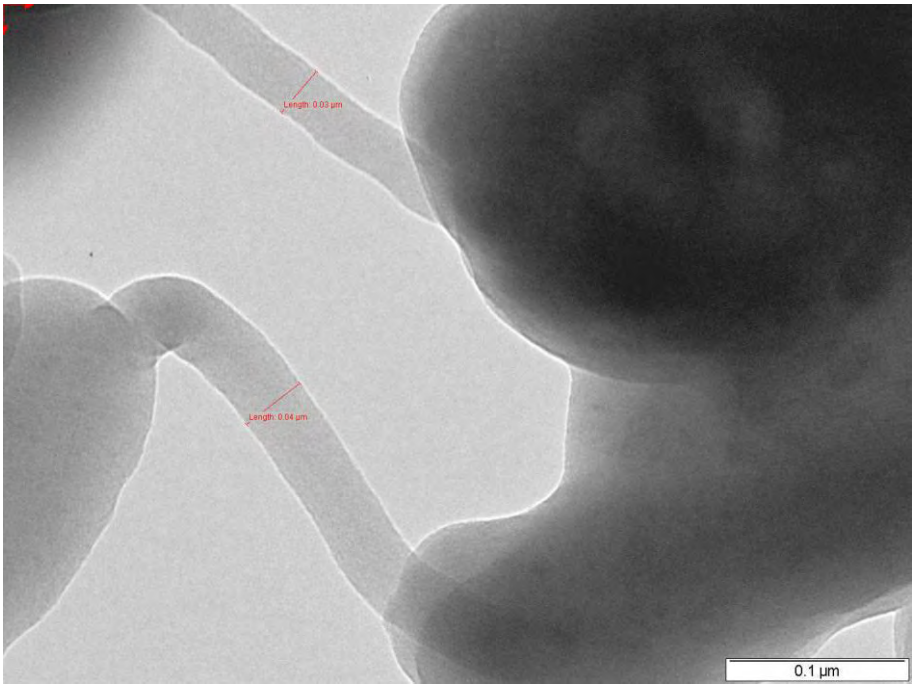

Figure 3-1: TEM micrograph of two carbon nanotubes found in Experiment A0 - these tubes are approximately 40 nm in diameter and were the only such tubes found in this sample

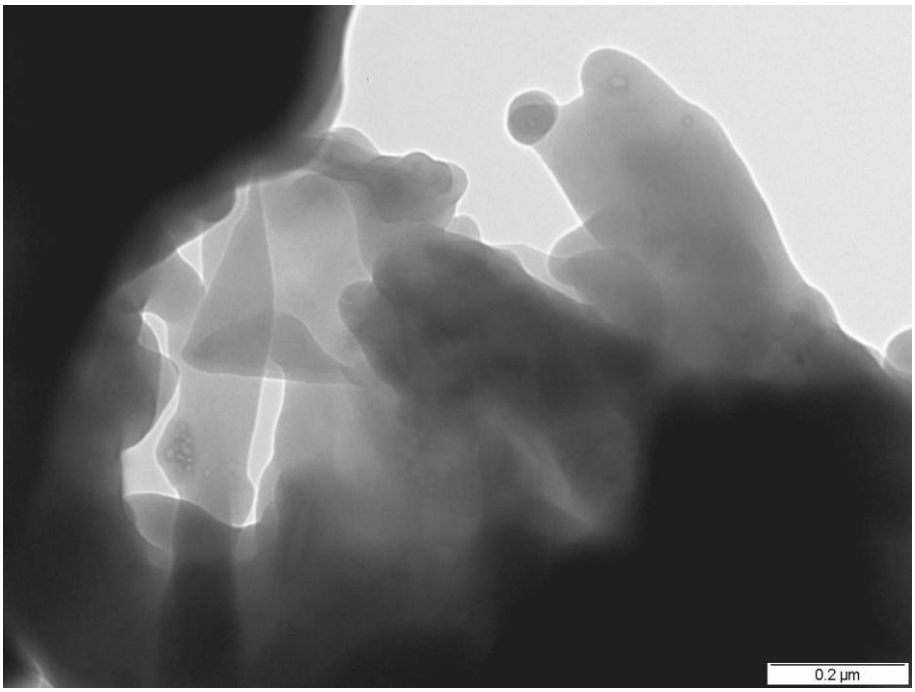

Figure 3-2: TEM micrograph of the amorphous carbon which dominated this sample.

3.1.2 Results of Experiment A1 (1 Lt/min Hydrogen)

The hydrocarbon source is pure ethanol with 1 Lt/min flow of hydrogen as a support gas. The Nilo K aerial was used as the catalyst. This run was also timed for five minutes. Here, the ethanol again bubbled furiously. The resulting plasma was again a bright purple turning orange. The plasma, however, was rather unstable and not well confined to the aerial tip. Within two minutes of plasma ignition, the plasma chamber had „melted' indicating a plasma temperature in excess of 1000 K had been achieved. The plasma chamber (with the hole formed by the „melting') is shown in Figure 3-3. The increased pressure as a result of the addition of hydrogen increases the possibility of the chamber melting. To prevent this undesirable event, experiments were, from this point onward, no longer conducted as a single 5 minute run, but were divided into ten segments of 30 seconds each.

When first analysed using TEM, negligible amounts of tube-like structures were found, with large quantities of amorphous carbon dominating the sample. The few tube-like structures that were found, however, were poorly formed and exhibited defects like branching as can be seen in Figure 3-4. Further analysis from SEM measurements, revealed a quantity of onion-like nanostructures. These ONSs are rather large, around 2 µm in diameter, but do exhibit the expected structure [**12**]. A SEM micrograph of these ONSs is presented in Figure 3-5.

Figure 3-3: Image of a hole formed in the plasma chamber as a result of the chamber side softening due to the high temperature plasma touching the side of the plasma chamber.

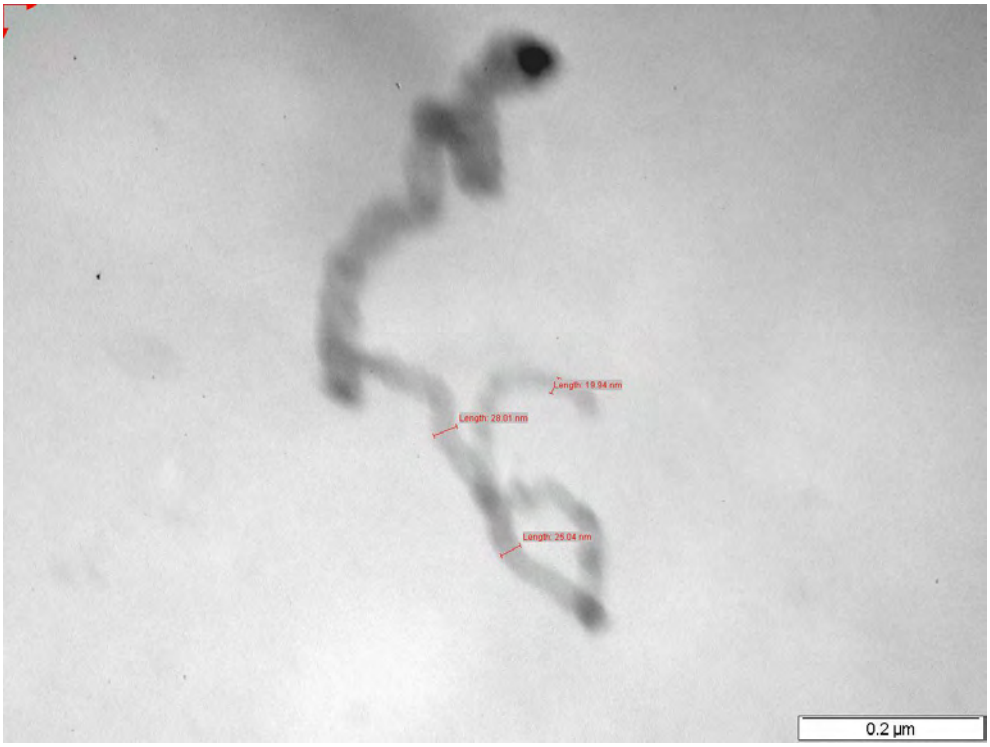

Figure 3-4: Poorly focussed TEM micrograph of tube-like structures found at 1 Lt/min H2. The dark spot towards the top of the structure is indicative of an growth site.

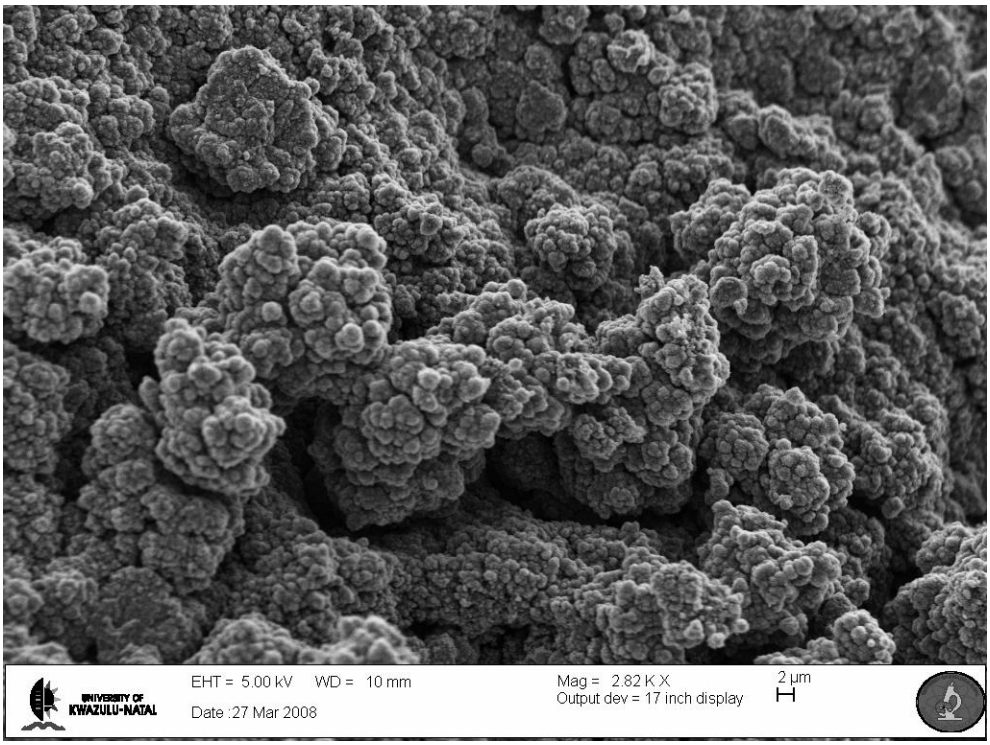

Figure 3-5: SEM micrograph of onion-like nanostructures found in the A1 sample.

3.1.3 Results of Experiment A2 (5 Lt/min Hydrogen)

Here, ethanol was used as the hydrocarbon source with 5 Lt/min of hydrogen as the support gas. The ethanol did not bubble as furiously as it did in the previous experiments, and the plasma remained bright purple – rather than changing to a bright orange glow. The plasma was, however, small and confined to the aerial tip

Again, this experiment was noted for the lack of carbon nanotubes and the appearance of onion-like nanostructures. The quantity of amorphous carbon decreased significantly; perhaps as a result of the increase in the hydrogen flow rate. The ONSs found in this sample (shown in Figure 3-6.) are considerably smaller than those found in Experiment A1.

3.1.4 Results of Experiment A3 (7.5 Lt/min Hydrogen)

In this run a small, but bright purple, plasma was well confined to the aerial tip. From the TEM analysis, there appeared to be no CNTs at all, but rather an abundance of ONSs and a further reduction of amorphous carbon.

3.1.5 Results of Experiment A4 (10 Lt/min Hydrogen)

The plasma, in this experiment, was again small, bright purple and well confined to the aerial tip. CNTs were found in abundance in this sample – with a further reduction in the quantity of amorphous carbon. No ONSs were found in this sample. Here, the CNTs are mainly smooth-walled, but with a variation in tube diameter from tube-to-tube (Figure 3-7 and Figure 3-8). There does exist, however, a small number of jagged-walled tubes in this sample – as shown in Figure 3-9.

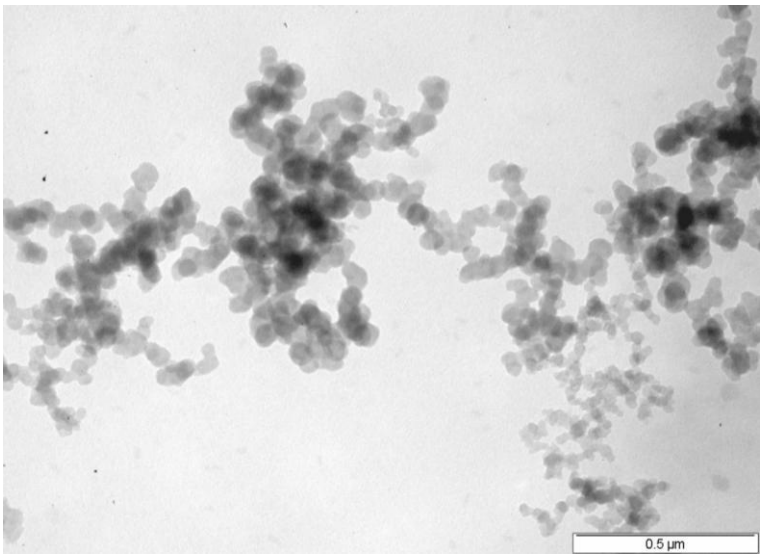

Figure 3-6: Onion-like nanostructures formed in Experiment A2. Note the reduction in size of the nano-onions from Experiment A1.

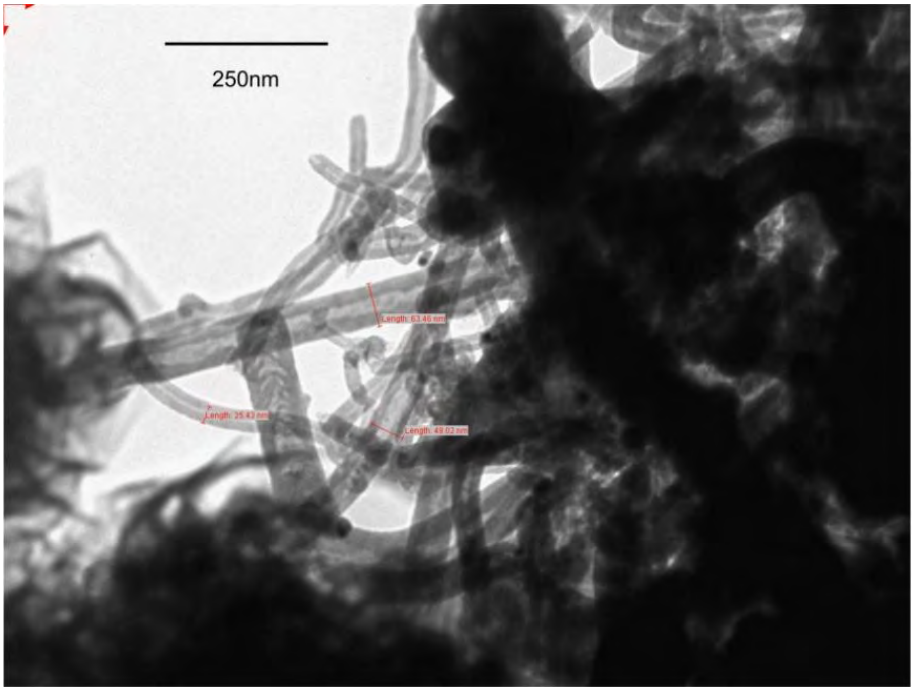

Figure 3-7: Carbon nanotubes produced in experiment A4. The tube diameters differ from tube-to-tube, but the nanotubes appear to have smooth walls. The darker area is a result of the density of the sample, rather than a collection of amorphous carbon.

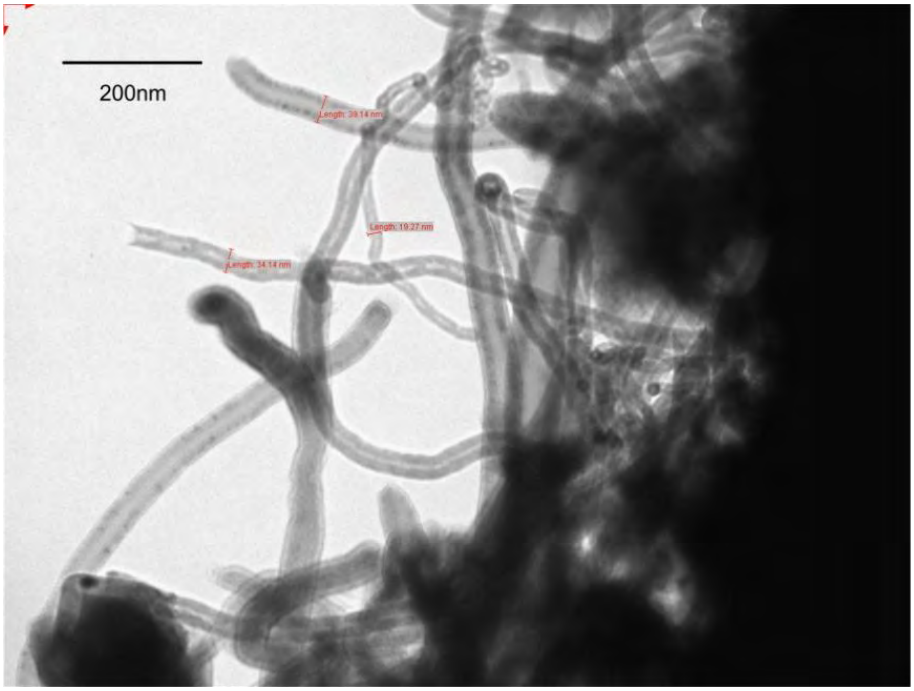

Figure 3-8: TEM micrograph of carbon nanotubes from Experiment A4. Here, the walls of the tubes are not as smooth as the nanotubes shown earlier.

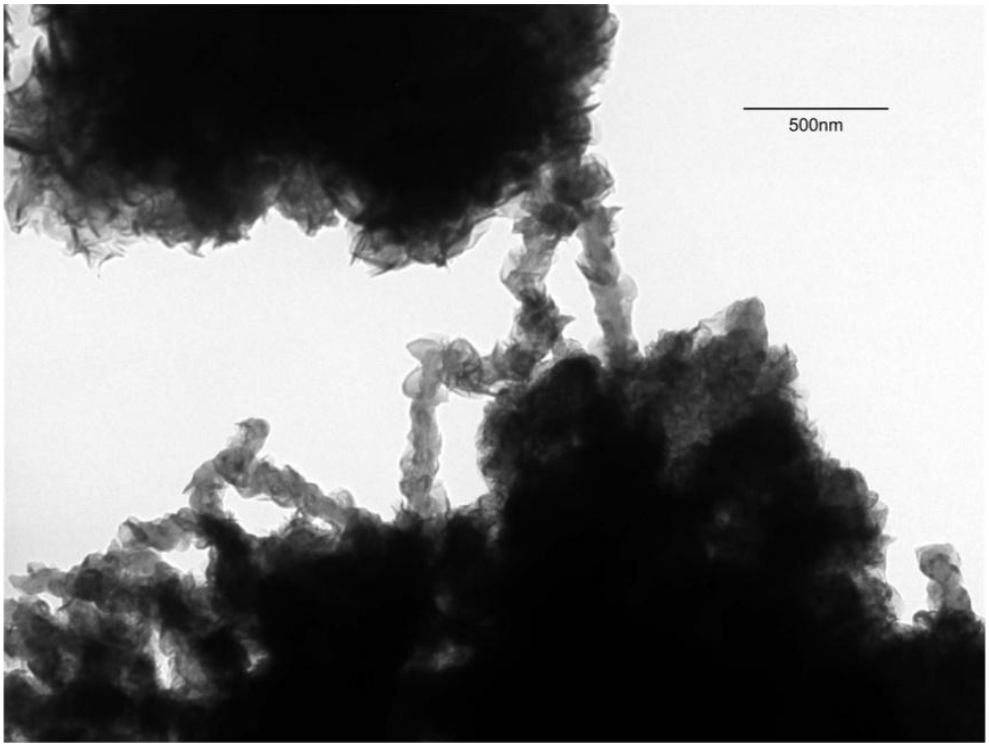

Figure 3-9: Rough walled tube-like structures. Examples like this may be found scattered sparsely around the sample.

3.2 Experiment Set B (Ethanol; 0.5% Thiophene)

3.2.1 Results of Experiment B0 (0 Lt/min Hydrogen)

The process input for this experiment was ethanol with 0.5% thiophene added to it. No hydrogen is added for this experiment. TEM analysis revealed that the addition of this small quantity of thiophene results in the formation of CNTs – even without hydrogen. A group of tangled CNTs are shown in Figure 3-10.

3.2.2 Results of Experiment B1 (1 Lt/min Hydrogen)

This experiment replicates the input parameters of B0, but with the introduction of 1 Lt/min of hydrogen. In this experiment, the plasma was bright white but not well confined to the aerial tip. Here, TEM analysis shows that neither CNTs nor ONSs are found, but rather a mass of jagged-walled structures which resemble CNTs. These jagged-walled structures are shown in Figure 3-11. There is also a small quantity of amorphous carbon present in this sample.

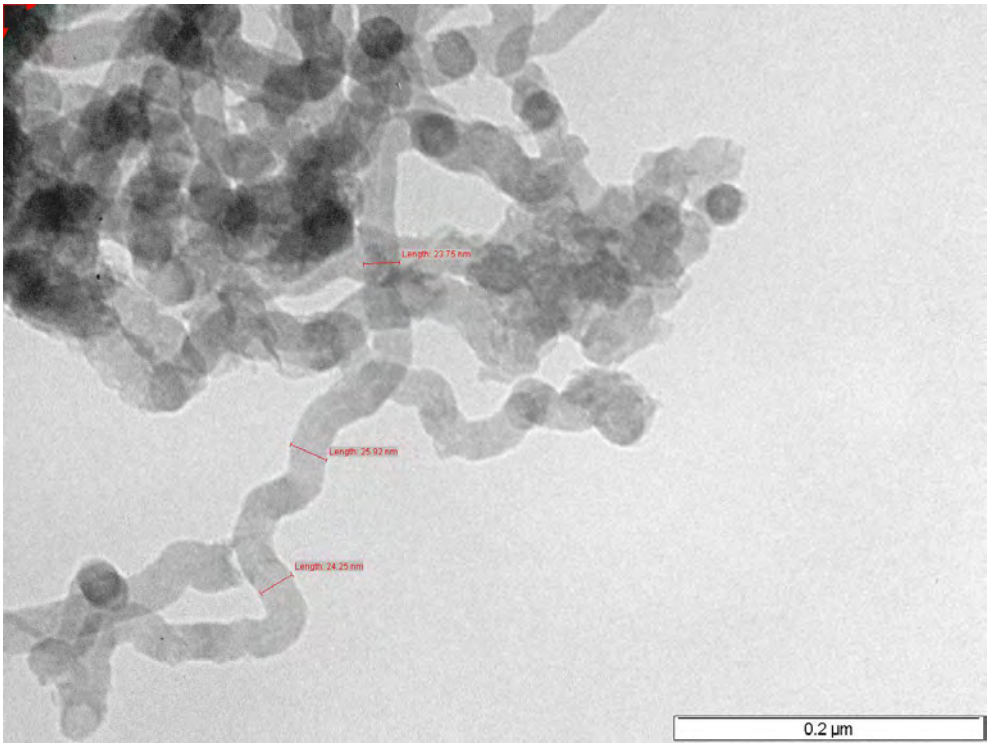

Figure 3-10: Tangled group of carbon nanotubes formed with the addition of 0.5% thiophene - but without hydrogen. Tube diameters are approximately 25 nm.

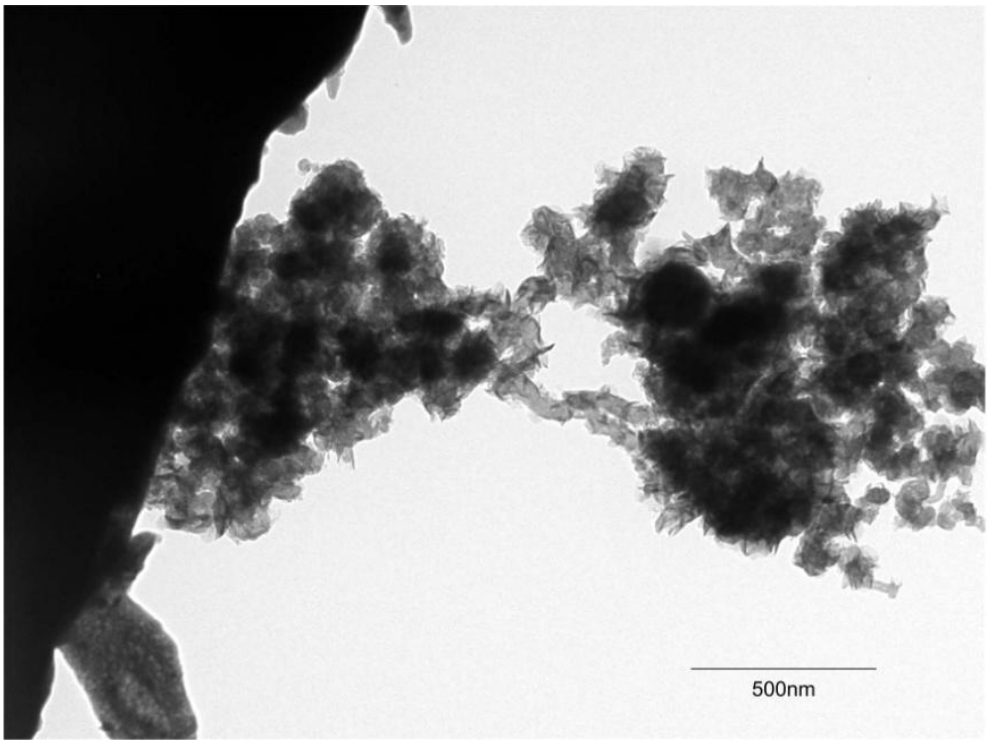

Figure 3-11: TEM micrograph of jagged-walled structures formed in Experiment B1. A quantity of amorphous carbon is observed in the bottom left corner of the image.

3.2.3 Results of Experiment B2 (5 Lt/min Hydrogen)

Here, the hydrogen flow rate is increased to 5 Lt/min. The other process inputs remain as in Experiment B1. Again, a bright white plasma was not well confined to the aerial tip. TEM analysis of the sample showed that the structures formed in this experiment (Figure 3-12) are a closer resemblance to CNTs than those from Experiment B1. Smooth-walled CNTs, with diameters of approximately 100 nm were found when the sample was analysed under SEM (Figure 3-13).

The formation of CNTs in this experiment is significant when compared to the experiments where ethanol alone was utilised as the precursor (Experiment set A). In set A, the CNTs were only found – in significant quantities – at a hydrogen flow rate of 10 Lt/min, compared to 5 Lt/min in this experiment. The trend thus far is noticeable: *the addition of hydrogen removes amorphous carbon and the addition of thiophene seems to promote the growth of CNTs at lower hydrogen levels.*

3.2.4 Results of Experiment B3 (7.5 Lt/min Hydrogen)

With the hydrogen flow rate increased to 7.5 Lt/min, the formation of ONSs is observed. It is noted that the formation of ONSs (Figure 3-14) is „delayed' (with respect to hydrogen flow rate) when compared to the ethanol only experiments of set A.

Small quantities of amorphous carbon are found in this sample (as can be seen in the lower right-hand corner of Figure 3-14). It is evident, from the trend observed in experiment set A, and the trend thus far in experiment set B, *that increasing the hydrogen flow not only reduces the quantity of amorphous carbon, but also delays the formation of ONSs.*

3.2.5 Results of Experiment B4 (10 Lt/min Hydrogen)

When the hydrogen flow rate is increased to 10 Lt/min, there is no amorphous carbon present in the sample. ONSs (Figure 3-15) are once again found in this experiment, along with poorly formed tube-like structures. It is certainly possible that, with our selected hydrogen source for this set of experiments (namely ethanol with 0.5% thiophene), the optimum hydrogen flow rate has been exceeded – resulting in these poorly formed „tubes'.

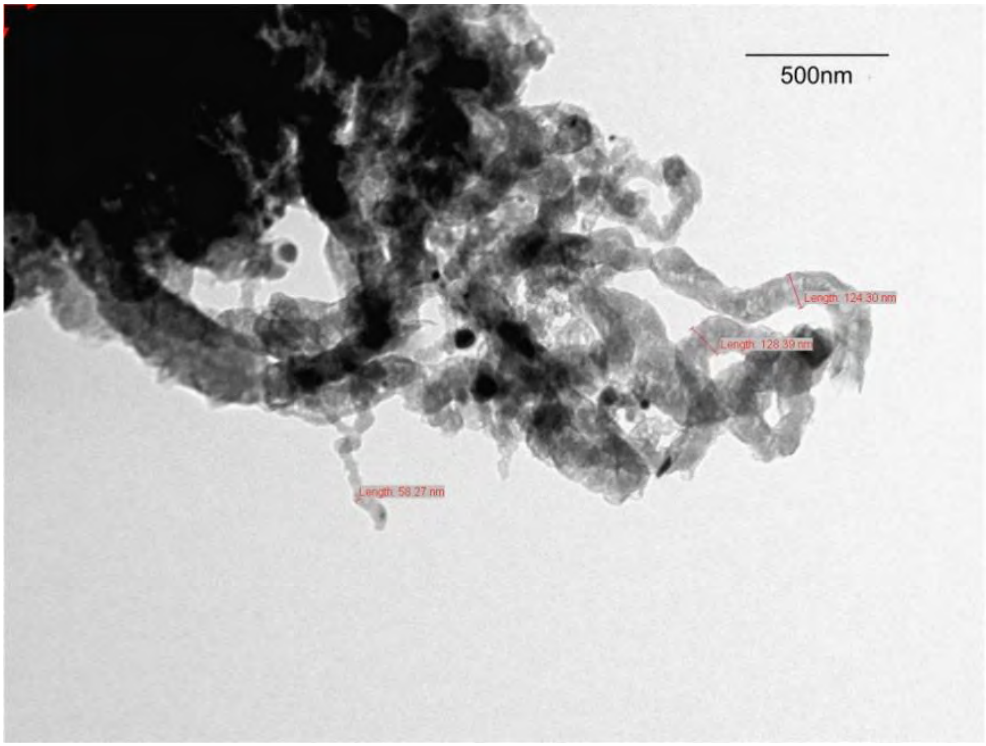

Figure 3-12: TEM micrograph of tube-like structures from Experiment B2.

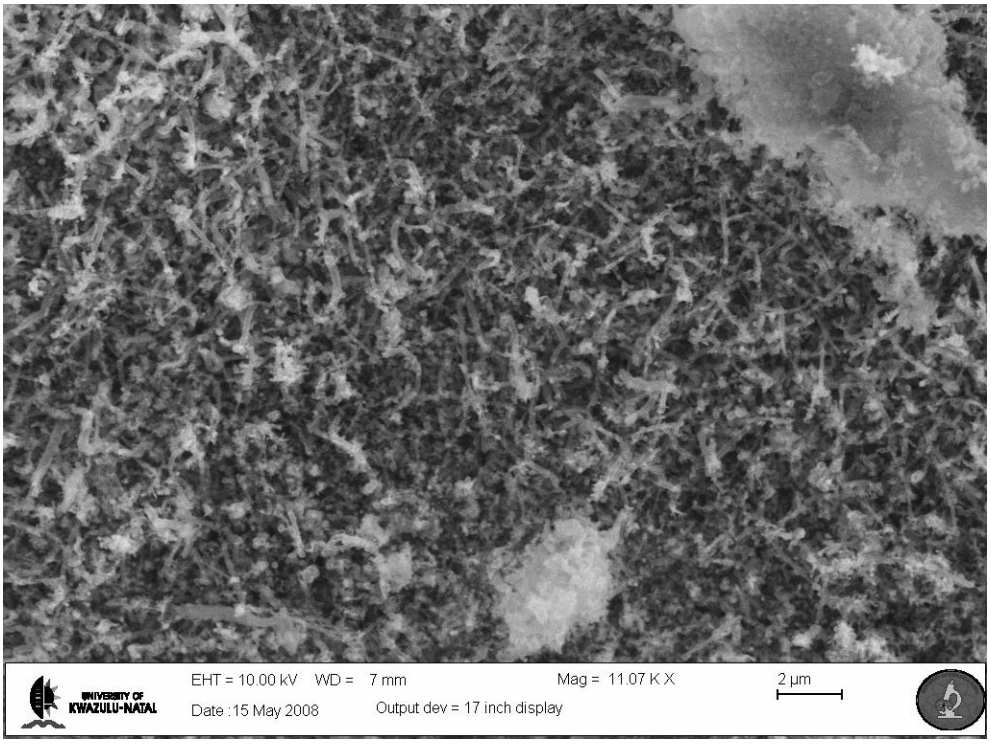

Figure 3-13: SEM micrograph of carbon nanotubes from B2; a small quantity of amorphous carbon is seen in the upper right corner of the micrograph. The scale bar is 2µm.

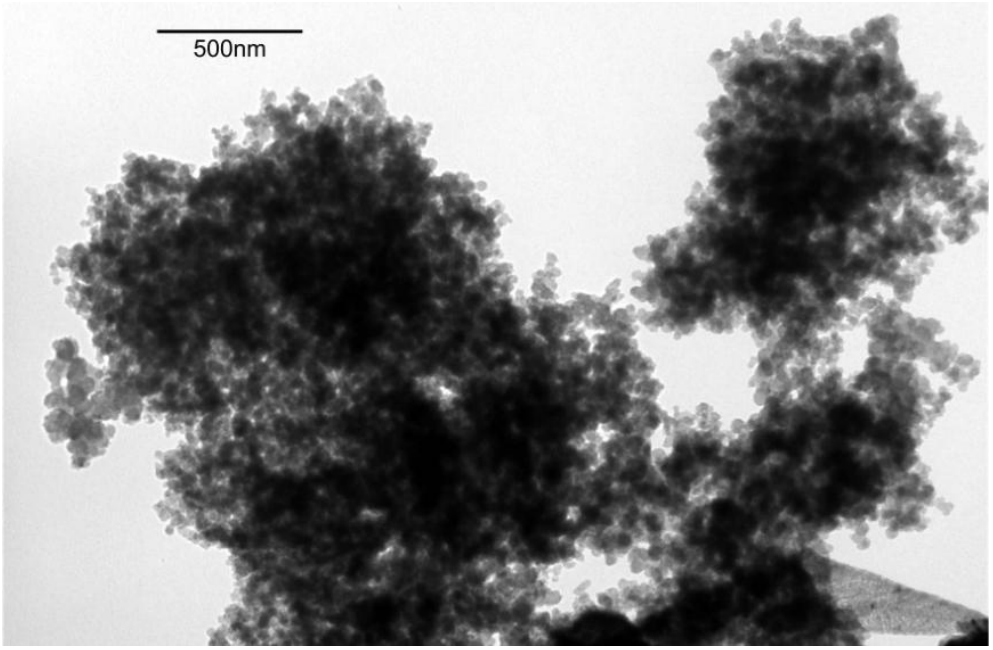

Figure 3-14: Onion-like nanostructures from the B3 experiment.

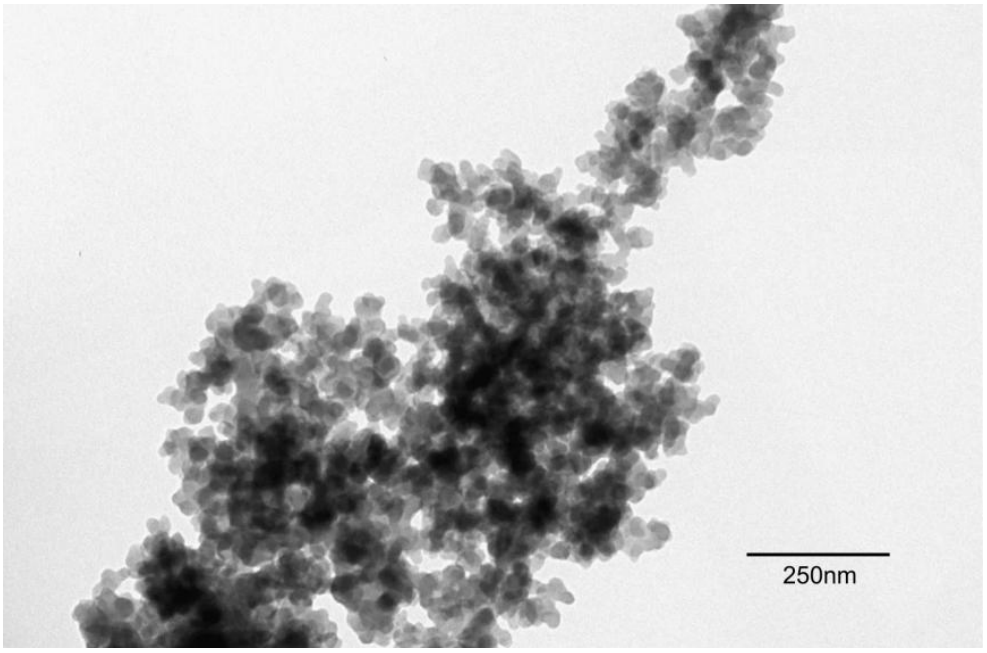

Figure 3-15: Onion-like nanostructures formed in Experiment set B4, at a hydrogen flow rate of 10 Lt/min.

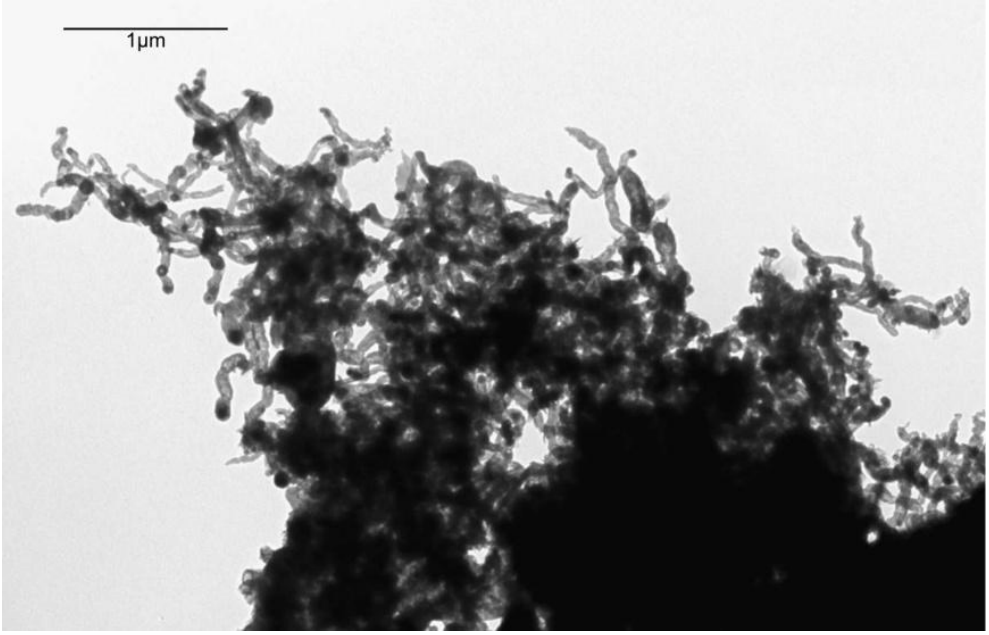

Figure 3-16: Poorly formed tubular structures formed in Experiment B4.

3.3 Experiment Set C (Ethanol; 1.5% Thiophene)

3.3.1 Results of Experiment C0 (0 Lt/min Hydrogen)

In this experiment, the thiophene content of the hydrocarbon solution has been increased to 1.5% by weight. The plasma is found to be small and well confined to the aerial tip and is a bright orange. As with Experiment B0 (Figure 3-10), TEM analysis reveals that poorly formed CNTs are present in the sample (Figure 3-17) – with uneven tube walls and numerous branching deformities present. SEM analysis (Figure 3-18), however, reveals that there are numerous well formed CNTs (along with some „branched' tubes) amongst a large quantity of amorphous carbon.

3.3.2 Results of Experiment C1 (1 Lt/min Hydrogen)

In this experiment, the hydrogen flow rate is increased from 0 Lt/min to 1 Lt/min. Again, the plasma is small, orange and well confined to the aerial tip. It is also apparent from TEM analysis that there is a reduction in the quantity of amorphous carbon present in the sample. The quality of the carbon nanotubes found in this sample is much improved from those present in Experiment C0 – exhibiting smoother wall and fewer branching deformities. The CNTs present, however, do exhibit variable tube diameters. This may be observed in Figure 3-19.

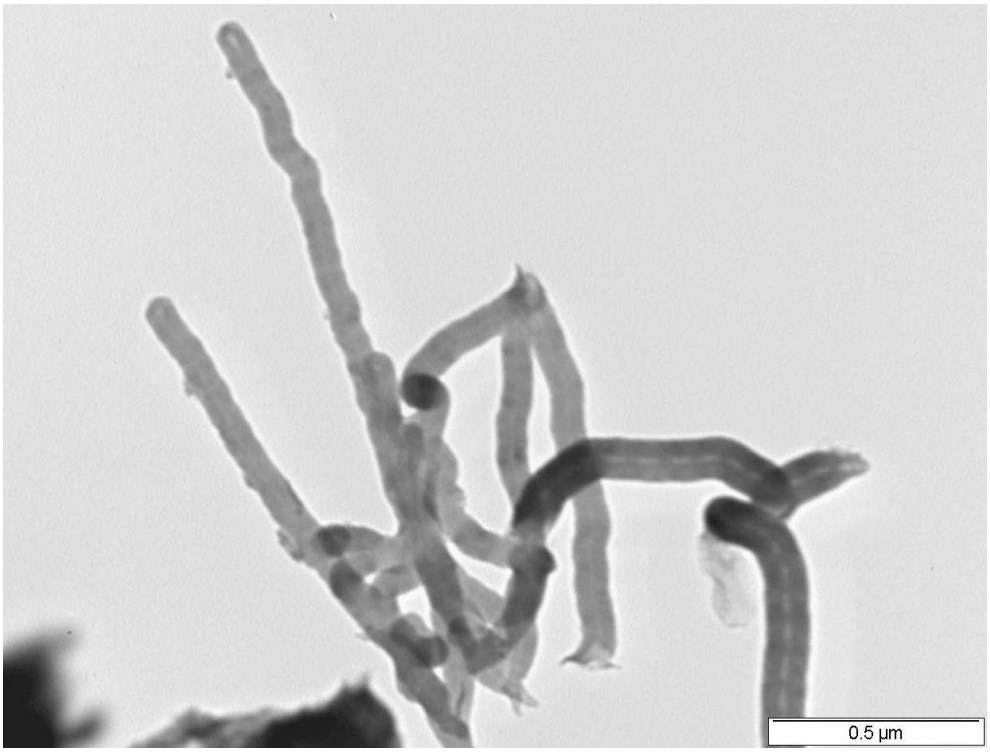

Figure 3-17: Poorly formed CNTs present in the C0 sample (Ethanol - 1.5% Thiophene; no hydrogen).

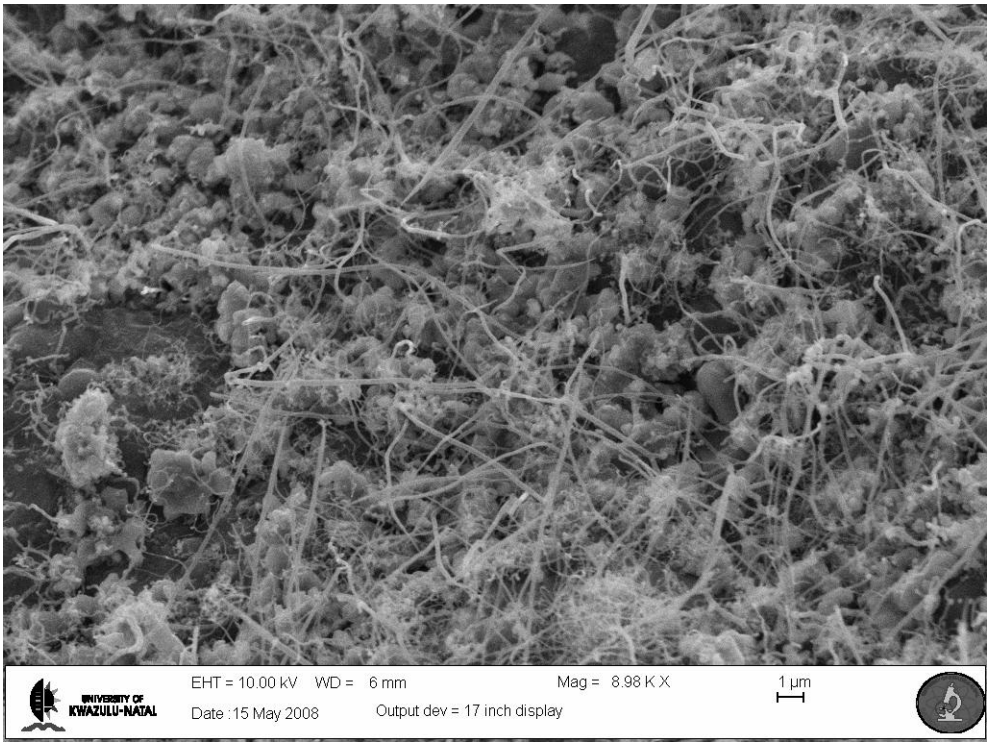

Figure 3-18: Scanning electron micrograph of well formed carbon nanotubes amongst amorphous carbon in the C0 sample. Scale bar is 1µm.

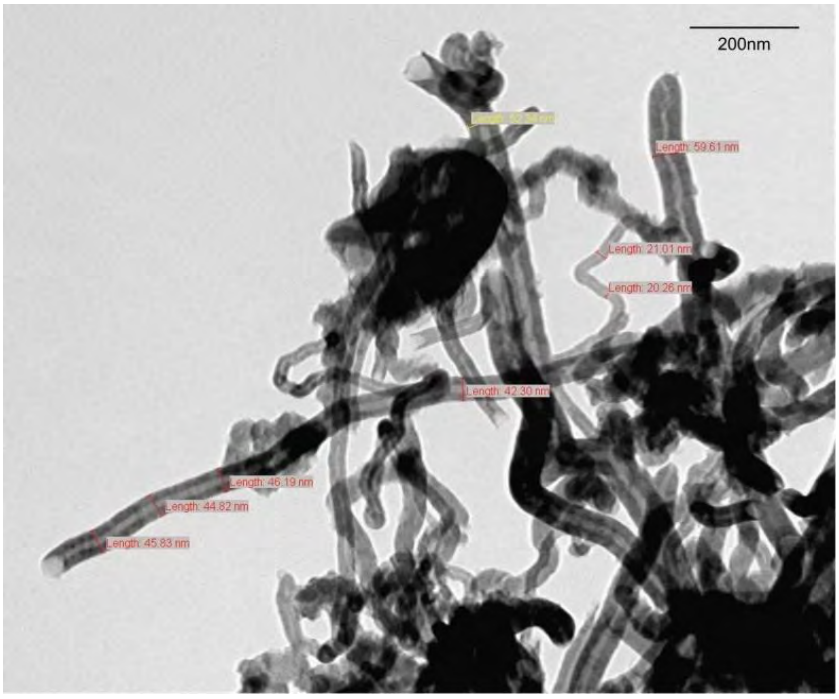

Figure 3-19: Smoother nanotubes found from Experiment C1. The tubes have variable diameters, but generally smoother walls than the tubes found in Experiment C0.

3.3.3 Results of Experiment C2 (5 Lt/min Hydrogen)

In this experiment, the H_2 flow rate was increased to 5 Lt/min. The plasma was large and purple, appearing almost column-like above the aerial tip. The plasma gradually changed to the familiar orange as it did in Experiment C1. In this experiment, the product was only found along the length of the Nilo K aerial tip. TEM analysis shows that the product formed in Experiment C2 resembles that of Experiment C1 closely. There are smooth-walled CNTs interspersed amongst poorly formed tubular structures and some amorphous carbon, as shown in Figure 3-20 and Figure 3-21.

3.3.4 Results of Experiment C3 (7.5 Lt/min Hydrogen)

With the H_2 increased to 7.5 Lt/min, the plasma begins bright purple, turning a dark orange; the plasma was small and well confined to the aerial tip. As with all experiments thus far, the product only formed on the Nilo K aerial tip. TEM analysis of the product shows that, unlike Experiments C1 and C2, smooth-walled CNTs do not form. Instead, there are numerous thick (almost 100 nm) tubular structures. There is, however, an absence of amorphous carbon in the sample. Compared to Experiment B3, there is no evidence of ONSs in this experiment. This is perhaps due to the effect of the increased thiophene content. The poorly formed tubular structures are shown in Figure 3-22

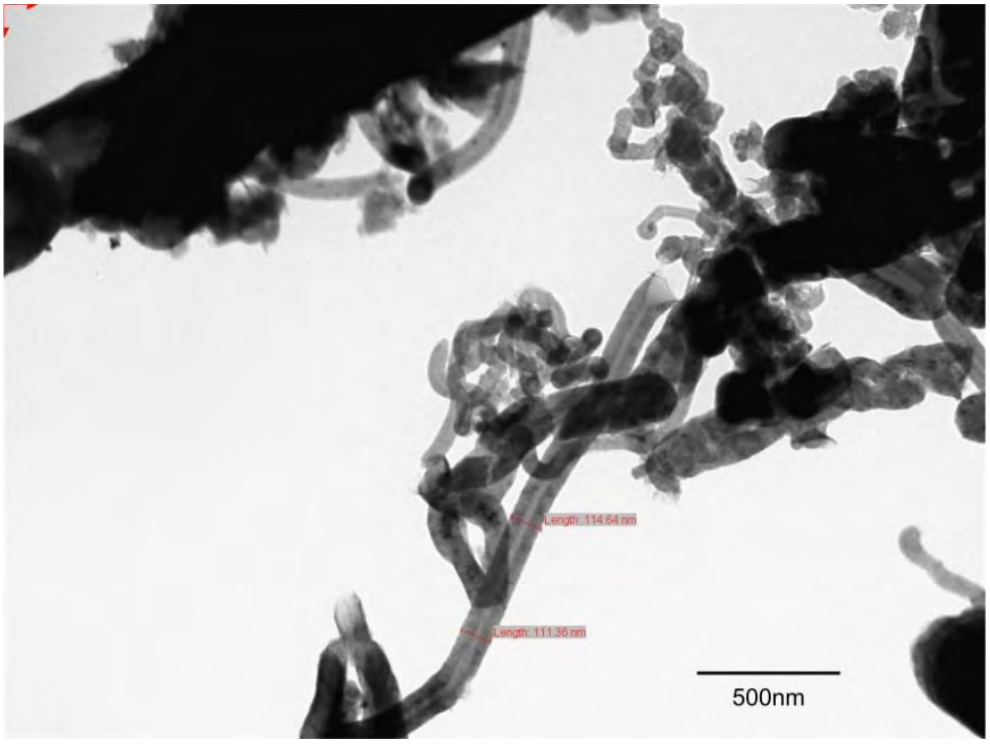

Figure 3-20: A smooth-walled carbon nanotube from Experiment C2.

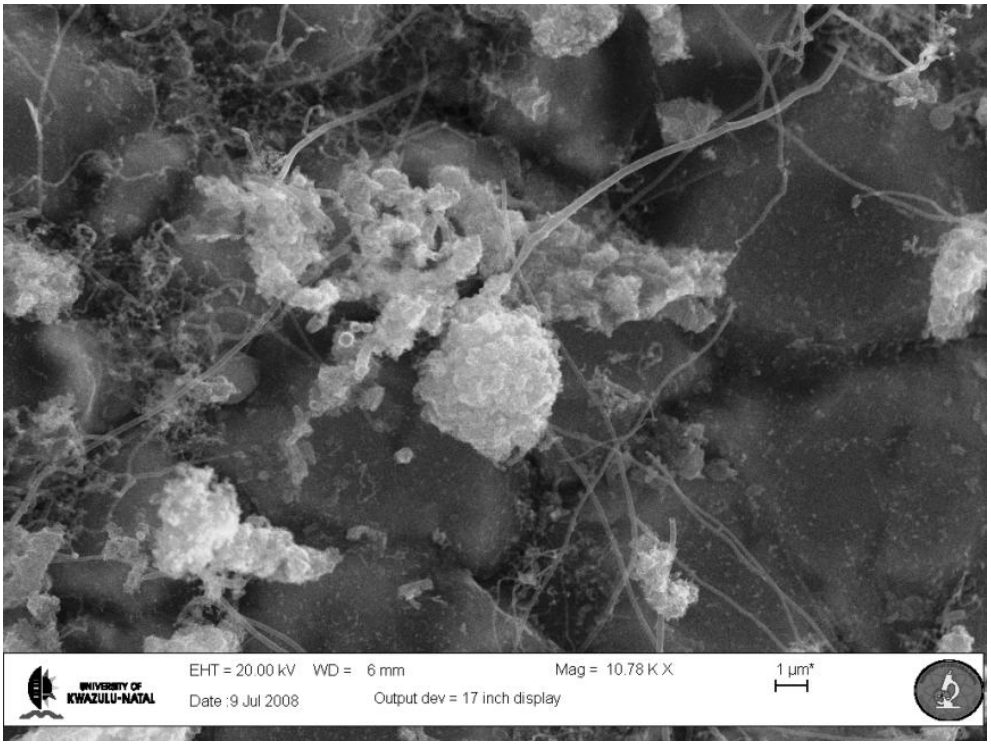

Figure 3-21: SEM micrograph of carbon nanotubes amongst some amorphous carbon grown in experiment C2.

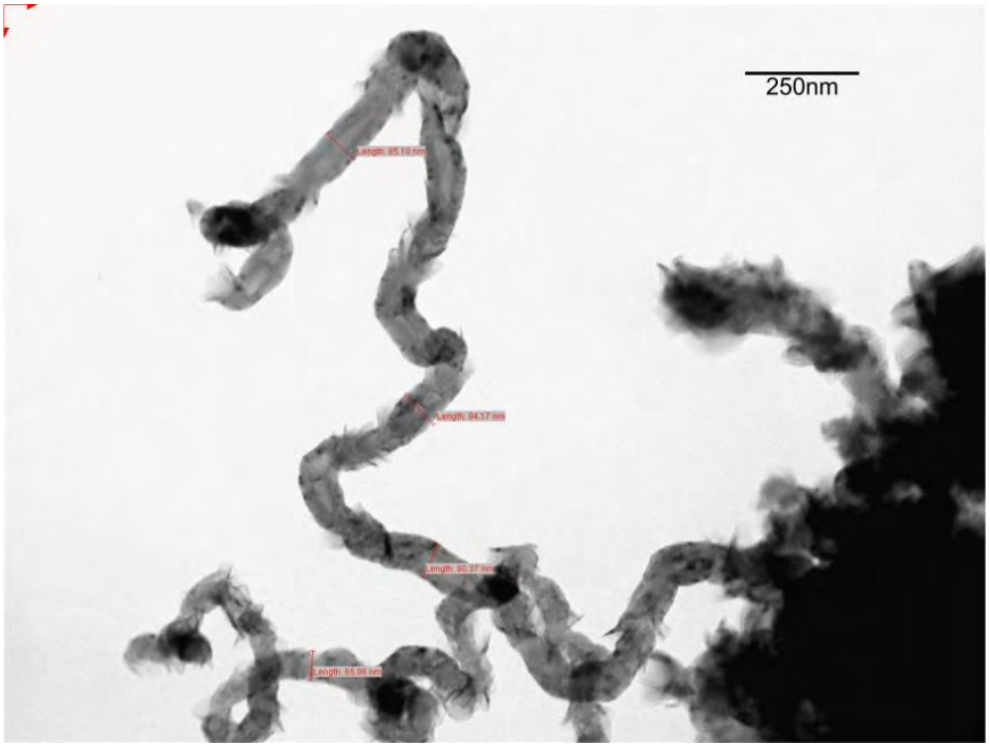

Figure 3-22: Poorly formed tubular structures formed in Experiment C3. This experiment has no amorphous carbon present; with the darker area in the bottom right corner resulting from an increased density of tubular structures.

3.3.5 Results of Experiment C4 (10 Lt/min Hydrogen)

Here, the hydrogen flow rate is increased to 10 Lt/min, and the resulting plasma begins as a large, bright purple glow, gradually changing to the familiar small, orange glow focussed on the aerial tip. In this experiment, the dominant carbon nanostructure present is uneven-walled carbon nanotubes (as shown in Figure 3-23). There is neither any amorphous carbon nor onion-like nanostructures present in the sample. It was observed, when comparing Experiment Set A and Experiment Set B, that the increase in thiophene content seems to delay the growth of ONSs. It is therefore unsurprising that there is no ONS growth in Experiment Set C. Note that a bamboo-like tube, similar to those found in the work by Li *et al.* [**99**] is found in the upper half of Figure 3-23. This is an indication that the reaction temperature may be too high in this particular experiment.

3.4 Experiment Set D (Xylene)

3.4.1 Results of Experiment D0 (0 Lt/min Hydrogen)

In this experiment, the hydrocarbon precursor was changed from ethanol to xylene and no hydrogen was introduced into the system. The plasma began as a bright purple glow, changing

to a brilliant orange. The orange glow appeared to darken during the ten 30s runs which make up the experiment. It was found that the darkening occurred as a result of a tremendous build up of product on the walls of the plasma chamber. In addition to the customary growth on the Nilo K aerial, the product also formed on the edges of the tube exposed to the plasma unlike experiments A, B and C where the product was only formed at the tip of the aerial.

Samples of the product, from both the sides of the chamber and the aerial, were analysed using TEM (Figure 3-24 and Figure 3-25) and it was found that the only nanostructure formed were onion-like nanostructures, along with a small quantity of amorphous carbon.

3.4.2 Results of Experiment D1 (1 Lt/min Hydrogen)

The input parameters for Experiment D1 are: xylene as the hydrocarbon source, 1 Lt/min of hydrogen as the support gas and the Nilo K aerial as the catalyst source. Much like Experiment D0, the plasma began bright purple, changing to a dark orange as the xylene entered the chamber. Again, the walls of the chamber and the portion of the tube were coated with the carbon product. A sample of the product formed on the aerial was taken and analysed utilising TEM. This is shown in Figure 3-26.

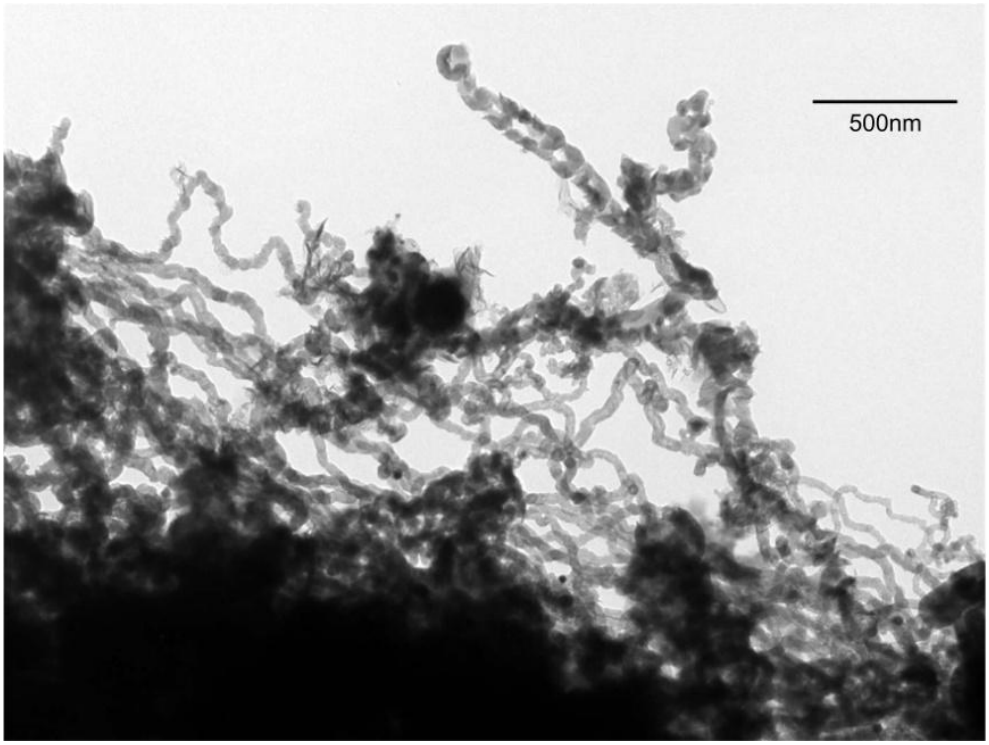

Figure 3-23: Uneven-walled carbon nanotubes formed in Experiment C4. These uneven-walled tubes are found across found throughout the sample.

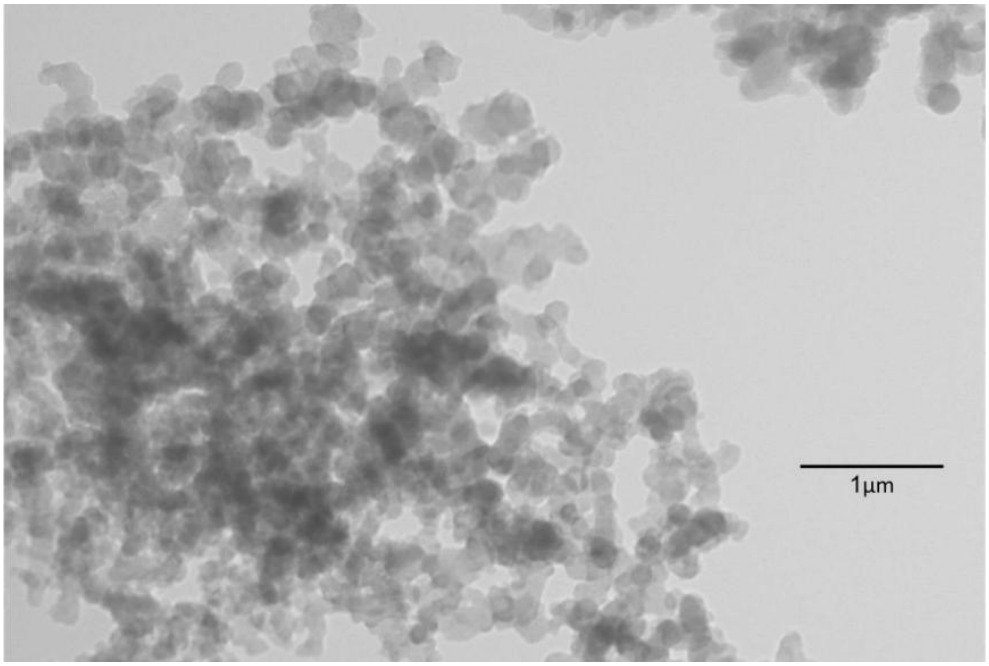

Figure 3-24: TEM micrograph of ONSs formed on the tube in Experiment D0.

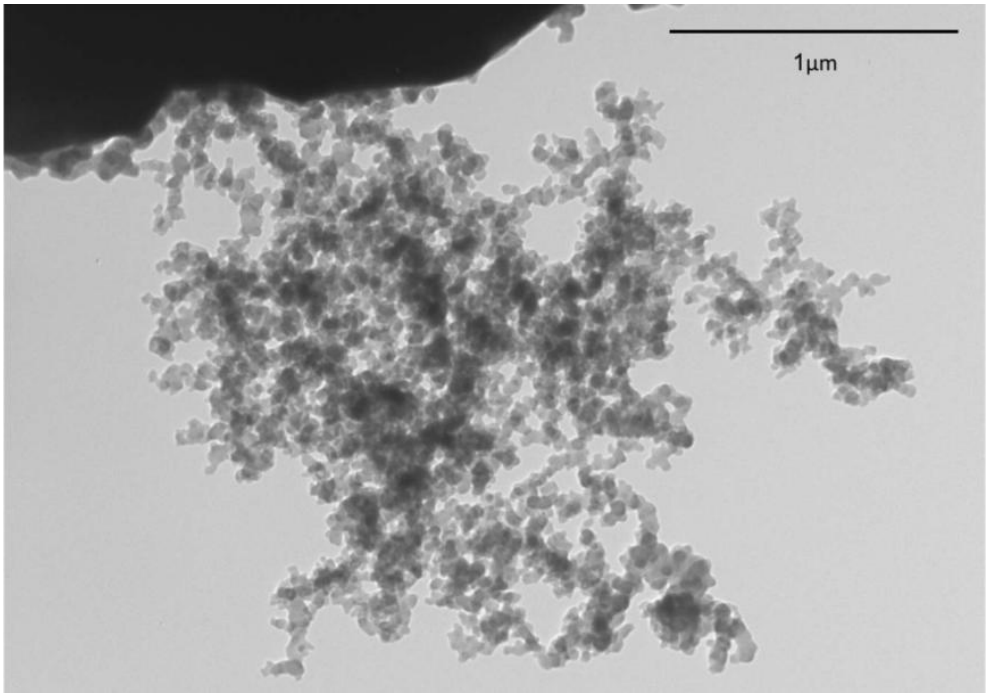

Figure 3-25: ONSs formed on the aerial in Experiment D0. Some amorphous carbon is observed in the upper section of the micrograph.

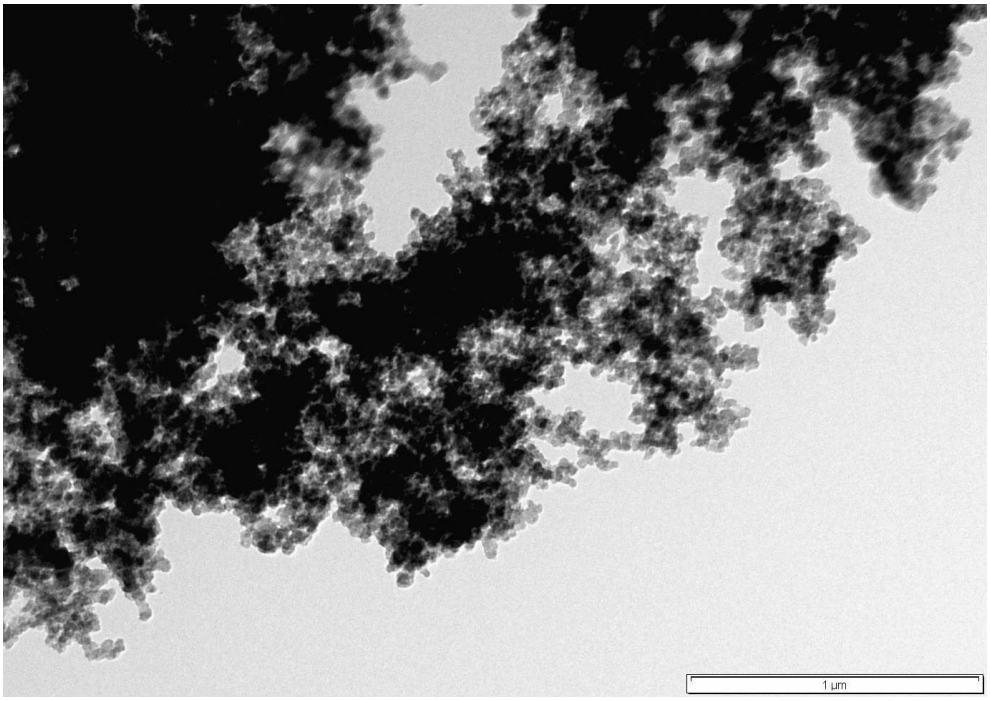

Figure 3-26: Transmission electron micrograph of onion-like nanostructures formed on the aerial in Experiment D1 (scale bar represents 1µm).

3.5 Experiment Set E0 (Toluene)

3.5.1 Results of Experiment E0 – (0 Lt/min Hydrogen)

The hydrocarbon precursor for this experiment is toluene and no support gas is added to the system. Here, the plasma begins bright purple, quickly changing to a dark orange as toluene enters the plasma chamber.

The aerial, plasma chamber and the portion of the tube exposed to the plasma is quickly covered in the product. Transmission electron microscopy reveals that the structures formed are onion-like nanostructures – similar to those found in Experiment set D. These are shown in Figure 3-27. A small quantity of amorphous carbon is found in the sample.

3.5.2 Results of Experiment E1 (1 Lt/min Hydrogen)

1 Lt/min of hydrogen is introduced in the experiment; with the other inputs remaining as in Experiment E0. The plasma again begins as a bright purple, turning dark orange as the hydrogen and toluene enter the system. The plasma is well confined to the aerial tip, but again, the product forms on the aerial, the portion of the tube exposed to the plasma and the side of the plasma chamber.

For this experiment, only the product formed on the aerial tip was analysed (the product from the other parts were not analysed in the interest of saving analysis time as experience showed that there was no discernable difference in the structures collected from Experiments D0, D1 and E0). The TEM analysis showed that, much like Experiments D0, D1 and E0, the only structures formed were ONSs, with a negligible quantity of amorphous carbon. The ONSs formed in this experiment are shown in Figure 3-28 below.

3.5.3 Results of Experiment E2 (5 Lt/min Hydrogen)

The hydrogen flow rate is increased to 5 Lt/min and, once again, the plasma starts bright purple – quickly turning a dark orange. The tube, aerial and plasma chamber is rapidly coated with the product. Analysis of the product formed on the aerial shows that ONSs are again produced in abundance, as shown in Figure 3-29.

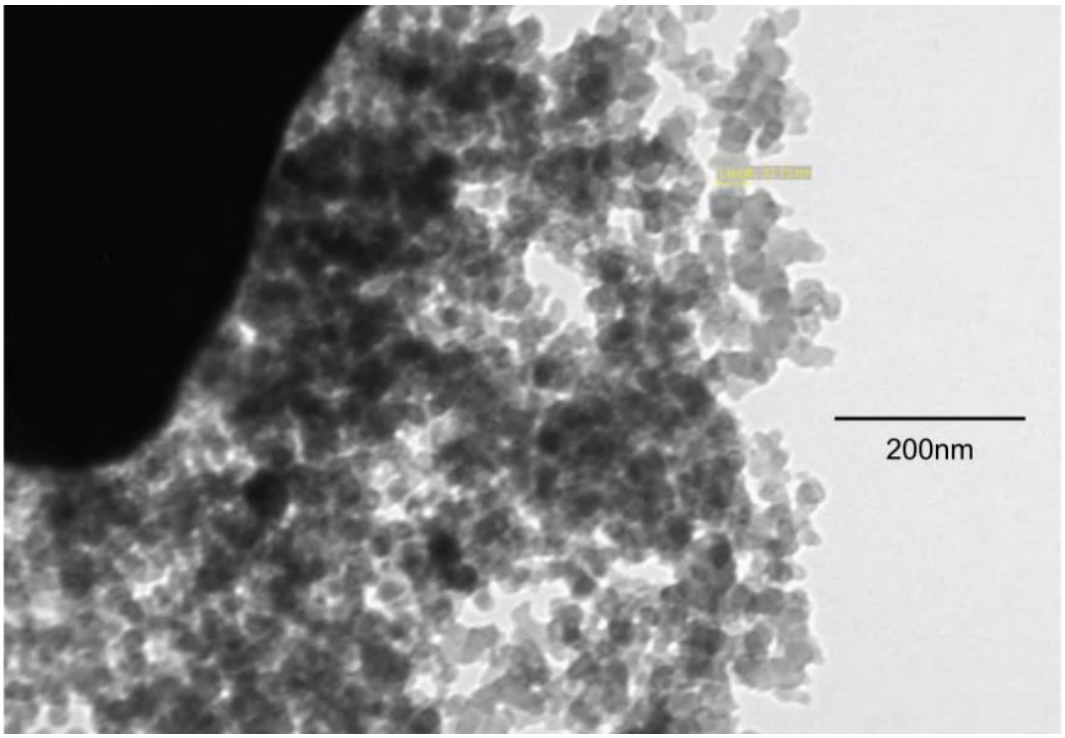

Figure 3-27: Transmission electron micrograph of onion-like nanostructures found in Experiment E0.

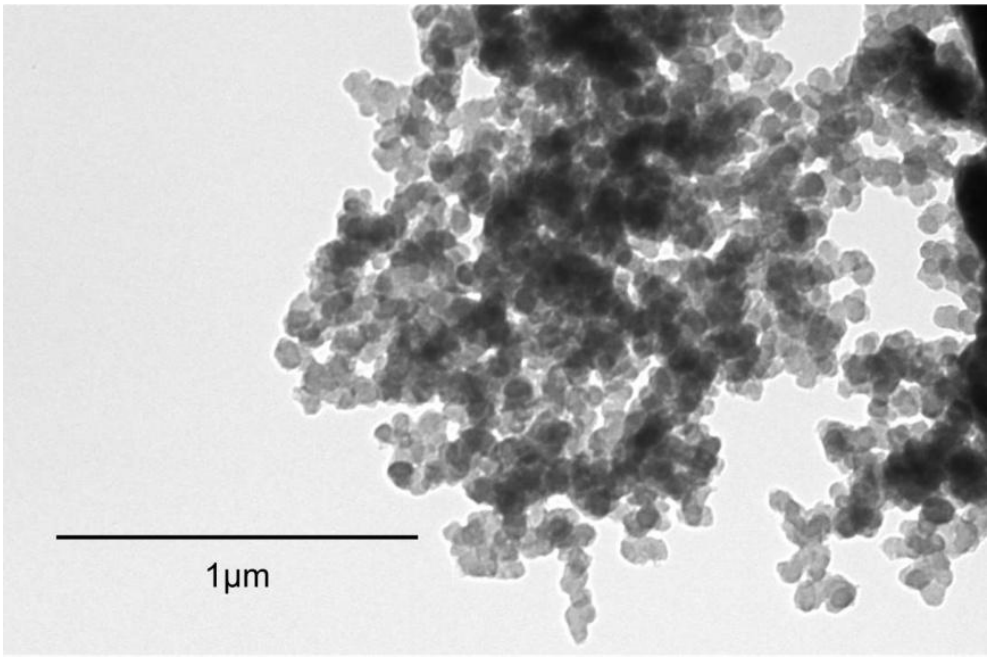

Figure 3-28: Transmission electron micrograph of onion-like nanostructures found when toluene and 1 Lt/min of hydrogen are used as the inputs.

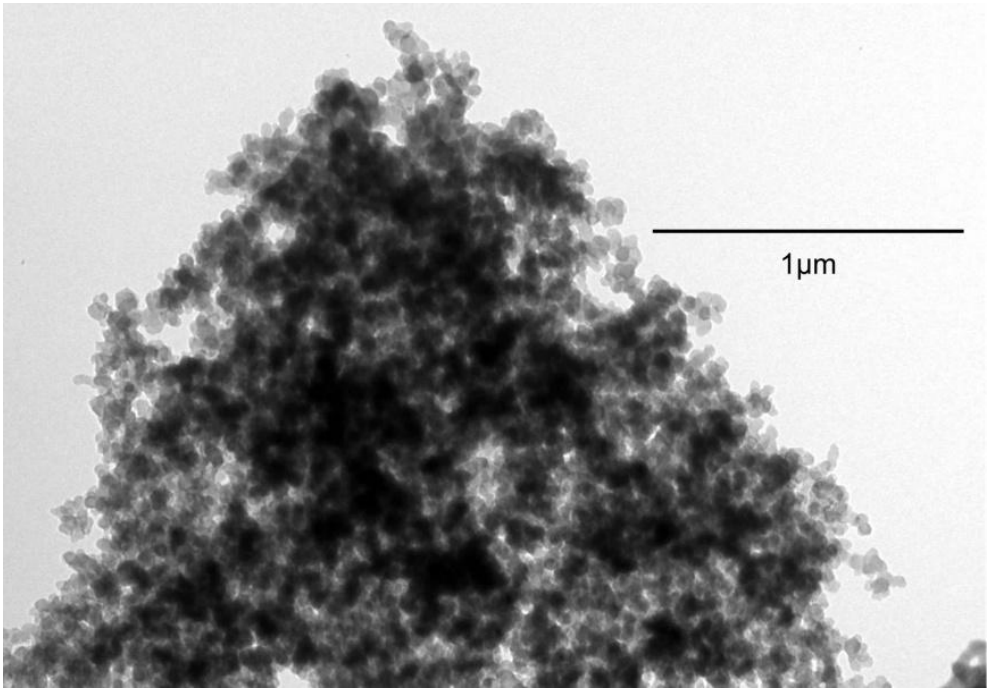

Figure 3-29: Onion-like nanostructures produced in Experiment E2.

3.5.4 Results of Experiment E3 (7.5 Lt/min Hydrogen)

In Experiment E3, the hydrogen flow rate is increased to 7.5 Lt/min. Here, again, the plasma begins as a bright purple glow, before turning a dark orange. The tube, aerial and the sides of the plasma chamber is quickly coated in the deposit, turning the plasma chamber black. TEM analysis of the product formed shows, once again, that ONSs are produced in abundance. The ONSs formed are shown in Figure 3-30.

3.5.5 Results of Experiment E4 (10 Lt/min Hydrogen)

Here, the hydrogen flow rate is increased to 10 Lt/min. Like the other experiments in Set E, the plasma begins bright purple before turning orange. The tube, aerial and plasma chamber are once again coated with the deposit. TEM analysis (Figure 3-31) shows the formation of ONSs.

3.6 Experiment Set F (Ethanol-1.5% Thiophene-1.5% Ferrocene)

3.6.1 Results of Experiment F1 (1 Lt/min Hydrogen)

As discussed earlier, the addition of iron particles in the form of ferrocene is common in the literature. Once the initial analysis was completed, it was decided that the effect of ferrocene on the experiment which „most successfully' produced carbon nanotubes should be investigated. The most successful nanotube experiment, without ferrocene, was Experiment C1 (that is an ethanol-thiophene (1.5% by weight) precursor and H_2 input of 1 Lt/min). Added to these inputs, for this experiment, was 1.5% (by weight) of ferrocene. A typical TEM micrograph of the product formed in this experiment is shown in Figure 3-32.

The tubes, which exhibit uneven walls and variable diameters, are clearly capped by the iron particles. It is apparent, however, that the nanotube yield has increased significantly.

3.7 Summary of Carbon Nanostructure Results

It is evident from the results of the experiments conducted that there exist optimal process inputs for the growth of carbon nanotubes utilising this method; namely the conditions of Experiment C1 (that is, a precursor solution of ethanol with 1.5% thiophene by weight and 1 Lt/min hydrogen). It was observed, in Experiment C1, that smooth-walled carbon nanotubes grow in abundance with significantly reduced quantities of amorphous carbon.

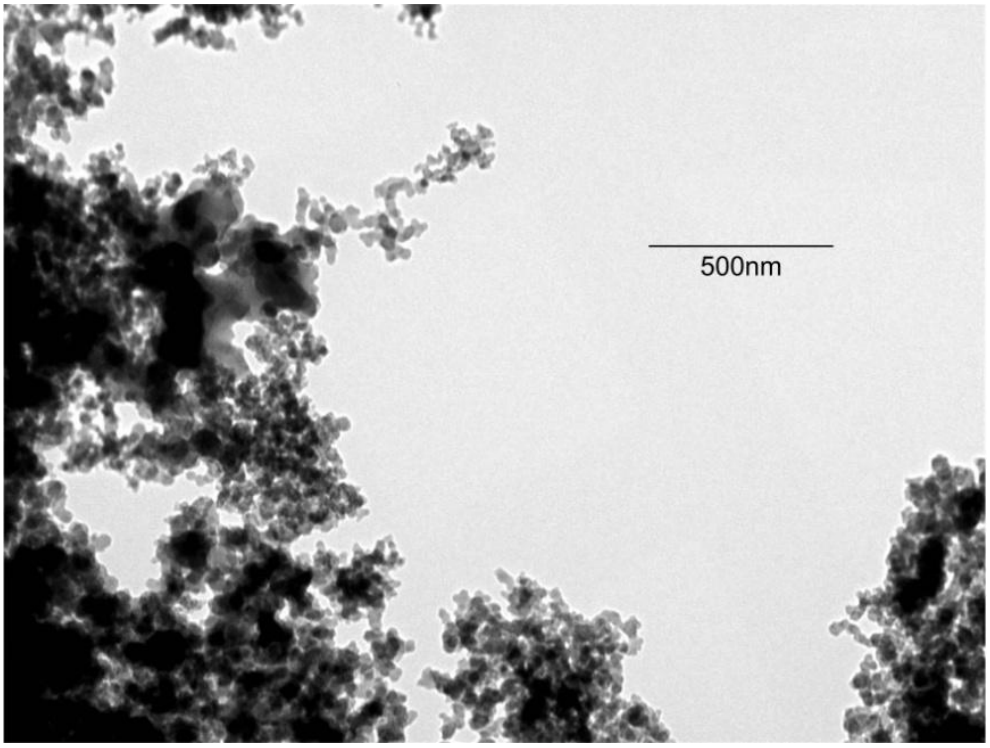

Figure 3-30: Onion-like nanostructures produced with Toluene and 7.5 Lt/min of hydrogen.

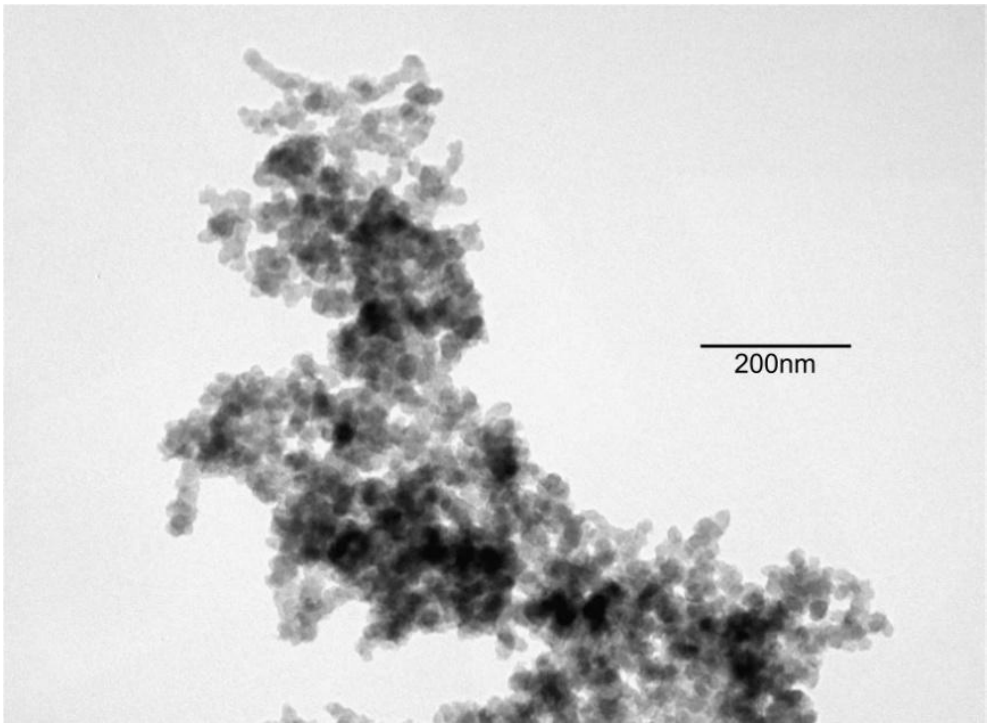

Figure 3-31: Onion-like nanostructures produced in the E4 experiment.

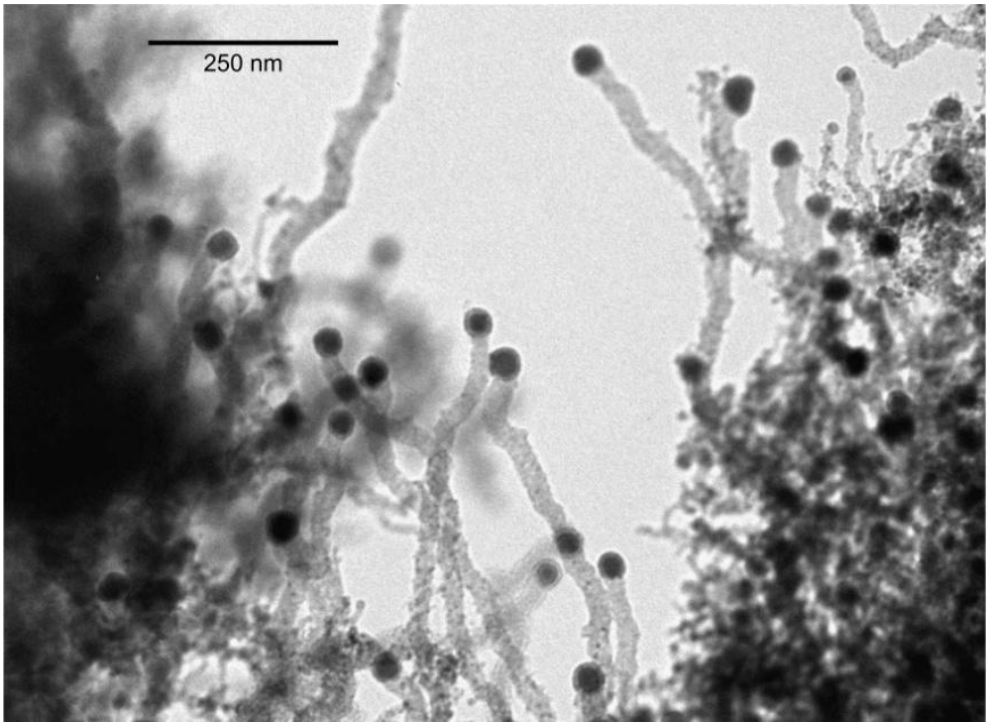

Figure 3-32: Nanotubes grown using ferrocene. The iron particles from the ferrocene are evident on the tips of the poorly formed nanotubes.

In the ethanol based experiments, it was observed that the introduction of an increasing quantity of hydrogen delays the formation of onion-like nanostructures. This could be a result of an increased hydrogen content combining with the oxygen component of ethanol, which then prevents catalytic poisoning by carbon (as suggested by Endo *et al.* [**69**] and Kim *et al.* [**86**]). It was found there was an optimal hydrogen point for the growth of carbon nanotubes (especially in Experiment Sets B and C), beyond which the quality of the grown tubes would suffer. This result is certainly not unexpected as the literature does suggest that too much hydrogen would suppress nanotube growth [**83**] .

Despite increasing the hydrogen flow rate, the toluene and xylene experiments did not show this delaying trend in the formation of onion-like nanostructures. This may be a result of the lack of the removal of the oxygen component in the experiments. It is interesting to note, from the literature, that xylene and toluene have been shown to grow CNTs [**69**,**70**,**72**,**97**] but there had been some additive, such as a species containing oxygen, which could lead to the preferential formation of nanotubes rather than onion-like structures.

The progressive reduction of amorphous carbon by hydrogen was observed across all five experiment sets. This was because hydrogen prevents ‚poisoning' of the catalyst by carbon and promotes the precipitation of graphitised structures from the metallic seeds.

The addition of thiophene in the ethanol-based experiments did indeed promote the growth of carbon nanotubes. This effect was most prominent in Experiment B0, where carbon nanotubes were grown without the explicit addition of hydrogen. Again this was not unexpected from the literature.

The production of a vast quantity of onion-like nanostructures in the toluene and xylene experiments was, however, not anticipated. Especially remarkable was that deposition of the onion-like structures also occurred on the sides of the plasma chamber – unlike the ethanol-based experiments. It has been noticed that although groups have noted the production of ONSs (also referred to as carbon nano-onions), the properties and potential uses of these structures have not been investigated as intensely as CNTs. It was thought that, as there was a vast quantity of onion-like structures produced in this work, there should be some further investigation into these structures. The remainder of this document is, therefore, dedicated to the investigation of the thermal conductivity of onion-like nanostructures.

CHAPTER 4. THERMAL CONDUCTIVITY

4.1 Introduction

Thermal conductivity is a measure of the ability of a material to conduct heat from one part of its body to another. A thermal conductor, such as diamond or carbon nanotubes, is characterised by a high thermal conductivity and is able to quickly conduct heat from its „hot end' to its „cold end', while an insulator, such as a ceramic will conduct heat at a much slower rate. The manner in which heat is conducted through a material depends on the phase of the material. In the solid phase, the energy is transferred via the movement of free electrons and the vibrations of molecules in the lattice structure. In fluids, heat also is transferred by the diffusion of molecules.

There are many applications where the knowledge of the thermal conductivity of a material is required. Such applications are those that require the addition or removal of heat, such as boiler applications, heat exchangers in aerospace vehicles or heat sinks for electronics. Indeed, the fact that more and more components may fit onto electronic circuit boards presents a challenge to systems designers who have to ensure that heat-related failure of components is kept to a minimum or completely eliminated [**109**].

Another application where the thermal conductivity of materials is relevant is that of the development of safe and efficient hydrogen fuel cells for vehicles. It has been observed that, in metal-hydride fuel cells, heat is dissipated during the process of hydrogen uptake and that heat is absorbed as hydrogen is released. Finding materials with good thermal conductivity and hydrogen storage capabilities is, therefore, highly desirable in order to satisfy the needs of the transport industry [**110**].

4.2 Fundamental law of heat transfer

Before discussing the potential application of the knowledge of thermal conductivities relating to carbon nanostructures, it is practical to first consider, briefly, the fundamental law of heat conduction. This law states that the instantaneous rate of heat flow is equal to the product of area, A, of the sample (perpendicular to the flow of heat), the temperature gradient, dT/dx, along the length of the sample and the thermal conductivity, κ, of the sample. These parameters are depicted graphically in Figure 4-1, with the discussion that follows based on the text books by McAdams [**111**], Zemansky [**112**] and Cheremisinoff [**113**].

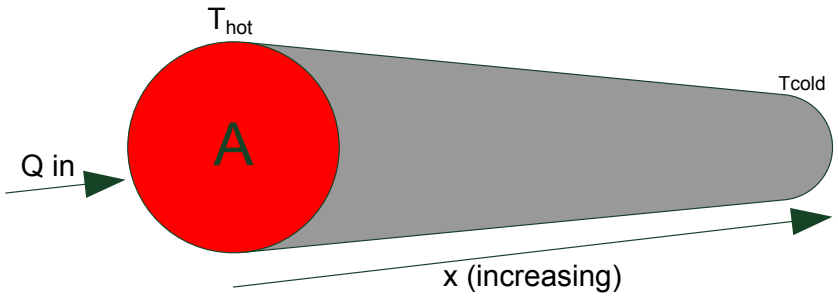

Figure 4-1: Illustration of the parameters relating to the fundamental law of heat conduction.

The fundamental law of heat conduction is also known as Fourier's Law and is mathematically expressed as

$$\frac{dQ}{dt} = -\kappa A \frac{dT}{dx}. \qquad \textbf{(4-1)}$$

In the illustration, heat flows in the direction of increasing *x,* but the temperature of the sample will actually decrease along this path. The negative sign in the equation is thus introduced to ensure that the constant, κ, representing thermal conductivity is positive.

Rearranging Equation (4-1) to make the thermal conductivity, κ, the subject, we obtain:

$$\kappa = -\frac{dQ}{dt}\frac{dx}{dT}\frac{1}{A}. \qquad \textbf{(4-2)}$$

Equation (4-1) refers to heat conduction in the unsteady state - where either the temperature gradient or the heat flow (or both) may be time-dependant. For the steady state, where heat flow and the temperature gradient are independent of time, the heat flow component, *dQ/dt*, is reduced to *Q/t* and the temperature gradient, *dT/dx*, reduces to $(T_2 - T_1)/(x_2 - x_1)$.

Equation (4-1) thus becomes, in the steady state:

$$\frac{Q}{t} = -\kappa A \frac{T_2 - T_1}{x_2 - x_1}. \qquad \textbf{(4-3)}$$

Equation (4-2) in the steady state then becomes:

$$\kappa = -\frac{Q}{t}\frac{x_2 - x_1}{T_2 - T_1}\frac{1}{A}. \qquad \textbf{(4-4)}$$

4.3 Thermal conductivity applications of nanostructures

4.3.1 Thermal management

Carbon nanotubes have been added to materials like epoxy or silicone elastomer to form composites with improved thermal conductivity for potential use in thermal management systems [**114**,**115**]. It has been shown that the addition of just a small quantity of SWNTs can increase the thermal conductivity of the interface material considerably. Biercuk *et al.* [**114**] added 1% SWNT (by weight) to an epoxy and found that the thermal conductivity increased by 70% at 40 K to 125% at room temperature. Biercuk *et al.* also found that the addition of SWNTs is far more effective at increasing the thermal conductivity of the epoxy than carbon fibres; that the nanotubes have larger aspect ratios than the carbon fibres – thus forming an improved „heat-percolation network' which accounted for this increased effectiveness. It has also been shown that an aligned array of CNTs increases the thermal conductivity of an epoxy-nanotube composite significantly when compared to a randomly arranged epoxy-nanotube composite [**116**,**117**]. Similar work has been conducted on micro- and nanostructured diamond fibres **[118-120]**.

4.3.2 Hydrogen storage

High thermal conductivity is also desirable for materials used in hydrogen storage [**110**]. To gain a better understanding of why a high thermal conductivity is desirable, hydrogen storage will be briefly discussed.

Carbon nanotubes, which exhibit good thermal conductivity, have been shown to store hydrogen **[121-123]**. There is, however, much variance in the reported hydrogen uptake perhaps as a result of the presence of impurities in the form of amorphous carbon or other carbon nanostructures, such as fullerenes. Hydrogen uptake as high as 60% H_2 by weight has been reported [**124**]. However, this amount is really anticipated to be much lower at somewhere between 1 and 6% by weight [**110**,**122**,**125**].

Adsorption of hydrogen may occur as a result of chemisorption, where hydrogen is stored within the structure of the nanomaterial by the formation of C-H bonds [**122**], or by physisorption, where the hydrogen molecules are weakly attracted to the surface of the storage material [**110**,**126**]. Molecular mechanics and molecular dynamics modelling [**127**,**128**] has indicated that physisorption of hydrogen is most likely to occur at low temperatures, either near the surface of a carbon nanotube in the interstitial sites in bundles of nanotubes or within the „hollow' of open tubes. The H_2 molecules surrounding the material in these models resemble a cloud (Figure 4-2), at low temperatures [**24**,**129**]. Wu *et al.* [**128**] performed molecular

dynamics simulations on Y-junction tubes at temperatures from 80 K to 300 K and found that an increase of temperature leads to the kinetic energy of hydrogen overpowering the attractive, non-bonding interactions between H_2 and the Y-junction tubes. The hydrogen is thus desorbed from its location near the carbon nanotube. A similar result was obtained by Dodziuk and Dolgonas [**127**] in their models of H_2 physisorption on more conventional nanotubes. In the case of chemisorption, C-H bonds are stable at intermediate temperatures, but these bonds begin to break at higher temperatures (around 600 °C), leading to hydrogen desorption [**122**].

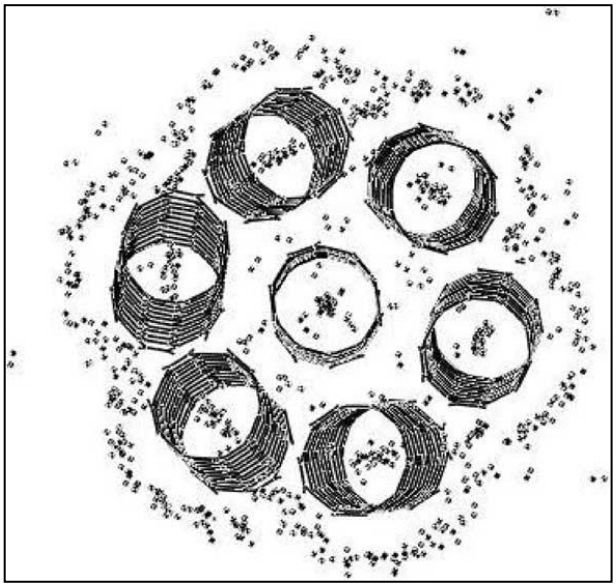

Figure 4-2: A nanotube bundle with hydrogen molecules physisorbed near the surface, within the tube hollows and between adjacent tubes [127**].**

As has been noted above, the temperature has an effect on the adsorption and desorption of hydrogen on carbon nanotubes. If a technique can be found to increase the hydrogen uptake above the 6.5% by weight threshold stipulated by the US Department of Energy for mobile application (lithium doping of graphitic nanofibres has been shown to increase hydrogen uptake of graphitic nanofibres significantly [**130**,**131**]), then the high thermal conductivity of carbon nanotubes certainly make them commercially attractive as the reduced cooling times will lead to faster refuelling. The higher thermal conductivity of carbon nanotubes will also lead to a shorter heating period to facilitate the quicker application of a power boost from the release of extra hydrogen.

It is interesting that, apart from carbon nanotubes, hydrogen storage in a few other carbon nanostructures has been investigated. These structures include the Y-junction tubes [**128**] and graphitic nanofibres mentioned earlier [**130**,**131**]. Also investigated were the „herringbone' fibres [**110**,**132**] and fullerenes [**133**]. The potential use of ONSs for hydrogen storage has,

however, not been thoroughly investigated as yet despite having some desirable properties As a result of the spherical structure, onion-like carbon nanostructures have a relatively large surface area which, in nanotubes, correlates to the quantity of reversibly adsorbed hydrogen [**125**]. In addition to the relatively large surface area, ONSs also have great curvature which is preferable in the physisorption of hydrogen as the curvature of the structure leads an increase in the potential field experienced by the hydrogen molecules when compared to an open, flat surface [**125**]. A study on the catalytic effect that carbon nanomaterials have on hydrogen storage in sodium alanate (a metal-hydride) suggested that the curvature of fullerenes make them a better catalyst for hydrogen storage than other carbon nanostructures like nanotubes and graphene [**133**].

4.4 Measurement methods

There are a few methods used to determine the thermal conductivity of materials, two of which are the „Searle's bar' technique and the „Lee's disk' method. In order to effectively utilise either method, one has to anticipate whether the material under test is either a good or a poor conductor of heat. Searle's bar is suited to the investigation of good conductors, whereas Lee's disk is used to determine the thermal conductivity of poor conductors.

There is, of course, some intuition used when determining which method is suitable for the investigation at hand. A new metal alloy is almost certain to be a good conductor of heat, requiring the use of the Searle's bar method. Ceramics and materials like glass or epoxies will have poor conductivity, thus requiring the Lee's disk method.

4.4.1 Searle's bar

Searle's bar is a useful steady-state technique for determining the thermal conductivity of good thermal conductors. The sample, in the Searle's bar technique, is in the form of a bar which is typically encapsulated by a good thermal insulator to ensure that heat loss to the environment by radiation is limited. The temperature gradient is usually determined by using two thermocouples embedded some distance apart in the bar and the cross-sectional area of the bar is determined by measuring the diameter, *d*, of the bar. An example of the Searle's bar technique is illustrated in Figure 4-3.

One end of the bar will be heated up, either resistively or by some other means such as steam. The other end is left to heat up as a result of the conduction. It is necessary, regardless of the

method of heating[4], to calculate the heat, Q, that flows through the bar in time, t. This may be done by introducing a passing a quantity of water, from a constant-head device, through tubing coiled around the unheated side of the bar. If the flow rate of the water is known then the mass, m, flowing through the tubing in time, t, may be calculated [**134**]. Two additional thermocouples are then used to determine the increase in the temperature of the water as it enters and exits the tubing around the end of the bar.

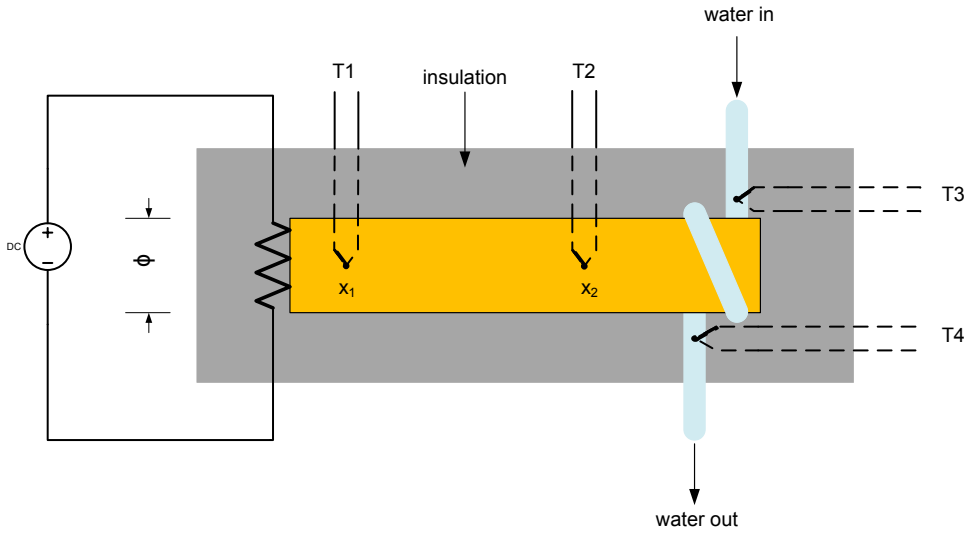

Figure 4-3: Illustration of the Searle's bar technique for good conductors.

Once the system has reached steady-state, the temperatures at thermocouples T_1, T_2, T_3 and T_4 are recorded. Q is calculated from the mass of the water and the temperature difference, $T_4 - T_3$, by the equation

$$Q = mc_w(T_4 - T_3) \qquad \textbf{(4-5)}$$

where c_w is the specific heat capacity of water.

The determined values for A, x_1, x_2, T_1, T_2, Q and t are then substituted into Equation (4-4) to determine the steady-state thermal conductivity of the material.

4.4.2 Lee's disk

In the Lee's disk method, which is illustrated in Figure 4-4, the sample is in the form of a thin disk which is sandwiched between two more disks known to be good conductors such as brass disks. One of the good conductors will, in turn be sandwiched by the sample and a very good

[4] In the case of resistive heating, one may use the power, $P=I^2R$, but one would have to ensure that there is no heat lost from the resistor to the environment.

thermal insulator, while the other conductor will be in contact with a heat source. Occasionally, the heater itself will also be in contact with a third disk made from the good conductor which is capped with a good thermal insulator. All of the brass disks used in the Lee's disk method should be identical. The ‚apparatus' may be held together with a long, thin bolt, to keep all the components in good contact. The entire apparatus may be encapsulated within thermal insulation, but if the thickness-to-area ratio of the sample is kept low then the heat lost to the environment may be assumed to be negligible **[135-137]**.

As the sample is usually very thin, the thermocouples are usually embedded in the brass disks – as close to the sample as possible. It would be possible to insert the thermocouples between the sample and the brass disks, but this would introduce small air-gaps which would reduce the quantity of heat flowing from the brass pieces to the sample. It is therefore assumed that the temperatures determined by the thermocouples approaches that of the sample surfaces. Once the apparatus has been assembled, the heat source is activated and heating continues until the steady-state is reached.

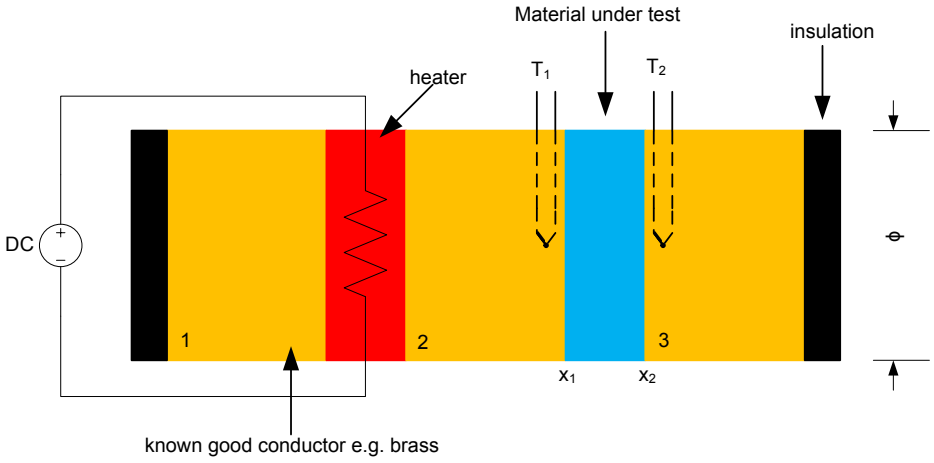

Figure 4-4: Illustration of the Lee's disk technique. Note that the thicknesses of the disks are exaggerated for the purposes of this illustration.

.The area of the disk is calculated from the diameter of the disk, which is easily measured. The temperature gradient across the disk is determined from the thermocouples by $T_2 - T_1$ and the thickness of the disk, dx (which is $x_2 - x_1$). It is now left to determine the heat flow, Q/t, which flows through the system. This is done by first considering the system again at steady-state. The heat flowing from the heater towards the sample through brass disk 2 equals the heat flowing out of brass disk 3 into the insulation. The heat that flows through brass disk 3 is determined in the following manner:

The sample and the other brass disks are removed, leaving just the insulation, the heater and brass disk 3 as shown in Figure 4-5. This solitary brass disk is now heated and the temperature of the disk is monitored using a thermocouple. Once this assembly has reached steady state and the temperature of the disk no longer increased over a period, the heater is removed. The rate at which the disk cools, that is *dT/dt*, is recorded and plotted. A typical plot of temperature versus time is shown in Figure 4-6.

The slope of the temperature versus time plot is determined at the relevant temperature for use in the calculation of the thermal conductivity. The quantity *dT/dt* is thus known, and the heat flow can thus be determined by

$$\left|\frac{dQ}{dt}\right| = mc_b \left|\frac{dT}{dt}\right| \qquad \textbf{(4-6)}$$

where m is the mass of the brass piece and c_b is the specific heat capacity of brass.

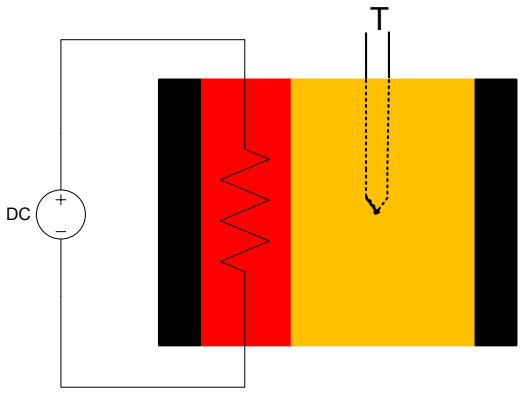

Figure 4-5: Setup used to determine the heat flow in the Lee's disk method.

4.5 Summary

The thermal conductivity of a material is certainly an important and useful property, and carbon nanomaterials with high thermal conductivities may have an important role to play in solving some of the pertinent problems facing the world of electronic manufacturing and equipment, or the world of hydrogen storage for mobile applications. Indeed, it has been observed that carbon nanotubes greatly increase the thermal conductivity of epoxies and silicone elastomers, especially so if the nanotubes are aligned in the direction of the heat flow. The potential for hydrogen storage in carbon nanostructures has also been noted in the preceding discussion.

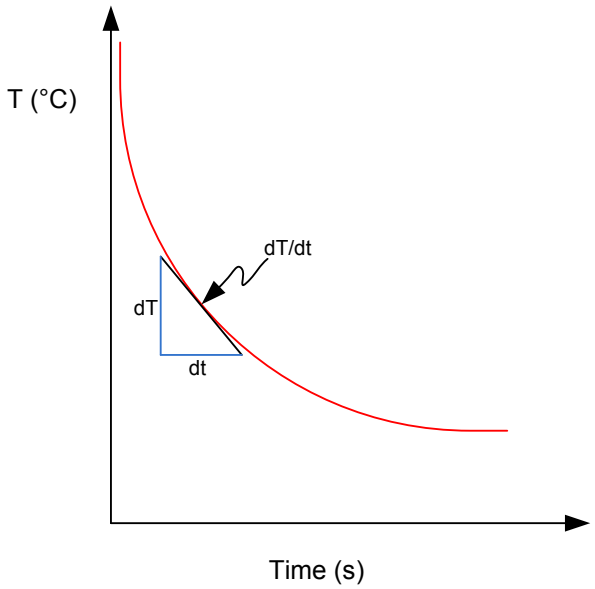

Figure 4-6: Typical shape of the plot of temperature versus time for the cooling of a brass disk.

While numerous investigations have been conducted on carbon nanotubes, fullerenes and graphitic nanofibres, ONSs have, in contrast, not been as thoroughly investigated. It is perhaps a bit fortunate, then, that the PECVD technique discussed in the earlier chapters of this document grows copious quantities of ONSs and therefore presents the opportunity to investigate ONS further, beginning with the thermal conductivity of these structures.

It is anticipated that although the addition of onion-like nanostructures to thermal interface materials, such as thermal grease, will increase the thermal conductivity of the thermal interface material. This increase will is not expected to be as significant as the increase seen with carbon nanotubes. The reason for this anticipated poorer increase is that the ONSs will populate the interface material's matrix in a very different manner. Rather than long, thermally conductive „strands' or ropes, the ONSs will tend to be randomly located throughout the matrix offering local increases in thermal conductivity. Determining the thermal conductivity of ONSs may aid the process of gauging the usefulness of ONSs for use in hydrogen fuel cells compared the CNTs.

A version of the Lee's disk method, similar to that used by Hickson [**135**] and has been used to measure the thermal conductivity of ONSs added to epoxy resin to form a disk. Varying quantities (% wt.) of ONSs was added to the epoxy resin and the thermal conductivities measured. The thermal conductivity of ONSs was compared against similar disks made from the epoxy resin and carbon dust. Further comparisons were made against a control sample made entirely from the epoxy resin.

CHAPTER 5. THERMAL CONDUCTIVITY OF ONION-LIKE NANOSTRUCTURES

A Lee's disk method, similar to that described in Section 4.4.2, was set up to determine the thermal conductivity of ONSs. ONSs were added to a resin-epoxy to produce the sample disks for these experiments. Thermal conductivity measurements were also made on disks made from carbon powder in order to provide a comparison with ONSs.

5.1 Experimental

5.1.1 Samples

The samples, in the form of disks, were prepared by first measuring the required mass of the relevant carbon „additive' and the required mass (4 g) of resin epoxy. The carbon additive was then added to the resin epoxy and stirred thoroughly until a uniform consistency was achieved. Once consistent, eight drops of hardening catalyst (methyl ethyl ketone peroxide) were added to the mixture. The mixture was again thoroughly stirred. The mixture was only transferred to a ring-mould once the viscosity of the mixture had noticeably changed. This was done to reduce the possibility of the carbon species from settling toward the bottom of the mould due to gravity. Once in the ring-mould, the samples were allowed to cure for at least 24 hours. Following removal from the ring-mould, the samples required filing to remove the meniscus that forms during the transfer of the mixture.

Once the processing of the samples was completed, the diameter and the thickness of the samples were measured using a vernier calliper and a micrometer respectively. One of the samples is shown in Figure 5-1.

5.1.2 Setup

The heater is 40 gauge tungsten wire wrapped around a mica disk with a diameter of approximately 30 mm. This wire-wrapped disk was, in turn, sandwiched between two identical mica disks to provide electrical insulation from the rest of the experimental assembly. The heater had a resistance of 10 Ω and was connected to a Topward dual-tracking 6303D DC power supply. An image of the tungsten heater is shown in Figure 5-2.

A solid 30 mm diameter brass cylinder was cut into three 5 mm thick disks, shown in Figure 5-3, weighing 26.81 g. A hole is drilled on the edge of the disk, extending to the centre, for the

thermocouple. Brass has a specific heat capacity of 0.370 J/g·K [**135**] and a thermal conductivity of 109 W/m·K [**138**].

The temperatures at the relevant locations were measured with type T thermocouples (copper-constantan). Type T thermocouples produce an output of 40 μV/K, and this signal requires amplification and cold-junction compensation, for which an AD595AQ thermocouple amplifier, which includes built-in cold-junction compensation is used; each thermocouple is connected to its own AD595AQ [**139**]. The connection of a thermocouple to an AD595AQ is shown in Figure 5-4.

Figure 5-1: Image of an epoxy-carbon sample after curing and filing.

Figure 5-2: Image of the heater, made from tungsten wire wrapped around a mica disk. Two more mica disks, also shown in the image, provide electrical insulation from the rest of the experimental assembly.

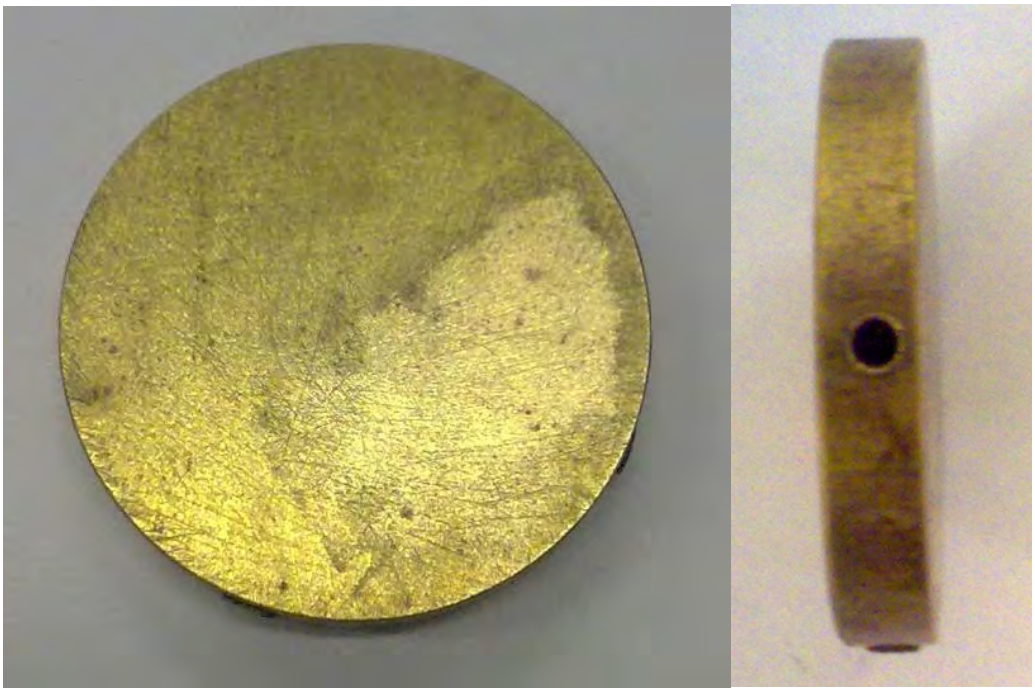

Figure 5-3: Brass disk used in the Lee's disk experiments. The hole for the thermocouple, drilled onto the side of the disk, is shown.

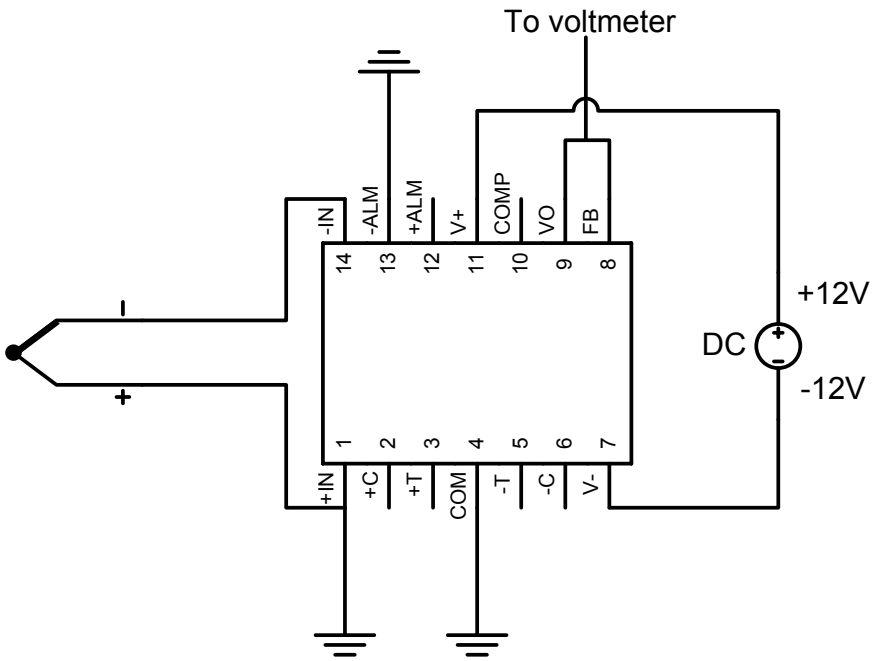

Figure 5-4: Thermocouple interface to AD595AQ thermocouple amplifier. The required voltage supply to the thermocouple amplifier is also shown.

The output from the AD595AQ integrated circuit is 10 mV/°C and connecting the thermocouple to the AD595AQ as shown in Figure 5-4 does not require any further circuitry – providing a simple method to measure the temperature. The output (pin 9) from the AD595AQ and the common (pin 4) is connected to a voltmeter, on which the output is observed. The temperature measured by the thermocouple is simple to calculate from the voltmeter's output display.

The Lee's disk apparatus for these experiments is shown in Figure 5-5. Three identical brass pieces have been used, with the sample sandwiched between the two brass disks towards the left in Figure 5-5. The heater is also sandwiched between two brass disks and shares a brass disk with the sample. In turn, the brass, sample and heater assembly is capped with two pieces of insulting white firebrick. The apparatus is clamped tightly together, firstly to hold everything in place and secondly to provide good thermal contact between the brass, heater and sample. The thermocouples (not shown in Figure 5-5) are inserted into the brass disks that sandwich the sample. The non-junction ends of the thermocouples are connected to the relevant pins of the AD595AQ thermocouple amplifier. The heater is connected to the DC power supply.

Once the apparatus has been installed, the power supply is turned on to a constant 1 A at 9 V. The temperatures of the disks are observed from the AD595AQ voltage output, displayed on the voltmeters. Heating continues until the system has reached steady state determined by no

change in temperature of both disks for a period of 15 minutes. The process of heating the system to steady state usually takes in excess of 4 hours. Once steady state was reached, the temperatures were recorded and the thermal conductivity calculated.

5.1.3 List of experiments

Eleven samples were made for these investigations: a control made entirely from resin; five samples made from as little as 3.5% (by weight) carbon powder content up to 25% carbon powder content and five ONS samples in the same ratios as the amorphous carbon powder samples. The properties of the samples used are summarised in Table 5-1.

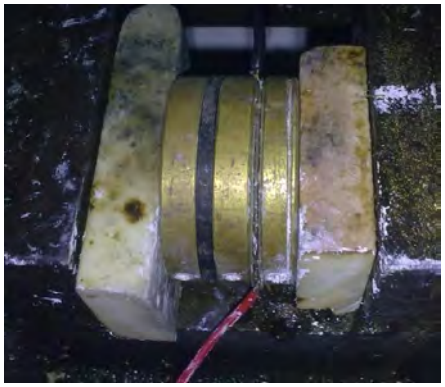

Figure 5-5: The Lee's disk setup for these experiments. The 3 brass disk and the sample can be clearly seen. The heater is connected from this assembly to the power supply via the black and red wires which can be seen.

Table 5-1: Sample properties for the thermal conductivity experiments.

Sample/Experiment Number	Carbon Species	Mass – resin (g)	Mass – Carbon Species (g)	Carbon Species:Resin (%)	Total Mass (g)
Control	-	4.00	0.00	0.00	4.00
GO	Amorphous carbon powder	4.00	0.13	3.25	4.13
G1		4.00	0.25	6.25	4.25
G2		4.00	0.38	9.50	4.38
G3		4.00	0.50	12.50	4.50
G4		4.00	1.00	25.00	5
HO	ONS	4.00	0.13	3.25	4.13
H1		4.00	0.25	6.25	4.25
H2		4.00	0.38	9.50	4.38
H3		4.00	0.50	12.50	4.50
H4		4.00	1.00	25.00	5

5.2 Results

Analysis of thermal conductivity experiments revealed that an increase in either the carbon powder or the ONSs content to a resin disk results in the increase of the thermal conductivity. Indeed, the addition of merely 3.25% (by weight) of ONSs to the epoxy resin results in a thermal conductivity increase of almost 20% when compared against the control sample.

In this chapter, the calculation of the heat flow, *dQ/dt*, and thermal conductivities of the samples are presented.

In order to calculate the thermal conductivity of the samples, the heat flow through the brass disk has to be known. This was done by heating up a single brass disk until it reached the steady state temperature and recording the rate at which the disk cooled.

In the „Lee's disk experiment', the temperature of the cold disk, T_c, is considered to be the working temperature and the heat flow is thus determined at this temperature. For this, the gradient, *dT/dt*, of Figure 5-6 is determined at that point (T_c). It should be noted that once all the experiments were completed there was an obvious variance in T_c. The gradient was therefore determined across the range of T_c rather than at the specific point for each experiment. The region over which *dT/dt* has been determined for these experiments is shown in Figure 5-7.

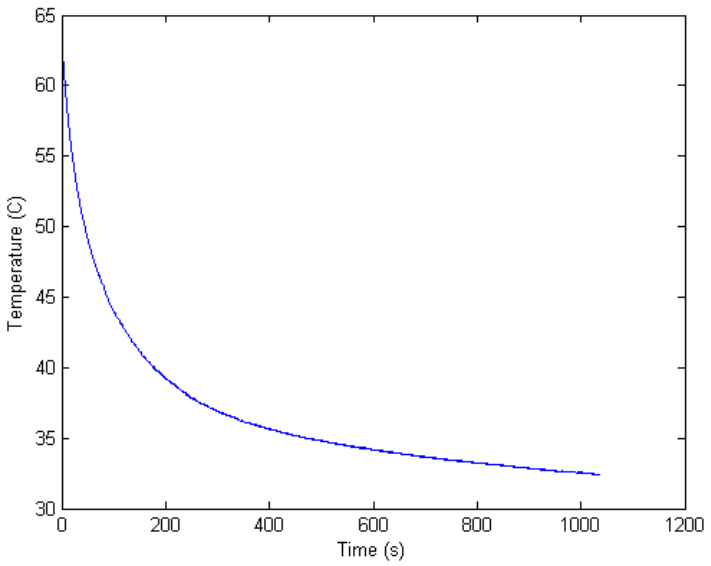

Figure 5-6: Plot of temperature versus time for the cooling of the brass disk from steady state. The plot was generated from the data captured from the data acquisition card, with the sample temperature recorded every 0.1 seconds.

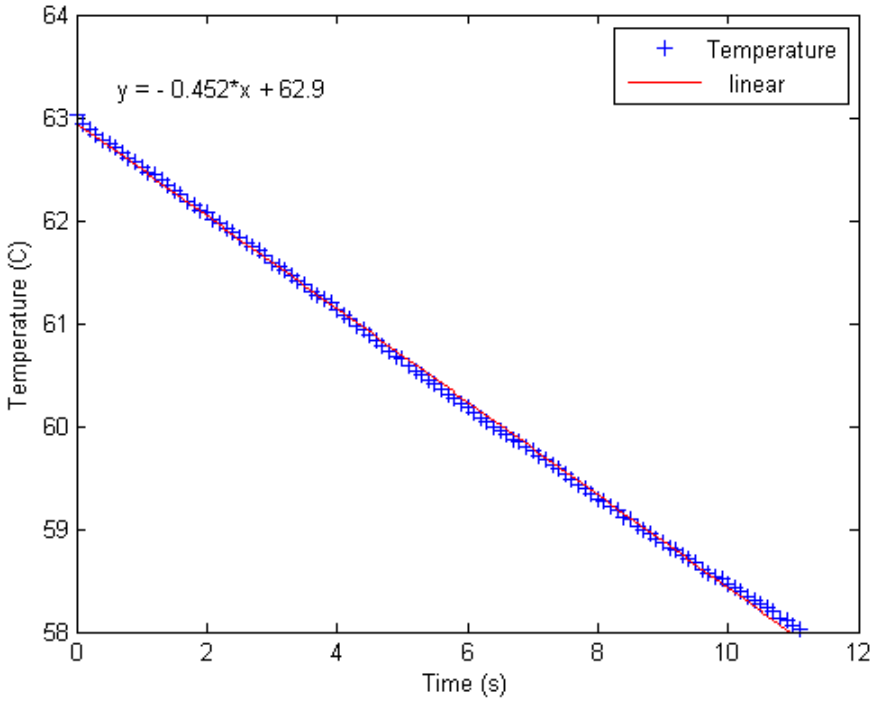

Figure 5-7: Plot of temperature versus time of the brass disk over the range of T_c values obtained from the experiments. The fitted line is used to determine the gradient dT/dt.

A linear fit to the data in Figure 5-7 has a gradient of -0.452±0.001 °C s^{-1}.

The mass of the brass disk, *m*, weighed on a Mettler Toledo PB3002-S digital mass balance is 26.810±0.005 g. The specific heat capacity, c_b, of brass is is 0.370 J/g·°C [**135**].

These values for c_b, *m* and *dT/dt* are substituted into Equation (4-6) to give *dQ/dt* = 4.48 W. This calculated ‚absolute' value for *dQ/dt* has been used in all the experiments.

The measurements for the control sample were:

$$x_2 - x_1 = 1.97 \times 10^{-3}\ m$$
$$A = 6.83 \times 10^{-4}\ m^2$$

At steady state, the temperature difference was $dT = -65.7$ K.

Substituting all of these values into Equation (4-4) reveals that $\kappa_{control}$ is 0.197 ± 0.007 W/m·K.

These calculations were repeated for the remaining samples, and the data plotted in Figure 5-8.

The results are summarised in Table 5-2.

Table 5-2 lists the results of all eleven thermal conductivity experiments, and it is immediately apparent that the thermal conductivity increases with even as little as 0.13 g of carbon powder or ONS. As may be expected, the addition of onion-like nanostructures to resin results in a

greater increase in thermal conductivity than the addition of carbon powder. The data for thermal conductivity listed in Table 5-2 is plotted in Figure 5-8 (the solid lines in Figure 5-8 are included merely to guide the eye and do not represent a fitted or theoretical curve). Again, it is clear from the data in Table 5-2 and the plots of Figure 5-8 that the thermal conductivity of the samples increases with an increase in the additive carbon powder or ONSs content.

Table 5-2: Summary of Thermal Conductivity Results.

Experiment	**x_2-x_1 (m)**	**A (m^2)**	**dT (°K)**	**κ (W/m·K) ±0.007**
Control	1.97E-03	6.83E-04	65.7	0.197
GO	2.09E-03	6.88E-04	66.0	0.206
G1	2.08E-03	6.77E-04	58.8	0.234
G2	2.18E-03	6.83E-04	58.8	0.243
G3	2.14E-03	6.88E-04	53.4	0.261
G4	2.14E-03	6.79E-04	46.1	0.306
HO	2.05E-03	6.97E-04	56.9	0.232
H1	1.98E-03	6.79E-04	50.1	0.261
H2	1.97E-03	6.83E-04	48.1	0.269
H3	2.14E-03	6.79E-04	49.1	0.288
H4	2.04E-03	6.97E-04	38.8	0.338

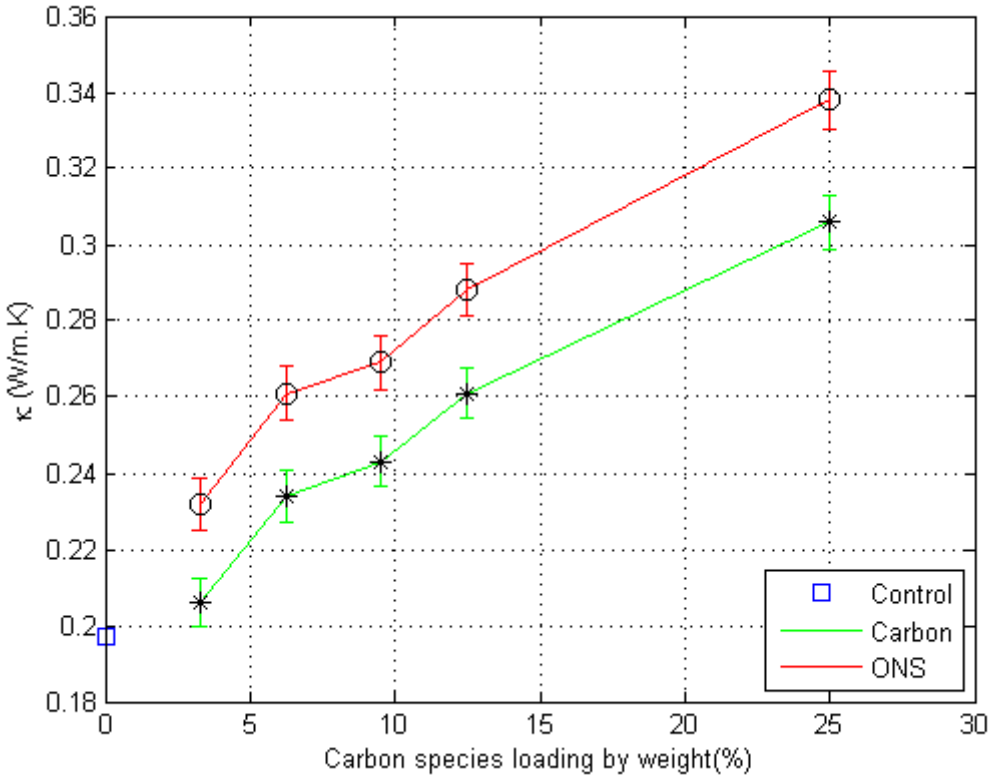

Figure 5-8: Plot of thermal conductivity versus additive content. The data points are joined by solid lines for each carbon species in order to guide the eye.

An almost a constant offset between the thermal conductivities of the carbon powder and the ONSs at corresponding content levels is observed in Figure 5-8. The actual differences are listed in Table 5-3. It is seen that there is a small variance of this „offset'.

The behaviour of the ONS conductivity compared to the conductivity of the carbon power is revealed by analysing the percentage increase in the thermal conductivity of ONS compared to carbon powder at the same carbon loading levels.

From the data listed in Table 5-3 and Figure 5-9, it is seen that the percentage increase in the thermal conductivity of the ONSs compared to carbon powder shows an initial decrease from 12.62% at level 0 to 10.34% at 12.5% at level 3 before a slight increase (from 10.34% to 10.46% between levels 3 and 4). The percentage increase in κ is listed in Table 5-3 and plotted in Figure 5-9 for each additive level. The solid line in the figure serves only to guide the eye and does not represent a fit.

Table 5-3: Table Showing the Calculation of the Difference between κ_{ONS} and κ_{Carbon_powder}.

Level Identifier Number[5]	Additive Content Level (%)	κ_{ONS} (W/m·K)	κ_{Carbon_powder} (W/m·K)	$\kappa_{ONS} - \kappa_{Carbon\_powder}$ (W/m·K)	Increase of κ_{ONS} versus κ_{carbon_powder} (%)
0	3.25	0.232	0.206	0.026	12.62
1	6.25	0.261	0.234	0.027	11.53
2	9.50	0.269	0.243	0.026	10.70
3	12.50	0.288	0.261	0.027	10.34
4	25.00	0.338	0.306	0.032	10.46

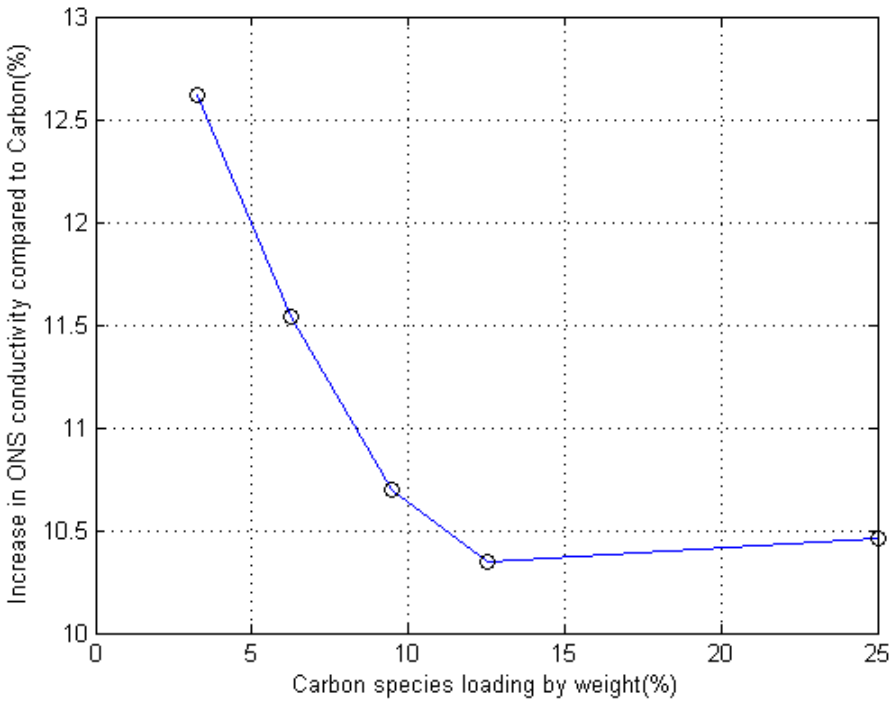

Figure 5-9: Percentage increase in thermal conductivity of ONS compared to carbon powder versus the additive content of the sample.

[5] Level identifier numbers have been introduced to ease the comparison of the percentage increase analysis.

It certainly would be interesting to obtain a few more data points between additive levels of 12.5% and about 50% to determine if this increasing trend is a behavioural trend or merely the result of potential anomalies in either of the level 4 samples.

Figure 5-10 shows the percentage increase for both carbon species compared to that of the control sample. Again, the solid lines merely provide a guide for the eye. With regard to the ONSs, there is a 20% increase in the thermal conductivity, when compared to the control sample, with the addition of as little as 4% (by weight) of ONSs to the resin, and a 50% increase in the thermal conductivity with the addition of just a little less than 15% (by weight) of ONSs.

To roughly predict the thermal conductivity of a disk made entirely of ONSs, the contribution of the ONS to the total mass of the sample has been calculated (Table 5-4) and κ plotted in Figure 5-11. The solid line is a fit to the data points and is extrapolated to reveal that the expected thermal conductivity of a disk made entirely from ONSs to be 0.740 W/m·K.

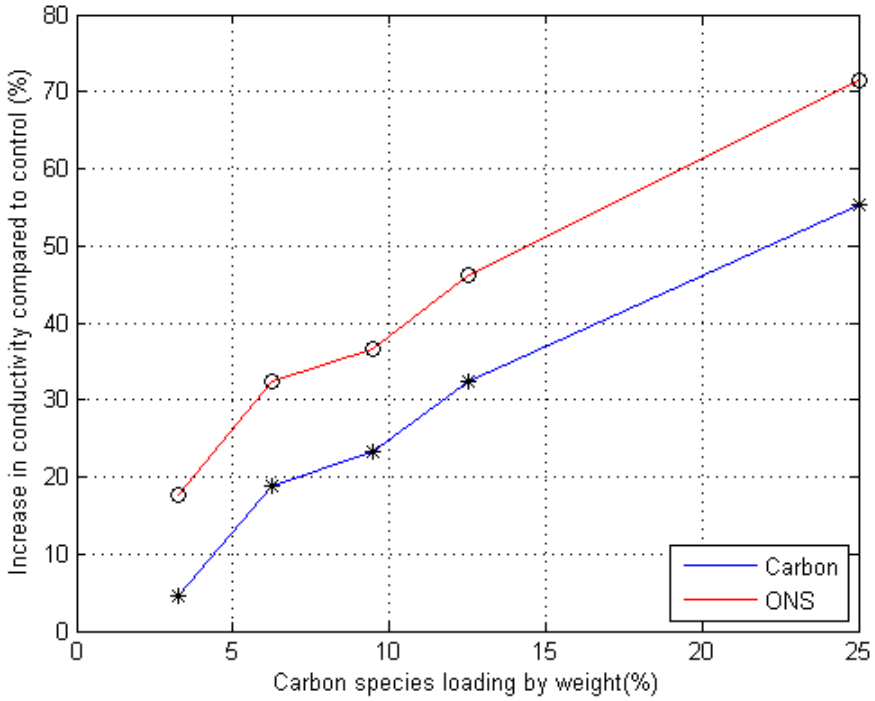

Figure 5-10: Plot of the percentage increase in thermal conductivity of ONSs and carbon powder versus the additive content.

Table 5-4: Contribution of ONSs to the Total Mass of the Samples.

Experiment	Mass ONS (g)	Total Sample Mass (g)	Contribution of ONS to Total Mass (%)	κ (W/m·K)
Control	0.00	4.00	0.00	0.197
H0	0.13	4.13	3.15	0.232
H1	0.25	4.25	5.88	0.261
H2	0.38	4.38	8.68	0.269
H3	0.50	4.50	11.1	0.288
H4	1.00	5.00	20.0	0.338

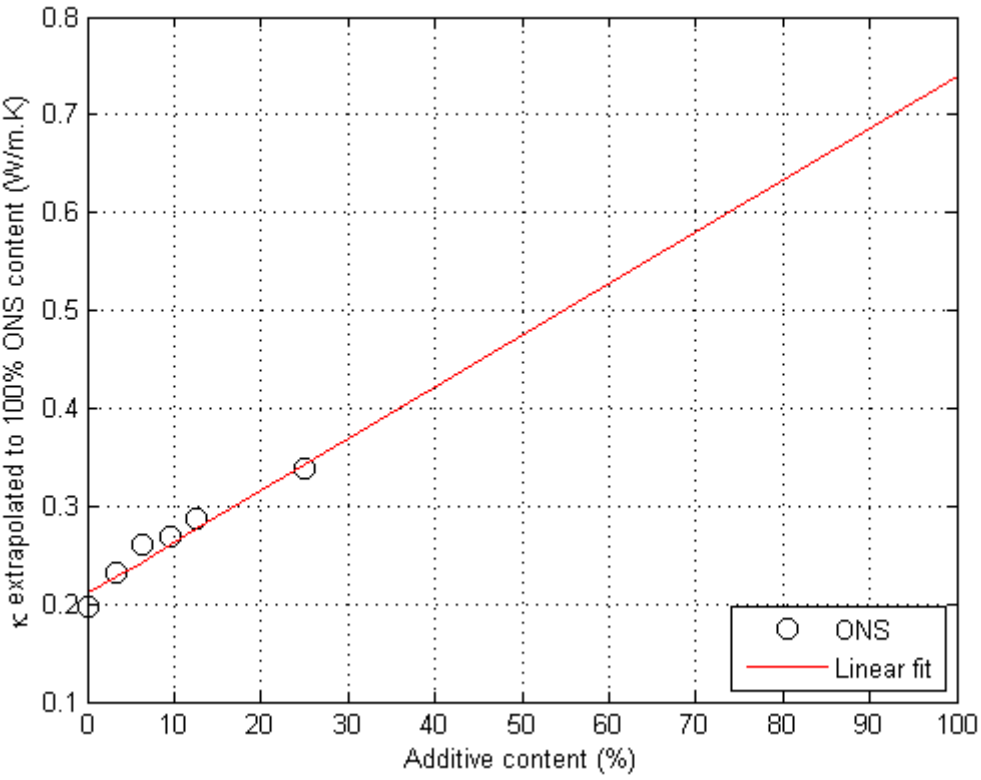

Figure 5-11: Linear fit for ONS thermal conductivity versus percentage content.

This predicted value of 0.740 W/m·K is, however, most likely to be a lower limit for the thermal conductivity of an „ONS only' sample as the thermal conductivity is likely to increase further as more-and-more ONSs replace the epoxy-resin in the matrix, resulting in a decrease in the influence of the resin on the thermal conductivity of the sample. For this particular investigation, it would have been best to keep the mass of the entire sample constant at 4 g, rather than keeping the resin content constant at 4 g, but unfortunately, the viscosity of the resin meant that as more of the ONSs were added the resin-ONS mixture became almost impossible to stir to achieve any form of consistency.

It is evident that the thermal conductivity of the resin-epoxy is increased by the addition of carbon powder, but an even more significant increase is observed by adding ONSs to the epoxy-resin. The thermal conductivity of the ONSs initially increases by more than 12% when compared to carbon powder, but this percentage increase itself starts to decrease as the loading levels increase. The thermal conductivity of an ONS-loaded disk increases by as much as 20% at a loading level of 3.23% by weight and by as much as 70% at a loading level of 25% by weight. This is quite a significant increase and actually lends some support to the suggestion that ONSs could be used to improve the thermal conductivity of thermal interface materials. The thermal conductivity of a pure ONS disk has been predicted to be about 0.740 W/m·K.

CHAPTER 6. CONCLUSIONS AND FUTURE WORK

It was the intention of this work to go some way in characterising the PECVD method that had been developed in-house in terms of mapping the optimal points for given inputs for the production of carbon nanotubes. Most of the experiments on the production of carbon nanotubes showed that although this method can produce carbon nanotubes, the grown structures are typically affected by poor structure or the proliferation of amorphous carbon. Onion-like carbon nanostructures were found to form by changing the carbon precursor, with the growth of these onion-like far exceeding that of carbon nanotubes.

In determining the optimal points for the production of carbon nanotubes, it was clear that the inputs would have a tremendous effect on the output structures. The introduction of hydrogen to the ethanol based experiments first removed amorphous carbon and delayed the growth of onion-like nanostructures. However, too much hydrogen, lead to a decrease in nanotube quality. The growth of carbon nanotubes was certainly promoted with the addition of just a small quantity of thiophene to the ethanol. The best results for carbon nanotubes were obtained in Experiment C1, where smooth-walled carbon nanotubes grow in abundance with significantly reduced quantities of amorphous carbon.

Unfortunately, however, the mass of carbon nanotubes grown is rather minute. A 5 minute long run of Experiment C1 may have produced sufficient tubes to visibly coat the aerial, but because nanotubes are so light the mass could not be determined. Ultimately, it would appear that this technique may not be suitable for the growth of abundant quantities of carbon nanotubes. It would be interesting to observe the effect of increasing the area of the catalyst exposed to the plasma. This would require some redesign of the plasma chamber and the aerial stand. This will most likely cause an increase in the quantity of carbon nanotubes grown.

The onion-like structures, on the other hand, grew in relatively copious quantities. A single experiment would typically produce a few hundred milligrams of onion-like structures (which is certainly remarkable when compared to the mass of nanotubes grown). It is somewhat fortunate that this method does produce such a generous quantity of onion-like structures as it presents the opportunity for the investigation of their properties.

It is evident from the data obtained from the Lee's disk technique that the addition of ONSs to an epoxy-resin results in a significant increase in the thermal conductivity even at levels as low as 3.25% ONS by weight. The thermal conductivity of the ONSs has been predicted to be 0.740 W/m·K. This is suspected to be a lower limit as the thermal conductivity is expected to increase

as the resin-epoxy ceases to occupy the space between the ONSs. The thermal conductivity of the ONSs is nowhere nearly as high as that of CNTs measured at 3000 W/m·K for a single MWNT [**140**].

When assessing the PECVD process used here, one must consider that just a few of the parameters have been analysed and ‚optimised' and there remain other parameters that should also be looked at before we can draw firm conclusions of the process.

Firstly, a quartz plasma chamber and tube were procured but initial attempts to incorporate them into this system were unsuccessful as a result of a few leaks here and there. If these leaks can be fixed it would be possible to run the experiments for a far longer duration than is currently possible.

One parameter is certainly the effect of the temperature of the plasma, which may be controlled by adjusting the power of the microwave oven. The suspicion is that, in Experiments C2 to Experiment C4, the reaction temperature is perhaps a bit too high – which results in the deformation of the tubes. Attempts to construct a Langmuir probe to measure the temperature of the plasma were made, but were ultimately beset with problems such as the introduction of air-leaks into the system which had a knock-on effect on the plasma itself. Proper integration of the Langmuir probe would require some redesign of the plasma chamber and tube, but the results may justify the expended effort.

Another parameter would be the effect of pressure – while the pressure is directly affected by the flow rates of hydrogen and the precursor, there is currently no measure of the pressure within the plasma chamber. The pressure itself may also be adjusted by controlling the pumping speed, or even including more pumping stages (such as adding a diffusion or turbo-molecular pump to drive the pressure down even further). As with temperature, is would certainly be interesting to observe the effect that pressure has on the output structures of this particular PECVD system.

It would also be interesting to investigate whether the nanotube yield could be increased by exposing a larger area of catalyst to the plasma and dissociated precursor, although this may require the redesign of the aerial or this could be accommodated in the redesign of the tube and chamber when incorporating the Langmuir probe into the system. This investigation looked at just a few parameters and there are many changes that could be made to provide a more comprehensive look at this system. A hydrogen-argon mixture may be introduced as the support gas, it may be worthwhile looking at the effect of adding thiophene and/or ferrocene to toluene and xylene has on the nanoproducts and, even further, hydrocarbons other than toluene and xylene may be used. One could even try to slightly heat the precursor in its container prior to the

introduction into the plasma chamber. There remain numerous experimental scenarios that could be modified which could have a significant impact of the products of this PECVD system.

The investigation of the thermal conductivity of ONS is merely the first step in investigating the properties of these structures. It may be worthwhile for other pertinent properties of these structures to be investigated such as the electrical conductivity, the thermoelectric properties of a bulk sample of ONSs.

REFERENCES

[1] D Coetsee, "Experiments in Thin Film Deposition: Plasma-Based Fabrication of Carbon Nanotubes and Magnesium DiBoride Thin Films," University of KwaZulu-Natal, Durban, MScEng Dissertation 2004.

[2] S.R. Singh and A.L.L. Jarvis, "Microwave plasma-enhanced chemical vapour deposition growth of carbon nanostructures," *South African Journal of Science*, vol. 106, no 5/6, Art #183, 2010.

[3] S Iijima, "Helical microtubules of graphitic carbon," *Nature*, vol. 354, pp. 56-58, 1991.

[4] M.S. Dresselhaus, G. Dresselhaus, and R. Saito, "Physics of carbon nanotubes," *Carbon*, vol. 33, no. 7, pp. 883-891, 1995.

[5] N. Hamada, S.-I. Sawada, and A. Oshiyama, "New One-Dimensional Conductors: Graphitic Microtubules," *Physical Review Letters*, vol. 68, no. 10, pp. 1579-1581, 1992.

[6] M. Kociak, A.Y. Kasumov, S. Guéron, B. Reulet, I.I. Khodos, Y.B. Gorbatov, V.T. Volkov, L. Vaccarini, and H. Bouchiat, "Superconductivity in Ropes of Single-Walled Carbon Nanotubes," *Physical review Letters*, vol. 86, no. 11, pp. 2416-2419, 2001.

[7] S. Iijima and T. Ichihashi, "Single-shell carbon nanotubes of 1-nm diameter," *Nature*, vol. 363, pp. 603-605, 1993.

[8] Y. Saito, M. Inagaki, H. Sinohara, H. Nagashima, M. Ohkohchi, and Y. Ando, "Yield of fullerenes generated by contact arc method under He and Ar: dependence on gas pressure," *Chemical Physics Letters*, vol. 200, pp. 643-648, 1992.

[9] N. Sano, H. Wang, M. Chhowalla, I. Alexandrou, and G.A.J Amaratunga, "Synthesis of carbon 'onions' in water," *Nature*, vol. 414, pp. 506-507, 2001.

[10] O.T. Heyning, L. Kouwenhover, P. Bernier, and M. Glerup, "A low cost method for the synthesis of carbon nanotubes and highly Y-branched nanotubes," *Chemical Physics Letters*, vol. 409, pp. 43-47, 2005.

[11] J.-M. Ting and J.B.C. Lan, "Beaded carbon tubes," *Applied Physics Letters*, vol. 75, no. 21, pp. 3309-3311, 1999.

[12] S.-S. Hou, D.-H. Chung, and T.-H. Lin, "High-yield synthesis of carbon nano-onions in counterflow diffusion flames," *Carbon*, vol. 47, pp. 938-947, 2009.

[13] P.G. Collins and P. Avouris, "Nanotubes for Electronics," *Scientific American*, vol. 283, pp. 62-69, 2000.

[14] J.W.G. Wildöer, L.C. Venema, A.G. Rinzler, R.E. Smaller, and C. Dekker, "Electronic structure of atomically resolved carbon nanotubes," *Nature*, vol. 391, pp. 59-62, 1998.

[15] J.W. Mintmire, B.I. Dunlap, and C.T. White, "Are Fullerene Tubules Metallic?," *Physical Review Letters*, vol. 68, no. 5, pp. 631-634, 1992.

[16] [Online]. http://www.uni-konstanz.de/sfb513/abstracts/A7.html.en

[17] [Online]. http://www.photon.t.u-tokyo.ac.jp/~maruyama/fticr/ft-icr.html

[18] Z.K. Tang, L. Zhang, N. Wang, X.X. Zhang, G.H. Wen, G.D. Li, J.N. Wang, C.T. Chan, and P. Sheng, "Superconductivity in 4 Angstrom Single-Walled Carbon Nanotubes," *Science*, vol. 292, pp. 2462-2465, 2001.

[19] M.M.J. Treacy, T.W. Ebbesen, and J.M. Gibson, "Exceptionally high Young's modulus observed for individual carbon nanotubes," *Nature*, vol. 381, pp. 678-680, 1996.

[20] F. Li, H.M. Cheng, S. Bai, G. Su, and M.S. Dresselhaus, "Tensile strength of single-walled carbon nanotubes directly measured from their macroscopic ropes," *Applied Physics Letter*, vol. 77, pp. 3161-3163, 2000.

[21] C. Zamora-Ledezma, L. Añez, J. Primera, P. Silva, S. Etienne-Calas, and E. Anglaret, "Photoluminescent single wall carbon nanotube-silica composite gels," *Carbon*, vol. 46, pp. 1253-1255, 2008.

[22] Y. Ohno, S. Kishimoto, and T. Mizutani, "Photoluminescence of single-walled carbon nanotubes in field-effect transistors," *Nanotechnology*, vol. 17, pp. 549-555, 2006.

[23] W. de Heer, A. Châtelain, and D. Ugarte, "A Carbon Nanotube Field-Emission Electron Source," *Science*, vol. 270, pp. 1179-1180, 1995.

[24] A.C. Dillon, K.M. Jones, T.A. Bekkedahl, C.H. Klang, D.S. Bethune, and M.J. Heben, "Storage of hydrogen in single-walled carbon nanotubes," *Nature*, vol. 386, pp. 377-379, 1997.

[25] C. Liu, Y.Y. Fan, M. Liu, H.T. Cong, H.M. Cheng, and M.S. Dressulhaus, "Hydrogen storage in Single-Walled Carbon Nanotubes at Room Temperature," *Science*, vol. 286, pp. 1127-1129, 1999.

[26] P. Chen, X. Wu, and K.L. Tan, "High H2 Uptake by Alkali-Doped Carbon Nanotubes Under Ambient Pressure and Moderate Temperatures," *Science*, vol. 285, pp. 91-93, 1999.

[27] D. Ugarte, A. Châtelain, and W.A. de Heer, "Nanocapillarity and Chemistry in Carbon Nanotubes," *Science*, vol. 274, pp. 1897-1899, 1996.

[28] S.J. Tans, A.R.M. Verschueren, and C. Dekker, "Room-temperature transistor based on a single carbon nanotube," *Nature*, vol. 393, pp. 49-52, 1998.

[29] W.B. Choi, J.U. Chu, K.S. Jeong, E.J. Bae, J.-W. Lee, J.-J. Kim, and J.-O. Lee, "Ultrahigh-density nanotransistors by using selectively grown vertical carbon nanotubes," *Applied Physics Letters*, vol. 79, no. 22, pp. 3696-3999, 2001.

[30] T. Rueckes, K. Kim, E. Joselevich, G.Y. Tseng, C.-L. Cheung, and C.M. Lieber, "Carbon Nanotube-Based Nonvolatile Random Access Memory for Molecular Computing," *Science*, vol. 289, pp. 94-97, 2000.

[31] M. Rinkio, A. Johansson, G.S. Paraoanu, and P. Törmä, "High-Speed Memory from Carbon Nanotube Field-Effect Transistors with High-k Gate Dielectric," *Nano Letters*, vol. 9, no. 2, pp. 643-647, 2009.

[32] J.L. Kwo, M. Yokoyama, W.C. Wang, F.Y. Chaung, and I.N. Lin, "Characterisitcs of flat panel display using carbon nanotubes as electron emitters," *Diamond and Related Materials*, vol. 9, pp. 1270-1274, 2000.

[33] P.M. Ajayan and J.M. Tour, "Nanotube Composites," *Nature*, vol. 447, pp. 1066-1068, 2007.

[34] Paul Rincon. (2007, October) BBC News: Science and Technology. [Online]. http://news.bbc.co.uk/2/hi/science/nature/7038686.stm

[35] T.W. Ebbesen and P.M. Ajayan, "Large-scale synthesis of carbon nanotubes," *Nature*, vol. 358, pp. 220-222, 1992.

[36] J. Qiu, Y. Li, Y. Wang, and W. Li, "Production of carbon nanotubes from coal," *Fuel Processing Technology*, vol. 85, pp. 1663-1670, 2004.

[37] D.S. Bethune, C.H. Klang, M.S. de Vries, G. Gorman, R. Savoy, J. Vazquez, and R. Beyers, "Cobalt-catalysed growth of carbon nanotubes with single-atomic-layer walls," *Nature*, vol. 363, pp. 605-607, 1993.

[38] M. Takiwaza, S. Bandow, M. Yudasaka, Y. Ando, H. Shimoyama, and S. Iijima, "Change of tube diameter distribution of single-wall carbon nanotubes induced by changing the bimetallic ratio of Ni and Y catalysts," *Chemical Physics Letters*, vol. 326, pp. 351-357, 2000.

[39] C. Journet, W.K. Maser, P Bernier, A. Loiseau, M. Lamy de la Chapelle, S. Lefrant, P. Deniard, R. Lee, and J.E. Fischer, "Large-scale production of single-walled carbon nanotubes by the electric-arc technique," *Nature*, vol. 388, pp. 756-758, 1997.

[40] S. Seraphin and D. Zhou, "Single-walled carbon nanotubes produced at high yield by mixed catalysts," *Applied Physics Letters*, vol. 64, no. 16, pp. 2087-2089, 1994.

[41] Y. Saito, Y. Tani, N. Miyagawa, K. Mitsushima, A. Kasuya, and Y. Nishina, "High yield of single-wall carbon nanotubes by arc discharge using Rh-Pt mixed catalysts," *Chemical Physics Letters*, vol. 294, pp. 593-598, 1998.

[42] T.W. Ebbesen, "Carbon Nanotubes," *Physics Today*, vol. 49, pp. 26-32, 1996.

[43] T. Zhao and Y. Liu, "Large scale and high purity synthesis of single-walled carbon nanotubes by arc discharge at controlled temperatures," *Carbon*, vol. 42, pp. 2735-2777,

2004.

[44] M. Nishio, S. Akita, and Y. Nakayama, "Cooling effect on the growth of carbon nanotubes and optical emission spectroscopy in short-period arc-discharge," *Thin Solid Films*, vol. 464-465, pp. 304-307, 2004.

[45] D.T. Colbert, J. Zhang, S.M. McClure, P. Nikolaev, Z. Chen, J.H. Hafner, D.W. Owens, P.G. Kotula, C.B. Carter, J.H. Weaver, A.G. Rinzler, and R.E. Smaller, "Growth and Sintering of Fullerene Nanotubes," *Science*, vol. 266, no. 5188, pp. 1218-1222, 1994.

[46] X. Zhao, M. Ohkohchi, M. Wang, S. Iijima, T. Ichihashi, and Y. Ando, "Preparation of high-grade carbon nanotubes by hydrogen arc discharge," *Carbon*, vol. 35, no. 6, pp. 775-781, 1997.

[47] X.K. Wang, X.W. Lin, V.P. Dravid, J.B. Ketterson, and R.P.H. Chang, "Carbon nanotubes synthesized in a hydrogen arc discharge," *Applied Physics Letters*, vol. 66, no. 18, pp. 2430-2432, 1995.

[48] I. Hinkov, S. Farhat, and C.D. Scott, "Influence of the gas pressure on single-wall carbon nanotube formation," *Carbon*, vol. 43, pp. 2453-2462, 2005.

[49] M. Ishigami, J. Cumings, A. Zettl, and S. Chen, "A simple method for the continuous production of carbon nanotubes," *Chemical Physics Letters*, vol. 319, pp. 457-459, 2000.

[50] S.-H. Jung, M.-R. Kim, S.-H. Jeong, O.-J. Lee, K.-H. Lee, J.-H. Suh, and C.-K. Park, "High-yield synthesis of multi-walled carbon nanotubes by arc discharge in liquid nitrogen," *Applied Physics A*, vol. 75, pp. 285-286, 2003.

[51] H.W. Zhu, X.S. Li, B. Jiang, C.L. Xu, Y.F. Zhu, D.H. Wu, and X.H. Chen, "Formation of carbon nanotubes in water by the electric-arc technique," *Chemical Physics Letters*, vol. 366, pp. 664-669, 2002.

[52] P.J.F. Harris, "Solid state growth mechanisms for carbon nanotubes," *Carbon*, vol. 45, pp. 229-239, 2007.

[53] E.G. Gamalay and T.W. Ebbesen, "Mechanism of carbon nanotube formation in the arc discharge," *Physical Review B*, vol. 52, no. 3, pp. 2083-2089, 1995.

[54] O.A. Louchev, "Transport-kinetical phenomena in nanotube growth," *Journal of Crystal Growth*, vol. 237-239, pp. 65-69, 2002.

[55] W.A. de Heer, P. Poncharal, C. Berger, J. Gezo, Z. Song, J Bettini, and D. Ugarte, "Liquid carbon, Carbon-Glass Beads, and the Crystallization of Carbon Nanotubes," *Sciene*, vol. 307, no. 5711, pp. 907-910, 2005.

[56] P.J.F Harris, S.C. Tsang, J.B. Claridge, and M.L.H. Green, "High-resolution electron microscopy studies of a microporous carbon produced by arc-evaporation," *Journal of the Chemical Society, Faraday Transactions* , vol. 90, no. 18, pp. 2799-2802, 1994.

[57] G. Radhakrishnan, P.M. Adams, and L.S. Bernstein, "Plasma characterization and room temperature growth of carbon nanotubes and nano-onions by excimer laser ablation," *Applied Surface Science*, vol. 253, pp. 7651-7655, 2007.

[58] T. Guo, P. Nikolaev, A. Thess, D.T. Colbert, and R.E. Smalley, "Catalytic growth of single-walled nanotubes by laser vaporization," *Chemical Physics Letters*, vol. 243, pp. 49-54, 1995.

[59] E. Muñoz, W.K. Maser, A.M. Benito, A.M. Martinez, G.F. de la Fuente, Y. Maniette, A. Righi, E. Anglaret, and J.L. Sauvajol, "Gas and pressure effects on the production of single-walled carbon nanotubes by laser ablation," *Carbon*, vol. 38, pp. 1445-1451, 2000.

[60] A. Thess, R. Lee, P. Nikolaev, H. Dai, P. Petit, J. Robert, C. Xu, Y.H. Lee, S.G. Kim, A.G. Rinzler, D.T. Colbert, G.E. Scuseria, D. Tomanek, J.E. Fischer, and R.E. Smalley, "Crystalline Ropes of Metallic Carbon Nanotubes," *Science*, vol. 273, no. 5274, pp. 483-487, 1996.

[61] M. Kusaba and Y. Tsunawaki, "Production of single-wall carbon nanotubes by a XeCl excimer laser ablation," *Thin Solid Films*, vol. 506-507, p. 2550258, 2006.

[62] H. Kataura, Y. Kumazawa, Y. Maniwa, Y. Ohtsuka, R. Sen, S. Suzuki, and Y. Achiba, "Diameter control of single-walled carbon nanotubes," *Carbon*, vol. 38, pp. 1691-1697, 2000.

[63] W.K. Maser, A.M Benito, and M.T. Martinez, "Prodcution of carbon nanotubes: the light

approach," *Carbon*, vol. 40, pp. 1685-1695, 2002.

[64] X.P. Zou, H. Abe, T. Shimizu, A. Ando, Y. Nakayama, H. Tokumoto, S.M. Zhu, and H.S. Zhou, "Simple thermal chemical vapor deposition synthesis and electrical property of multi-walled carbon nanotubes," *Physica E*, vol. 24, pp. 14-18, 2004.

[65] B. Zheng, C. Lu, G. Gu, A. Mkarovski, G. Finkelstein, and J. Liu, "Efficient CVD Growth of Single-Walled Carbon Nanotubes on Surfaces Using Carbon Monoxide Precursor," *Nano Letters*, vol. 2, no. 8, pp. 895-898, 2002.

[66] Y. Li, D. Mann, M. Rolandi, W. Kim, A. Ural, S. Hunt, A. Javey, J. Cao, D. Wang, E. Yenilmez, Q. Wang, J.F. Gibbons, Y. Nishi, and H. Dai, "Preferential Growth of Semiconducting Single-Walled Carbon Nanotubes by a Plasma Enhanced CVD Method," *Nano Letters*, vol. 4, no. 2, pp. 317-321, 2004.

[67] S.B. Sinnott, R. Andrews, D. Qian, A.M. Rao, Z. Mao, E.C. Dickey, and F. Derbyshire, "Model of carbon nanotube growth through chenical vapour deposition," *Chemical Physics Letters*, vol. 315, pp. 25-20, 1999.

[68] F. Li, X.-P. Zou, J. Cheng, H.-D. Zhang, and P.-F. Ren, "Preparation of carbon nanotube by ethanol catalytic combustion technique using nickel salt as catalyst precursor," *transactions of Nonferrous Metals Society of China*, vol. 16, pp. 381-384, 2006.

[69] H. Endo, K. Kuwana, K. Saito, D. Qian, R. Andrews, and E.A. Grulke, "CFD prediction of carbon nanotube production in a CVD reactor," *Chemical Physics Letters*, vol. 387, pp. 307-311, 2004.

[70] R. Andrews, D. Jacques, A.M. Rao, F. Derbyshire, D. Qian, X. Fan, E.C. Dickey, and J. Chen, "Continuous production of aligned carbon nanotubes: a step closer to commercial realiation," *Chemical Physics Letters*, vol. 303, pp. 467-474, 1999.

[71] H. Ago, T. Komatsu, S. Ohshima, Y. Kuriki, and M. Yumura, "Dispersion of metal nanoparticles for aligned carbon nanotube arrays," *Applied Physics Letters*, vol. 77, no. 1, pp. 79-81, 2000.

[72] C. Singh, M. Shaffer, I. Kinloch, and A. Windle, "Production of aligned carbon nanotubes

by the CVD injection method," *Physica B*, vol. 323, pp. 339-340, 2002.

[73] H. Ago, S. Ohshima, K. Tsukuagoshi, M. Tsuji, and M. Yumura, "Formation mechanism of carbon nanotubes in the gas-phase synthesis from colloidal solution of nanoparticles," *Current Applied Physics*, vol. 5, pp. 128-132, 2005.

[74] C.L. Cheung, A. Kurtz, H. Park, and C.M. Liemer, "Diameter-Controlled Synthesis of Carbon Nanotubes," *Journal of Physical Chemistry B*, vol. 106, pp. 2429-2433, 2002.

[75] M. Hiramatsu, K. Shiki, H. Amano, and M. Hori, "Fabrication of vertically aligned carbon nanowalls using capacitively coupled plasma-enhanced chemical vapor deposition assisted by hydrogen radical injection," *Applied Physics Letters*, vol. 84, no. 23, pp. 4708-4710, 2004.

[76] P. Nikolaev, M.J. Bronikowski, R.K. Bradley, F. Rohmund, D.T. Colbert, K.A. Smith, and R.E. Smalley, "Gas-phase catalytic growth of single-walled carbon nanotubes from carbon monoxide," *Chemical Physics Letters*, vol. 313, pp. 91-97, 1999.

[77] M. Kumar and Y. Ando, "A simple method of producing aligned carbon nanotubes from an unconventional precursor - Camphor," *Chemical Physics Letters*, vol. 374, pp. 521-526, 2003.

[78] R.J. Andrews, C.F. Smith, and A.J. Alexander, "Mechanism of carbon nanotube growth from camphor and camphor analogs by chemical vapor deposition," *Carbon*, vol. 44, pp. 341-347, 2006.

[79] J. Qiu, Q. Li, Z. Wang, Y. Sun, and H. Zhang, "CVD synthesis of coal-gs-derived carbon nanotubes and nanocapsules containing magnetic iron carbide and oxide," *Carbon*, vol. 44, pp. 2565-2568, 2006.

[80] S.Y. Brichka, G.P. Prikhod'ko, Y.I. Sementsov, A.V. Brichka, G.I. Dovbeshko, and O.P. Paschuk, "Synthesis of carbon nanotubes from a chlorine-containing precursor and their properties," *Carbon*, vol. 42, pp. 2581-2587, 2004.

[81] J. Liu, M. Shao, Q. Xie, L. Kong, W. Yu, and Y. Qian, "Single-source precursor route to carbon nanotubes at mild temperatre," *Carbon*, vol. 41, pp. 2101-2104, 2003.

[82] Y.-F. Shi, H.-J. Quan, G.-B. Zheng, H. Sano, and Y. Uchiyama, "Synthesis of double-walled carbon nanotubes from tetraethoxysilane," *Carbon*, vol. 41, pp. 1674-1677, 2002.

[83] Y.-L. Li, A. Kinloch, and A.H. Windle, "Direct spinning of carbon nanotube fibres from chemical vapour deposition synthesis," *Science*, vol. 304, pp. 276-278, 2004.

[84] N. van Quy, Y.S. Cho, G.S. Choi, I.K. Song, W.J. Yu, and D. Kim, "Synthesis of a long strand of single-wall carbon nanotubes," *Nanotechnology*, vol. 16, pp. 386-390, 2005.

[85] X. Wang, Z. Hu, X. Chen, and Y. Chen, "Preparation of carbon nanotubes and nano-particles by microwave plasma-enhanced chemical vapour deposition," *Scripta Materialia*, vol. 44, pp. 1567-1570, 2001.

[86] W. Kim, H.C. Choi, M. Shim, Y. Li, D. Wang, and H. Dai, "Synthesis of Ultralong and High Percentage of Semiconducting Single-walled Carbon Nanotubes," *Nano Letters*, vol. 2, no. 7, pp. 703-708, 2002.

[87] R.A. Afre, T. Soga, T. Jimbo, M. Kumar, Y. Ando, and M. Sharon, "Growth of vertically aligned carbon nanotubes on silicon and quartz substrate by spray pyrolysis of a natural precurosr: Turpentine oil," *Chemical Physics Letters*, vol. 414, pp. 6-10, 2005.

[88] W.Z. Li, S.S. Xie, L.X. Qian, B.H. Chang, B.S. Zou, W.Y. Zhou, R.A. Zhao, and G. Wang, "Large-Scale Synthesis of Aligned Carbon Nanotubes," *Science*, vol. 274, pp. 1701-1703, 1996.

[89] O. Smiljanic, B.L. Stansfield, J.-P. Dodelet, A. Serventi, and S. Désilets, "Gas-phase synthesis of SWNT by an atmospheric pressure plasma jet," *Chemical Physics Letters*, vol. 356, pp. 189-193, 2002.

[90] S. Maruyama, R. Kojina, Y. Miyauchi, S. Chiashi, and M. Kohno, "Low-temperature synthesis of high-purity single-walled carbon nanotubes from alcohol," *Chemical Physics Letters*, vol. 360, pp. 229-234, 2002.

[91] J. Gonzalez-Aguilar, M. Moreno, and L. Fulcheri, "Carbon nanostrucutres production by gas-phase plasma processes at atmospheric pressure," *Journal of Physics D: Applied Physics*, vol. 40, pp. 2361-2374, 2007.

[92] Q. Ye, A.M. Cassell, H. Liu, K.-J. Chao, J. Han, and M. Meyyappan, "Large-Scale Fabrication of Carbon Nanotube Probe Tips for Atomic Force Microscopy Critical Dimension Imaging Applications," *Nano Letters*, vol. 4, no. 7, pp. 1301-1308, 2004.

[93] D. Harbec, J. Meunier, L. Guo, R. Gauvin, and N. Mallah, "Carbon nanotubes from the dissociation of C2Cl4 using a DC plasma torch," *Journal of Physics D: Applied Physics*, vol. 37, pp. 2121-2126, 2004.

[94] H. Ago, K. Marata, M. Yumura, J. Yotani, and S. Uemura, "Ink-jet printing of nanoparticle catalyst for site-selective carbon nanotube growth," *Applied Physics Letters*, vol. 82, no. 5, pp. 811-813, 2003.

[95] C.-H. Kiang, "Carbon rings and cages in the growth of single-walled carbon nanotubes," *Journal of Chemical Physics*, vol. 113, no. 11, pp. 4763-4766, 2000.

[96] L. Ci, Z. Rao, Z. Zhou, D. Tang, X. Yan, Y. Laing, D. Liu, H. Yuan, W. Zhou, G. Wang, W. Liu, and S. Xie, "Double wall carbon nanotubes promoted by sulfur in a floating iron catalyst CVD system," *Chemical Physics Letter*, vol. 359, pp. 63-67, 2002.

[97] H. Ago, S. Ohshima, K. Uchida, and M. Yumura, "Gas-Phase Synthesis of Single-wall Carbon Nanotubes from Colloidal Solution of Metal Nanoparticles," *The Journal of Physical Chemistry B*, vol. 105, no. 43, p. 1045310456, 2001.

[98] M.S. Kim, N.M. Rodriguez, and R.T.K. Baker, "The Interplay Between Sulphur Adsorption and Carbon Deposition on Cobalt Catalysts," *Journal of Catalysts*, vol. 143, no. 2, pp. 449-463, 1993.

[99] W.Z. Li, J.G. Wen, and Z.F. Ren, "Effect of temperature on growth and structure of carbon nanotubes by chemical vapour deposition," *Applied Physics A: Materials Science and Processing*, vol. 74, pp. 397-402, 2002.

[100] Z.F. Ren, Z.P. Huang, D.Z. Wang, J.G. Wen, J.W. Xu, J.H. Wang, L.E. Calvet, J. Chen, J.F. Klemic, and M.A. Reed, "Growth of a single freestanding multiwall carbon nanotube on each nanonickel dot," *Applied Physics Letter*, pp. 1086-1088, 1999.

[101] M. Chhowalla, K.B.K. Teo, C. Ducati, N.L. Rupesinghe, G.A. Amaratunga, A.C. Ferrari,

D. Roy, J. Robertson, and W.I. Milne, "Growth process conditions of vertically aligned carbon nanotubes using plasma enhanced chemical vapor deposition," *Journal of Applied Physics*, vol. 90, no. 10, pp. 5308-5317, 2001.

[102] H. Kinoshita, I. Kume, H. Sakai, M Tagawa, and N. Ohmae, "High growth rate of vertically aligned carbon nanotubes using a plasma shield in mocrowave plasma-enhanced chemical vapor deposition," *Carbon*, vol. 42, pp. 2753-2756, 2004.

[103] C. Bower, O. Zhou, W. Zhu, J. Werder, and S. Jin, "Nucleation and growth of carbon nanotubes by microwave plasma chemical vapor deposition," *Applied Physics Letters*, vol. 77, pp. 2767-2769, 2000.

[104] Y.C. Choi, Y.M. Shin, Y.H. Lee, B.S. Lee, G.-S. Park, W.B. Choi, N.S. Lee, and J.M. Kim, "Controlling the diameter, growth rate, and density of vertically aligned carbon nanotubes synthesized by microwave plasma-enhanced chemical vapor deposition," *Applied Physics Letters*, vol. 76, no. 17, pp. 2367-2369, 2000.

[105] L. Delzeit, I. McAninch, B.A. Cruden, D. Hash, B. Chen, J. Han, and M. Mayyappan, "Growth of multiwall carbon nanotubes in an inductively coupled plasma reactor," *Journal of Applied Physics*, vol. 91, no. 9, pp. 6027-6033, 2002.

[106] Z.F. Ren, Z.P. Huang, J.W. Xu, J.H. Wang, P. Bush, M.P. Siegal, and P.N. Provencio, "Synthesis of Large Arrays of Well-Aligned Carbon Nanotubes on Glass," *Science*, vol. 282, pp. 1105-1107, 1998.

[107] Y. Zhang, A. Chang, J. Cao, Q. Wang, W. Kim, Y. Li, N. Morris, E. Yenilmez, J. Kong, and H. Dai, "Electric-field-dirceted growth of aligned single-walled carbon nanotubes," *Applied Physics Letters*, vol. 79, no. 19, pp. 3155-3157, 2001.

[108] C. Bower, W. Zhu, S. Jin, and O. Zhou, "Plasma-induced alignment of carbon nanotubes," *Applied Physics Letters*, vol. 77, no. 6, pp. 830-832, 2000.

[109] K.A. Brucker and J. Majdalani, "Effective thermal conductivity of common geometric shapes," *International Journal of Heat and Mass Transfer*, vol. 48, pp. 4779-4796, 2005.

[110] A.C. Dillon and M.J. Heben, "Hydrogen storage using carbon adsorbents: past, present

and future," *Applied Physics A*, vol. 72, pp. 133-142, 2001.

[111] W.H. McAdams, *Heat Transmission*, 3rd ed., S.D. Kirkpatrick, Ed. New York: McGraw-Hill, 1954.

[112] M.W. Zemansky, *Heat and thermodynamics : an intermediate textbook*, 5th ed. Japan: McGraw-Hill, 1968.

[113] N.P. Cheremisinoff, Ed., *Handbook of heat and mass transfer, Volume 1: Heat Transfer Operations*. Houston, Texas: Gulf Publishing, 1986.

[114] M.J. Biercuk, M.C. Llaguno, M. Radosavljevic, J.K. Hyun, A.T. Johnson, and J.E. Fischer, "Carbon nanotube composites for thermal management," *Applied Physics Letters*, vol. 80, pp. 2767-2769, 2002.

[115] C.H. Liu, H. Huang, Y. Wu, and S.S. Fan, "Thermal conductivity improvement of silicone elastomer with carbon nanotube loading," *Applied Physics Letters*, vol. 84, pp. 4248-4250, 2004.

[116] Y.-M. Chen and J.-M. Ting, "Ultra high thermal conductivity polymer composites," *Carbon*, vol. 40, pp. 359-362, 2002.

[117] S. Shaikh, L. Li, K. Lafdi, and J. Huie, "Thermal conductivty of an aligned carbon nanotube array," *Carbon*, vol. 45, pp. 2608-2613, 2007.

[118] P.W. May, R. Portman, and K.N. Rosser, "Thermal conductivity of CVD diamond fibres and diamond fibre-reinforced epoxy composites," *Diamond and Related Materials*, vol. 14, pp. 598-603, 2005.

[119] P.G. Partridge, G. Lu, P. May, and J.W. Steeds, "Potential high-strength high thermal conductivity metal-matrix composites based on diamond fibres," *Diamond and Related Materials*, vol. 4, pp. 848-851, 1995.

[120] A. Vaslov, V. Ralchenko, S. Gordeev, D. Zakharov, I. Vlasov, A. Karabutov, and P. Belobrov, "Thermal properties of diamond.carbon composites," *Diamond and Related Materials*, vol. 9, pp. 1104-1109, 2000.

[121] H.-M. Cheng, Q.-H. Yang, and C. Liu, "Hydrogen storage in carbon nanotubes," *Carbon*, vol. 39, pp. 1447-1454, 2001.

[122] A. Nikitin, H. Ogasawara, D. Mann, R. Denecke, Z. Zhang, H. Dai, K. Cho, and A. Nilsson, "Hydrogenation of Single-Walled Carbon Nanotubes," *Physical Review Letters*, vol. 95, pp. 225507.1-225507.4, November 2005.

[123] P. Sudan, A. Zuttel, P. Mauron, C. Emmenegger, P. Wenger, and L. Schlapbach, "Physisorption of hydrogen in single-walled carbon nanotubes," *Carbon*, vol. 41, pp. 2377-2383, 2003.

[124] A. Chambers, C. Park, R.T.K. Baker, and N.M. Rodriguez, "Hydrogen storage in graphite nanofibers," *Journal of Physical Chemistry B*, vol. 102, pp. 4253-4256, 1998.

[125] L. Schlapbach and A. Züttel, "Hydrogen-storage materials for mobile application," *Nature*, vol. 414, pp. 353-358, 2001.

[126] H. Lee, Y.-S. Kang, S.-H. Kim, and J.-Y. Lee, "Hydrogen desorption properties of multiwall carbon nanotubes with closed and open structures," *Applied Physics Letters*, vol. 80, no. 4, pp. 577-579, 2002.

[127] H. Dodziuk and G. Dolgonos, "Molecular modeling study of hydrogen storage in carbon nanotubes," *Chemical Physics Letters*, vol. 2002, pp. 79-83, 2002.

[128] H. Wu, J. Qiu, C. Hao, Z. Tang, and K. Han, "Molecular dynamics study of hydrogen adsorption in Y-junction carbon nanotubes," *Journal of Molecular Structure*, vol. 684, pp. 75-80, 2004.

[129] M.G. Nijkamp, J.E.M.J. Raaymakers, A.J. van Dillen, and K.p. de Jong, "Hydrogen storage using physisorption - materials demands," *Applied Physics A*, vol. 72, pp. 619-623, 2001.

[130] U. Bünger and W. Zittel, "Hydrogen storage in carbon nanostructures - still a long way from science to commerce?," *Applied Physics A*, vol. 72, pp. 147-151, 2001.

[131] V. Meregalli and M. Parrinello, "Review of theoretical calculations of hydrogen storage in

carbon-based materials," *Applied Physics A*, vol. 72, pp. 143-146, 2001.

[132] M. Ritschel, M. Uhlemann, O. Gutfleish, A. Leonhardt, A. Graff, C. Taschner, and J. Fink, "Hydrogen storage in different carbon nanostructures," *Applied Physics A*, vol. 80, pp. 2985-2987, 2002.

[133] P.A. Berseth, A.G. Harter, R. Zidan, A. Blomqvist, C.M. Araujo, R.H. Scheicher, R. Ahuja, and R. Jena, "Carbon Nanomaterials as Catalysts for Hydrogen Uptake and Release in NaAlH4," *Nano Letters*, vol. 9, no. 4, pp. 1501-1505, 2009.

[134] Mark Davison. (1997) Universityof Paisley. [Online]. http://media.paisley.ac.uk/~davison/labpage/searle/searle.html

[135] Ian Hickson. (1997) Ian Hickson's Lee's Disk experiment. [Online]. http://academia.hixie.ch/bath/Thermal/home.html

[136] Mark Davison. (1997) University of Paisely. [Online]. http://media.paisley.ac.uk/~davison/labpage/leedisk/leedisk.html

[137] D.M. Price and M. Jarratt, "Thermal conductivity of PTFE and PTFE composites," *Thermochimica Acta*, vol. 392-393, pp. 231-236, 2002.

[138] Thermal Conductivities of Various Metals. [Online]. http://www.oberlin.edu/physics/catalog/demonstrations/thermo/conductivity.html

[139] Analog Devices, Monolithic Thermocouple Amplifiers with Cold Junction Compensation AD594/AD595 Data Sheet, http://www.datasheetcatalog.org/datasheet/analogdevices/AD594AQ.pdf.

[140] J. Hone, "Carbon Nanotubes: Thermal Properties," in *Dekker Encyclopedia of Nanoscience and Nanotechnology*, J.A. Schwartz, C.I. Contescu, and K. Putyera, Eds. London, United kingdom: Taylor & Francis, 2004, pp. 603-610.

[141] Laura Mgrdichain. (2009, January) physorg.com. [Online]. http://www.physorg.com/news152202897.html

[142] C.-W. Nan, Z. Shi, and Y. Lin, "A simple model for thermal conductivity of carbon

nanotube-based composites," *Chemical Physics Letters*, vol. 375, pp. 666-669, 2003.

[143] T. Kato, G.-H. Jeong, T. Hirata, R. Hatakeyama, K. Tohji, and K. Motomiya, "Single-walled carbon nanotubes produced by plasma-enhanced chemical vapor deposition," *Chemical Physics Letters*, vol. 381, pp. 422-426, 2003.

[144] Y. Liu, R.L. Vander Wal, and V.N. Khabashesku, "Functionalization of Carbon Nano-onions by Direct Flourination," *Chemistry of Materials*, vol. 19, no. 4, pp. 778-786, 2007.

[145] E.W. Weisstein. (2009) MathWorld--A Wolfram Web Resource. [Online]. http://mathworld.wolfram.com/AbsoluteError.html

[146] E.A. Wiesstein. (2009) Mathword - A Wolfram Web Resource. [Online]. http://mathworld.wolfram.com/RelativeError.html